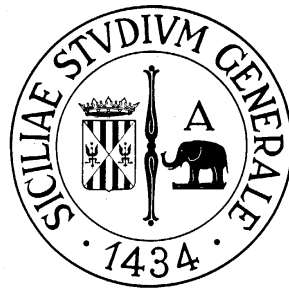# Università degli Studi di Catania

## Facoltà di Scienze Matematiche, Fisiche e Naturali

Dipartimento di Matematica e Informatica

Dottorato di Ricerca in Matematica Pura e Applicata

XXVIII ciclo

# Numerical Methods for All Mach Number flows for Gas Dynamics

Leonardo Scandurra

*Advisor*

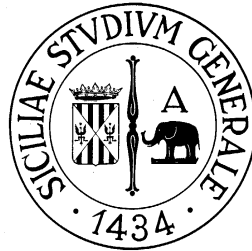Prof. Giovanni Russo

Anno Accademico 2016-2017

# Università degli Studi di Catania

## Facoltà di Scienze Matematiche, Fisiche e Naturali

Dipartimento di Matematica e Informatica

Dottorato di Ricerca in Matematica Pura e Applicata

XXVIII ciclo

# Numerical Methods for All Mach Number flows for Gas Dynamics

*Tutor*
Chiar.mo Prof. Giovanni Russo

*Candidato*
Leonardo Scandurra

*Coordinatore*
Prof. Giovanni Russo

*A Carlo Foti*

# Numerical Methods for All Mach Number flows for Gas Dynamics

Leonardo Scandurra[1]

December 9, 2016

[1]Dipartimento di Matematica e Informatica, Università di Catania, Catania, Italy

# Contents

# Introduction

My research is about numerical methods for hyperbolic systems of conservation laws. In particular in my PhD project I focus on gas dynamics, but in general I worked during these years on numerical methods for computational fluid dynamics (CFD). The use of these methods is nowadays widespread in scientific and engineering applications such as aerodynamics, design process of aircraft, engines or wind turbines, simulation of meteorology and weather prediction, astrophysical modeling, modeling the plasma in a fusion reactor, magnetohydrodynamics, electromagnetic effects, study of explosions and blast waves, simulation of geophysical and enviromental flows, and many others.

The equations that describe the motion of inviscid gases (non rarefied regime) are Euler equations in the compressible regime. These equations have the structure of a hyperbolic system of conservation laws. The initial value problem for Euler equations, also in presence of regular initial data, admits strong solutions only for a short time. For a long time it develops singularity type jump (*shocks*) and it is therefore necessary to resort to weak solutions. The theory of hyperbolic systems of conservation laws provides a good mathematical basis for the study of such systems. A conservative structure, combined with the selection conditions for the solutions (viscosity solution, entropy condition) allows to prove existence and uniqueness of the solution in several cases (scalar equation in multiple dimensions, system of equations in one dimension). The most widely used methods for the solution of such systems are the *shock-capturing* schemes: the system is discretized and the equations are solved on the whole computational domain; discontinuities are automatically determined as areas of strong variation of the fields. Among the most popular schemes for this kind of problems there are finite volume schemes (FV) [10, 21, 26] and finite difference schemes (FD) [7], both in conservative form.

For example, consider a finite volume scheme based on an uniform discretization of the computational domain. The modern conservative schemes shock capturing finite volume are based on three main ingredients:

- the numerical flux function;

- the reconstruction of non-oscillatory field variables;

- the time integration scheme (typically explicit).

For explicit schemes, the time step is subject to a stability restriction (CFL, from the name of mathematicians Richard Courant, Kurt Friedrichs and Hans Lewy) of the type

$$\Delta t \leqslant c\Delta x/\lambda_{\max}$$

where $\Delta x$ and $\Delta t$ represent, respectively, the space and time steps, while $\lambda_{\max}$ represents the maximum speed characteristic of the system (basically the maximum spectral radius of the Jacobian matrix of the system on the computational domain). In the case of gas dynamics, the maximum speed characteristic in a point is given by $\lambda_{\max} = |\mathbf{u}| + c_s$, where $\mathbf{u}$ represents the velocity of the gas, and $c_s$ is the speed of sound.

The compressible phenomena are observed when the velocity of the fluid is comparable with the speed of sound. In dimensionless number that characterizes the compressibility is the Mach number

$$M \equiv U/C_s$$

where $U$ represents a typical velocity of a gas, and $C_s$ a typical speed of sound. If $M \ll 1$ the gas behaves in practice as an incompressible fluid.

In the incompressible limit, the equation structure changes: the system has no more a hyperbolic structure, the density of the gas is constant, the flow has zero divergence: $\nabla \cdot \mathbf{u} = 0$ (incompressible condition) and the gas pressure acts as a Lagrange multiplier that forces the incompressibility of the flow. Incompressible Euler equations can be written in the form

$$\frac{\partial u}{\partial t} = -\mathbb{P}u \cdot \nabla u$$

where $\mathbb{P}$ denotes the projection operator on the fields to zero divergence. The CFL time constraint for the explicit schemes is:

$$\Delta t < \Delta x/u_{\max}(t^n)$$

where $u_{\max}(t^n) = \max_\Omega |u(x, t^n)|$.

On the other hand, when we are near the incompressible regime, and the Mach number is very small, but not negligible, in many cases the majority of the energy of the system is carried by the so-called *material wave* (the one that moves with the velocity of the fluid), while the acoustic waves carry a negligible signal and we are not interested in their resolution.

Research objective and purpose of the thesis is the construction of an universal numerical method, efficient and accurate, for the solution of the Euler equations, able to work perfectly in all compressibility regimes. When $M \approx 1$ the method becomes a FV scheme for compressible Euler equations, while $M \ll 1$ the scheme deals with the material waves explicitly, and acoustic waves implicitly, bypassing the stability restriction of CFL type. In the limit $M \to 0$ the scheme becomes a projection method for incompressible fluid dynamics.

Compressible flow equations converge to incompressible equations when the Mach number becomes small. This convergence has been rigorously studied mathematically by Klainerman and Majda [18, 19]. Of course, when the Mach number is of order one, modern shock capturing methods are able to capture shocks and other complex structures with high numerical resolutions. A difficulty in the construction such schemes consists in the different nature of the equations and then in different numerical techniques traditionally used for solving them: methods for compressible Euler is usually based on a conservative form, explicit schemes in time and non-linear reconstruction, while the methods for Euler incompressible are usually based on a non-conservative formulation, on the implicit treatment of the pressure and on reconstructions which are often linear.

However, to solve a problem that works for both low-Mach and high-Mach numbers, we have adopted an original finite volume method for the Euler equations of the gas dynamics on staggered grids.

The system is discretized to second order in space on staggered grid, in a fashion similar to the Nessyahu-Tadmor central scheme for 1D model [22] and Jang-Tadmor central scheme for 2D model [15], thus simplifying the flux computation. This approach turns out to be extremely simple, since it requires no equation splitting. We consider the isentropic case and the general case. For simplicity we assume a $\gamma$-law gas in both cases.

Both approaches are based on IMEX strategy, in which some term is treated explicitly, while other terms are treated implicitly, thus avoiding the classical CFL restriction due to acoustic waves.

By rescaling the variables the (possibly small) Mach number $\varepsilon$ appears in the equations.

1. Isentropic Euler Case:

$$\begin{cases} \rho_t + \nabla \cdot (\rho \mathbf{u}) = 0, \\ \\ (\rho \mathbf{u})_t + \nabla \cdot (\rho \mathbf{u} \otimes \mathbf{u}) + \frac{1}{\varepsilon^2} \nabla p(\rho) = 0, \end{cases} \tag{1}$$

completed with the relation $p = k\rho^\gamma$. The core if the implicit term contains a non-linear elliptic equation for the pressure, which has to be treated by a fully implicit technique. Because of the non-linearity, it is necessary to adopt an iterative method to compute the pressure. In our numerical experiments Newton's method worked with few iterations. As an alternative, a semi-implicit method based writing $\nabla(\nabla p) = \nabla(p'(\rho)\nabla\rho)$ is described in Chapter 3.

**Remark 1.** *These equations will be introduced in dimensionless form in the section* (3.3.1).

2. General Euler Case:

$$\begin{cases} \rho_t + \nabla \cdot (\rho \mathbf{u}) = 0 \\ \\ (\rho \mathbf{u})_t + \nabla \cdot (\rho \mathbf{u} \otimes \mathbf{u}) + \frac{1}{\varepsilon^2} \nabla p = 0 \\ \\ E_t + \nabla \cdot [(E + p)\mathbf{u}] = 0, \end{cases} \tag{2}$$

The system is closed by the (suitably scaled) equation of state

$$E = \rho \varepsilon^2 \mathbf{u}^2 / 2 + p/(\gamma - 1)$$

In this case the implicit term is treated in a semi-implicit fashion, thus avoiding the use of Newton's iterations.

In both cases the schemes are implemented to second order accuracy in time. Suitably *well-prepared* initial conditions are considered, which depend on the Mach number $\varepsilon$. In one space dimension we obtain the same profiles found in the literature [11, 23] for the isentropic case and [9, 23] for the general Euler system) for all Mach numbers.

**Structure of the thesis**   The thesis is composed of five chapters: the first two are introductory, while the original results are presented in the last three chapters. The phisical context is described in the first chapter, while the second chapter is devoted to a brief overview of a second order staggered central schemes in one and two space dimensions. Third chapter is devoted to one-dimensional case, while chapter 4 presents results in two dimensions. The last chapter is an application to the piston problem.

# Fluid dynamics

We start introducing the equations of the fluid dynamics in conservative form that govern the fluid motion. Fluid dynamics is the disclipine that deals with the fluids in motion. Fluids include both liquids or gases and their structure do not have a preferred shape unlike a solid and can be easily deformed. The most relevant difference between liquids and gases lies in their compressibility. The density $\rho$ is the mass per unit volume. In liquids it is almost constant, and it is much larger than in gases where changes in density are due to changes in the pressure $p$ and temperature $T$ through the ideal gas equation

$$p = \rho \mathcal{R} T \tag{1.1}$$

where $\mathcal{R}$ is the gas constant.

## 1.1 Governing equations

Consider a volume $\Omega \subseteq \mathbb{R}^d$ and assume that it is filled by a fluid.
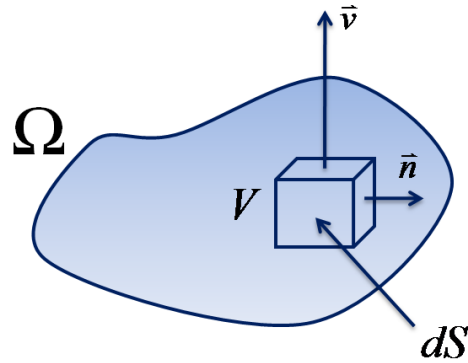
The description of this fluid needs two quantities: a density of mass $\rho(\vec{x}, t)$ that depends on the position in space $\vec{x}$ and at time $t$, that we can write as mass per unit volume:

$$\rho = \lim_{\Delta V \to 0} \frac{\Delta m}{\Delta V},$$

and the velocity $u(\vec{x}, t)$. The governing equations of such quantities will be determined by imposing conservation of mass and momentum.

## 1.1.1 Continuity Equation

Let us consider a region $V$ of space around the point $\vec{x}$, the amount of mass enclosed in this region is

$$\int_V \rho(\vec{x}, t) \, d\vec{x}.$$

We calculate the derivative with respect to time to see how this can vary the amount of mass within the volume. Since there is no source or sink of mass, the only thing that can change it, is the mass flow $\vec{F}_m$ through the surface $\partial V$. Denoting by $\mathbf{n}$ the unit outward normal vector of the small volume $V$, then we put the minus sign in front of the integral:

$$\frac{d}{dt} \int_V \rho(\vec{x}, t) d\vec{x} = -\int_{\partial V} \vec{F}_m \cdot \mathbf{n} \, dS, \tag{1.2}$$

because if the total mass flow through the surface of V is positive, the derivative is negative. The mass flow $\vec{F}_m$ is given exclusively by the mass density $\rho$ times the velocity $\vec{u}$.

$$\vec{F}_m = \rho \vec{u}.$$

On the left hand side of Equation (1.2), by choosing the volume $V$ to be fixed in space, we can bring the time derivative inside the integral, getting

$$\int_V \frac{\partial}{\partial t} \rho(\vec{x}, t) d\vec{x} = -\int_{\partial V} \rho \vec{u} \cdot \mathbf{n} \, dS. \tag{1.3}$$

Applying Gauss (divergence) theorem to the right hand side of Equation (1.3), which transforms a surface integral in a volume integral, and writing it under a single integral we obtain

$$\int_V \left[ \frac{\partial \rho}{\partial t} + \nabla \cdot (\rho \vec{u}) \right] d\vec{x} = 0 \quad , \quad \forall V \subseteq \Omega.$$

The volume $V$ is arbitrary, so this implies that the integrand vanishes:

$$\frac{\partial \rho}{\partial t} + \nabla \cdot (\rho \vec{u}) = 0. \tag{1.4}$$

Equation (1.4) is the mass-conservation or continuity equation in conservative form.

## 1.1.2   Momentum Equation

The amount of momentum enclosed in a volume $V$ is given by

$$\int_V \rho \vec{u} \, d\vec{x}; \tag{1.5}$$

this amount may change in time, for two reasons:

1. the flow of momentum through the surface $\partial V$

$$\int_{\partial V} (\rho \vec{u}) \vec{u} \cdot \mathbf{n} \, dS,$$

   where $\rho \vec{u}$ is the momentum carried by the fluid and $\vec{u} \cdot \mathbf{n}$ how much of it comes out, namely the velocity normal to the surface of the volume, indeed

   - if $\vec{u}$ is parallel to $\mathbf{n}$ then $\vec{u} \cdot \mathbf{n}$ is maximum;
   - if $\vec{u}$ is perpendicular to $\mathbf{n}$ nothing comes out;

   By the Gauss theorem, applied to each component of $\rho \vec{u}$, we have

$$\int_{\partial V} (\rho \vec{u}) \vec{u} \cdot \mathbf{n} \, dS = \int_V \nabla \cdot (\rho \vec{u} \otimes \vec{u}) \, d\vec{x} \tag{1.6}$$

2. due to Newton's second law ($m\vec{a} = \vec{F}$), namely to the forces acting on the fluid contained in V, which in turn are of two types:

    2.1. *Body forces*, which are volumetric forces, indeed act directly on the volumetric mass of the fluid element and are proportional to the density

    $$\rho \vec{F} d\vec{x} \qquad (1.7)$$

    where by $d\vec{x}$ we denote an infinitesimal volume element.
    For istance, in the case of the gravity $\vec{F} = \vec{g}$.

    2.2. *Surface forces*, are due to the interaction of the fluid contained in the volume $V$ with the surrounding fluid. They are also called contact forces because the forces of the surrounding fluid acting on the volume $V$ is exerted through the surface and these are only of two types: the pressure distribution acting on the surface and the shear and normal stress distribution acting on the surface by means of friction.

We consider separately the case of inviscid or viscous fluids.

**Inviscid Fluids:** Under the strong assumption that these contact forces are perpendicular to the surface, then the only surface force is due to the pressure

$$d\vec{F} = -\int_{\partial V} p\mathbf{n}\, dS$$

where $p$ is a function of position that we can assume constant if the volume $V$ is small enough. We use the minus sign because $\mathbf{n}$ denotes the external normal. By the Gauss theorem:

$$-\int_{\partial V} p\mathbf{n}\, dS = -\int_{V} \nabla p\, d\vec{x} \qquad (1.8)$$

putting it all together from (1.5), (1.6), (1.7) and (1.8), we get

$$\frac{d}{dt}\int_{V} \rho\vec{u}\, d\vec{x} = \int_{V} \rho\vec{F}\, d\vec{x} - \int_{V} \nabla p\, d\vec{x} - \int_{V} \nabla \cdot (\rho\vec{u} \otimes \vec{u})\, d\vec{x}.$$

Since volume $V$ is arbitrary, the derivative with respect to time to the left hand side can be carried inside the integral, getting the second equation of fluid dynamics in conservative form

$$\frac{\partial}{\partial t}(\rho\vec{u}) + \nabla\cdot(\rho\vec{u}\otimes\vec{u}) + \nabla p = \rho\vec{F}. \tag{1.9}$$

A non-conservative form can be obtained by splitting the first term as

$$\frac{\partial}{\partial t}(\rho\vec{u}) = \frac{\partial\rho}{\partial t}\vec{u} + \rho\frac{\partial\vec{u}}{\partial t}$$

and using the continuity Equation (1.4):

$$\rho\frac{\partial\vec{u}}{\partial t} + \rho\vec{u}\cdot\nabla\vec{u} + \nabla p = \rho\vec{F}. \tag{1.10}$$

**Remark 2.** *In the case in which the contact forces $\vec{F}_c = -p\mathbf{n}$ then the fluids are called **ideal fluids**.*

**Remark 3.** *We have four equations and the unknowns are $\rho$, $\vec{u}$ and $p$.*

 - *if the pressure $p$ depends only on the density, then the system is closed and is called **barotropic**;*

 - *if instead the pressure also depends for example from the temperature $T$, then we need another equation to close the system.*

**Viscous Fluids:**   In general is not so simple, because in the contact forces there is a matrix tensor $\tilde{\sigma}$ for which

$$(\vec{F}_c)_i = \sigma_{ij}n_j$$

where $\sigma_{ij}$ is called *stress tensor*.

**Remark 4.** *If this tensor is isotropic $\sigma_{ij} = -p\delta_{ij}$, then we get the previous case of the ideal fluids*
$$(\vec{F}_c)_i = -pn_i$$

Consider an element of the surface and try to calculate the mean of all the forces that act on the surface

$$\frac{1}{4\pi}\int_{\partial V} F_i n_i \, dS \quad = \frac{1}{4\pi}\int_{\partial V} \sigma_{ij}n_j n_i \, dS =$$
$$\frac{1}{4\pi}\sigma_{ij}\int_{\partial V} n_i n_j \, dS \quad = \frac{1}{4\pi}\sigma_{ij}\frac{4\pi}{3}\delta ij = \frac{1}{3}\sigma_{ii} = \frac{1}{3}\mathrm{tr}(\tilde{\sigma}) \tag{1.11}$$

Hence to call $p = -\frac{1}{3}\text{tr}(\tilde{\sigma})$ is the generalization of the concept of pressure for ideal fluids, because it gives us how it compresses an element of fluid.
We can decompose

$$\sigma_{ij} = -p\delta ij + d_{ij}$$

where $d_{ij} = \sigma_{ij} - \frac{1}{3}\text{tr}(\tilde{\sigma})\delta_{ij}$ is the zero trace part of $\tilde{\sigma}$ that is clearly anisotropic because we are removing an isotropic part.
Consider the tangential component of the force

$$F_\tau = F_i\tau_i = \sigma_{ij}n_j\tau_i = (-p\delta_{ij} + d_{ij})n_j\tau_i = d_{ij}n_j\tau_i$$

This tangential component arises because there is a volume element which slides on another volume element for a friction effect due to the sliding part of the fluid on other parts of the fluid, so it is natural to think that $d_{ij}$ is associated with the velocity differences, namely with the gradient tensor of velocity

$$d_{ij} \sim \frac{\partial u_j}{\partial x_i}.$$

If there were no differences in velocity between the fluid parts, then the tangential stress would be null. We try to think of a linear relationship

$$d_{ij} = A_{ijkl}\frac{\partial u_k}{\partial x_l}$$

where $A_{ijkl}$ is an isotopic tensor of 4th order.

**Remark 5.** *In a generic fluid there could be privileged directions. This is the case, for example, of liquid crystals, but if we are in a generally homogeneous fluid, the tensor $A_{ijkl}$ is an isotopic tensor.*

It can be proved that the general expression for a 4th order isotopic tensor is

$$A_{ijkl} = \mu\delta_{ik}\delta_{jl} + \mu'\delta_{il}\delta_{jk} + \mu''\delta_{ij}\delta_{kl}$$

We shall make use of the following decomposition of the velocity gradient

$$\frac{\partial u_i}{\partial x_j} = e_{ij} + \Omega_{ij}$$

where

$$e_{ij} = \frac{1}{2}\left(\frac{\partial u_i}{\partial x_j} + \frac{\partial u_j}{\partial x_i}\right) \quad \text{symmetric tensor}$$

$$\Omega_{ij} = \frac{1}{2}\left(\frac{\partial u_i}{\partial x_j} - \frac{\partial u_j}{\partial x_i}\right) \quad \text{skew-symmetric tensor}$$

**Remark 6.** *We note that*

- *$\mu = \mu'$ because $\tilde{\sigma}$ is symmetric (is a consequence of conservation of angular momentum)*

- *$tr(\tilde{e}) = e_{ii} = \frac{1}{2}\left(\frac{\partial u_i}{\partial x_i} + \frac{\partial u_i}{\partial x_i}\right) = \nabla \cdot \vec{u}$*

- *$\tilde{\sigma}$ is symmetric then $\tilde{d}$ is symmetric*

So we have that

$$d_{ij} = A_{ijkl}e_{kl} = \mu''\delta_{ij}\text{tr}(\tilde{e}) + (\mu + \mu')e_{ij} = \mu''\nabla \cdot \vec{u}\,\delta_{ij} + 2\mu e_{ij}.$$

Since $d_{ij}$ has null trace, if we apply the trace on $d_{ij}$ we obtain

$$\mu''\nabla \cdot \vec{u}\,\text{tr}(\delta_{ij}) + 2\mu\,\text{tr}(e_{ij}) = 0,$$

but $\text{tr}(\delta_{ij}) = 3$ and $\text{tr}(e_{ij}) = \nabla \cdot \vec{u}$, for which

$$3\mu'' + 2\mu = 0 \quad \Longrightarrow \quad \mu'' = -\frac{2}{3}\mu.$$

$d_{ij}$ will be written as

$$d_{ij} = 2\mu[e_{ij} - \frac{1}{3}\nabla \cdot \vec{u}\,\delta_{ij}],$$

then the stress tensor now we can be written as

$$\sigma_{ij} = -p\delta_{ij} + 2\mu[e_{ij} - \frac{1}{3}\nabla \cdot \vec{u}\,\delta_{ij}].$$

Hence the momentum equation becomes

$$\rho\left(\frac{\partial u}{\partial t} + u_j\frac{\partial u_i}{\partial x_j}\right) = \rho F_i - \frac{\partial p}{\partial x_i} + \frac{\partial}{\partial x_i}[2\mu(e_{ij} - \frac{2}{3}\nabla \cdot \vec{u}\,\delta_{ij})]. \qquad (1.12)$$

Since $e_{ij} = \frac{1}{2}\left(\frac{\partial u_i}{\partial x_j} + \frac{\partial u_j}{\partial x_i}\right)$ then the derivative respect to space will be

$$\frac{\partial e_{ij}}{\partial x_j} = \frac{1}{2}\frac{\partial^2 u_i}{\partial x_j\partial x_j} + \frac{\partial}{\partial x_i}\frac{\partial u_j}{\partial x_j},$$

where $\frac{\partial u_j}{\partial x_j} = \nabla \cdot \vec{u}$ and $\Delta u_i = \frac{\partial^2 u_i}{\partial x_j \partial x_j}$. Using this expression in (1.12) we get the Navier-Stokes equation

$$\rho \left( \frac{\partial u}{\partial t} + u_j \frac{\partial u_i}{\partial x_j} \right) = \rho F_i - \frac{\partial p}{\partial x_i} + \mu \left( \Delta u_i + \frac{1}{3} \frac{\partial}{\partial x_i} \nabla \cdot \vec{u} \right). \qquad (1.13)$$

If the viscosity coefficient $\mu$ is equal to zero, then we get the Euler equation. At the end the second equation of fluid dynamics, in the case of viscous fluids, will be

$$\rho \left( \frac{\partial \vec{u}}{\partial t} + \vec{u} \cdot \nabla \vec{u} \right) + \nabla p = \rho F + \mu \left[ \Delta \vec{u} + \frac{1}{3} \nabla (\nabla \cdot \vec{u}) \right]. \qquad (1.14)$$

**Incompressible Fluids**
In the case in which the fluid is incompressible $\nabla \cdot \vec{u} = 0$ and the (1.14) can be written as

$$\begin{cases} \rho \left( \frac{\partial \vec{u}}{\partial t} + \vec{u} \cdot \nabla \vec{u} \right) + \nabla p = \rho F + \mu \Delta \vec{u} \\ \nabla \cdot \vec{u} = 0 \end{cases} \qquad (1.15)$$

**Remark 7.** *Tensor $\tilde{\sigma}$ proves to be symmetrical, otherwise there would arise a torque on the volume element, which is not allowed for the fluids we consider here. Indeed in modern materials such as graphene, LCD, polarized, a good way to model them it is that they are born to endless forces couples. So in these materials are considered non-symmetric stress tensors.*

The surface forces are due to the pressure as before but also to the stress tensor $\tilde{\sigma}$ that produces a stress in any direction (this because the fluid is viscous). If denote by $\tilde{\tau}$ the viscous stress tensor, than we have

$$\tilde{\sigma} = -p\tilde{I} + \tilde{\tau}$$

Consequently, the second equation of the fluid dynamics becomes

$$\frac{\partial}{\partial t} (\rho \vec{u}) + \nabla \cdot (\rho \vec{u} \otimes \vec{u}) + \nabla p = \rho \vec{F} + \nabla \cdot \tilde{\tau} \qquad (1.16)$$

### 1.1.3   Energy Equation

We consider the total energy $E_{TOT}$ relative to the volume $V$. The first law of thermodynamics tales us that

$$dE_{TOT} = \delta Q + \delta L \tag{1.17}$$

where

- ○ $\delta Q$ is the heat released to $V$ from the external fluid

$$\delta Q = \left(-\int_{\partial V} \vec{q} \cdot \mathbf{n}\, dS\right) dT \tag{1.18}$$

  where $-\vec{q} \cdot \mathbf{n}\, dS$ represents the heat flowing inside $V$ per unit mass of the fluid that crosses the surface $dS$ in the unit of time

- ○ $\delta L$ is the work executed by the external forces on the volume $V$

$$\delta L = \left(\int_V \rho \vec{F} \cdot \vec{u}\, dV - \int_{\partial V} p\mathbf{n} \cdot \vec{u}\, dS\right) dl \tag{1.19}$$

  where to the right hand side, the first term is the work of surface forces, while the second term is the work of body forces.

We denote with $E$ the total energy per unit volume, then the variation of the amount of energy enclosed in a volume $V$ in the unit of time is given by

$$\frac{d}{dt} \int_V E\, dV$$

similarly as already seen for the mass balance we obtain

$$\frac{d}{dt} \int_V E\, dV = \int_V \frac{\partial E}{\partial t}\, dV + \int_{\partial V} E\vec{u} \cdot \mathbf{n}\, dS \tag{1.20}$$

using the Gauss theorem, from (1.18), (1.19) and (1.20) we get

$$\int_V \frac{\partial E}{\partial t}\, dV + \int_V \nabla \cdot (E\vec{u})\, dV = -\int_V \nabla \cdot \vec{q}\, dV + \int_V \rho \vec{F} \cdot \vec{u}\, dV - \int_V \nabla \cdot (p\vec{u})\, dV.$$

This integral is valid for each volume $V$ we are considering, then it can be written as

$$\frac{\partial E}{\partial t} + \nabla \cdot [(E + p)\vec{u}] = \rho \vec{F} \cdot \vec{u} - \nabla \cdot \vec{q}, \tag{1.21}$$

getting the third equation of the fluid dynamics in conservative form.

## 1.2 Euler equations

Now we introduce the Euler equations of gas dynamics for compressible fluids considering that the total energy $E$ is decomposed as

$$E = \mathcal{K} + \mathcal{E}$$

where

- $E$ represents the **internal energy** that characterizes the fluid within the volume $V$

$$E = \rho e$$

- while $\mathcal{K}$ represents the **kinetic energy** associated with the motion of the volume $V$

$$\mathcal{K} = \frac{1}{2}\rho u^2$$

In order to get the Euler equations, we assume that thermal conductivity and viscosity are zero, therefore the heat flucx is zero

$$\vec{q} = 0.$$

We assume that the specific internal energy $e$ is a function of pressure and density

$$e = e(p, \rho). \tag{1.22}$$

Equation (1.22) is called equation of state for the gas. If we consider an ideal gas, then the equation of state becomes a function of temperature $T$

$$e = e(T).$$

In several gases, at normal condition, the relation between $e$ and $T$ can be assumed to be linear:

$$e = c_V T,$$

where $c_V$ is the specific heat at constant volume $V$.

$$c_p = c_V + \mathcal{R} \tag{1.23}$$

where $c_p$ is the specific heat at constant pressure. For polytropic gas we can get an expression for the internal energy which depends by the pressure, in

order to get an equation of state for a polytropic gas. Using Equation (1.23) and denoting by $\gamma = \frac{c_p}{c_V}$ the polytropic gas constant, we have

$$\rho e = \rho \frac{c_v}{\mathcal{R}} \mathcal{R}T = \rho \frac{c_V}{c_p - c_V} \mathcal{R}T = \rho \frac{1}{1-\gamma} \frac{p}{\rho} = \frac{p}{\gamma - 1}.$$

From the equations of fluid dynamics, under these assumptions, we can therefore write the Euler equations of gas dynamics for a polytropic gas as

$$\begin{cases} \dfrac{\partial \rho}{\partial t} + \nabla \cdot (\rho \vec{u}) = 0 \\[2mm] \dfrac{\partial (\rho \vec{u})}{\partial t} + \nabla \cdot (\rho \vec{u} \otimes \vec{u} + p) = 0 \\[2mm] \dfrac{\partial E}{\partial t} + \nabla \cdot [(E + p)\vec{u}] = 0 \end{cases} \tag{1.24}$$

with the following equation of state

$$E = \frac{1}{2}\rho u^2 + \frac{p}{\gamma - 1}. \tag{1.25}$$

## 1.3 Acoustic Waves

The **acoustic waves** are produced in response to oscillations in a medium. In a fluid such oscillations take place in the same direction in which the energy, propagates. The perturbation, are typically longitudinal waves and material waves.

The waves that propagate in a gas can be seen both as *displacement waves* $y(\vec{x}, t)$, in the sense that the medium undergoes oscillations but can be seen as *pressure waves* $p(\vec{x}, t)$ because the oscillations change the gas pressure or *density waves* $\rho(\vec{x}, t)$ as well because the density changes as well.

An important quantity in the propagation of waves in gases is the **coefficient of compressibility**

$$\beta = -V \frac{\partial p}{\partial V},$$

that is a quantity that characterizes the medium that depends also on the thermodynamic properties of the medium.

For small amplitude waves propagating on a constant medium with density $\rho_0$ and compressibility $\beta$, the displacement $y(x,t)$ of one-dimensional waves satisfies the equation

$$\frac{\partial^2 y}{\partial x^2} - \frac{\rho_0}{\beta}\frac{\partial^2 y}{\partial t^2} = 0 \qquad (1.26)$$

whose solutions are

$$y(x,t) = F(x - ut) + G(x + ut)$$

with $u = \sqrt{\beta/\rho_0}$. $F(x - ut)$ is a *progressive wave*, while $G(x + ut)$ is a *regressive wave* and $u$ is the speed of the waves. Instead of $y$ in the (1.26) we can replace the pressure $p$ or the density $\rho$. For istance for the pressure we can write:

$$p = p_0 - \beta\frac{\partial y}{\partial x}$$

where $p_0$ is the equilibrium pressure. Once we know the quantities defined before they are able to know the velocity of acoustic waves $u = \sqrt{\beta/\rho_0}$. The acoustic waves (that is, the materials waves in an elastic medium such as a gas) can be seen at the same time as pressure, displacement or density waves. What we call **sound** is heard at a certain frequency band:
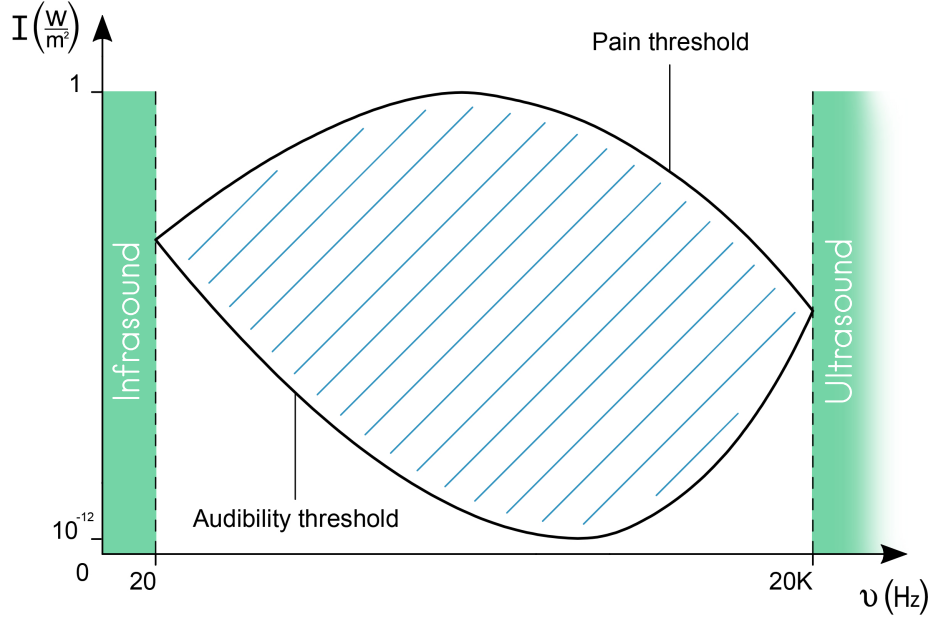
About acoustic waves in a gas. We assume that the gas is ideal. Then the equation of state $pV = n\mathcal{R}T$ is valid. We consider two cases:

1. $pV = K_1$ (isotermal case)

$$p = \frac{K_1}{V} \Rightarrow \frac{\partial p}{\partial V} = -\frac{1}{V^2}K_1 = -\frac{p}{V}$$

    hence

$$\beta_{iso} = -V\left(-\frac{p}{V}\right) = p$$

    then the sound speed will be $v_{iso} = \sqrt{p_0/\rho_0}$

2. $pV^\gamma = K_2$ (adiabatic case)

$$p = \frac{K_2}{V^\gamma} = K_2 V^{-\gamma} \Rightarrow \frac{\partial p}{\partial V} = -\gamma K_2 V^{-\gamma-1} = -\frac{\gamma p}{V}$$

    hence

$$\beta_{adi} = (-V)\left(-\gamma\frac{p}{V}\right) = \gamma p$$

    then the sound speed in this case will be $v_{adi} = \sqrt{\gamma p_0/\rho_0} > v_{iso}$

In most cases the adiabatic approximation is the better one.

Calculating the velocity in the case of the air:

$$\begin{cases} \rho_0 = 1.293 \ Kg/m^3 \\ \gamma = 1.4 \\ T = 0°C \\ p_0 = 1 \ atm = 9.81 \times 10^4 \ N/m^2 \end{cases}$$

The adiabatic velocity $v_{adi} = 326 \ m/s = 3.6 \times 326 \ Km/h = 1173.6 \ Km/h$ that is the velocity of propagation of the acoustic waves in the air. Then if an airplane wants to be supersonic must exceed this velocity. Obviously the line airplanes do not work in these conditions, but they travel at a cruising velocity $\sim 900 \ Km/h$.
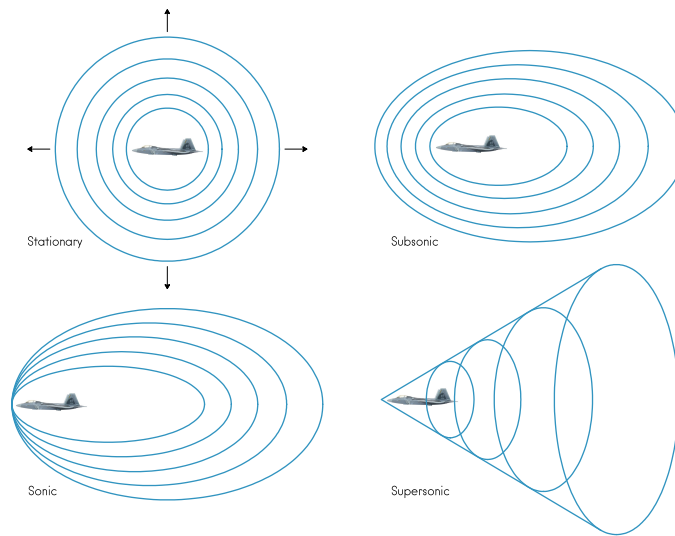


The ratio between the speed of airplane and the speed of sound is called **Mach number**.

$$\mathcal{M} = \frac{u}{c_s}$$

It is a dimensionless number according to which we know whether we are in the compressible or incompressible regime.
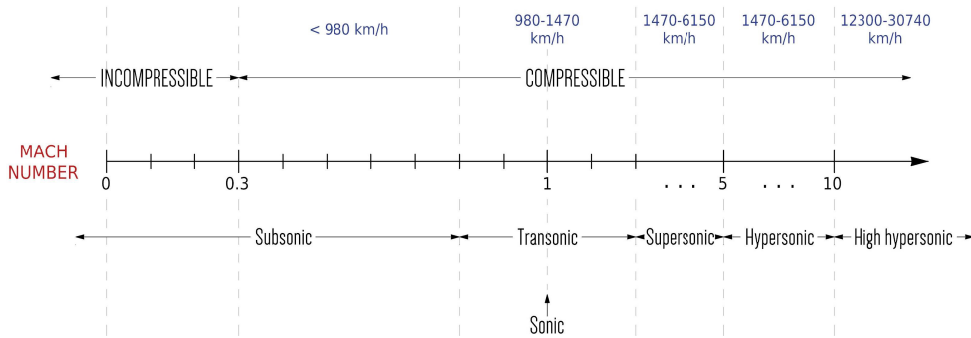
- If $\mathcal{M} << 1$, the flow speed is much lower than the speed of sound - and the fluid is incompressible.

- If $\mathcal{M} < 1$, the flow speed is lower than the speed of sound - and the speed is **subsonic**.

- If $\mathcal{M} \sim 1$, the flow speed is approximately like the speed of sound - and the speed is **transonic**.

- If $\mathcal{M} > 1$, the flow speed is higher than the speed of sound - and the speed is **supersonic**.

- If $\mathcal{M} >> 1$, the flow speed is much higher than the speed of sound - and the speed is **hypersonic**.

Calculating the velocity in the case of the water:

$$\begin{cases} \beta \sim 2.1 \times 10^9 \ N/m^2 \\ \rho_0 = 10^3 \ Kg/m^3 \end{cases}$$

then the velocity is

$$v \simeq 1450 \ m/s \simeq 5220 \ km/h$$

in the water the acoustic waves are essentially longitudinal. The propagation of waves in solids is more complicated, since besides longitudinal waves, transversal as well as surface waves appear. Such waves are carefully studied by seismologists.

# 1.4 AP Property

This thesis presents an asymptotic preserving (AP) all Mach number finite volume method for the numerical solution of compressible Euler equations of gas dynamics (in conservative form). Both isentropic and full Euler equations are considered. The equations are discretized on a staggered grid. This simplifies flux computation and guarantees a natural central discretization in the low Mach limit, thus dramatically reducing the excessive numerical diffusion of upwind discretizations. Furthermore, second order accuracy in space is automatically guaranteed. For the time discretization we adopt a Semi-IMplicit/EXplicit (S-IMEX) discretization, obtaining an elliptic equation for the pressure in the isentropic case and for the energy in the full Euler equations. Such equations can be linearized, so that we do not need any iterative solver and we reduce the computational cost. Second order in time is obtained by a suitable S-IMEX strategy taken from [3]. Moreover, the CFL stability condition is independent of the Mach number and depends essentially on the fluid velocity. Numerical tests are displayed in one and two dimensions to demonstrate performances of our scheme in both compressible and incompressible regimes.

## 1.4.1 Small Mach number

For sake of clarity, we start considering the isentropic gas dynamics case and successively we extend the results to the case of the full Euler system.

**Isentropic Euler Case:**

The isentropic Euler equations in d-dimensions, $x \in \Omega \subset \mathbb{R}^d$, $t \geq 0$, are given by:

$$\begin{cases} \rho_t + \nabla \cdot (\rho \vec{u}) = 0 \\ \\ (\rho \vec{u})_t + \nabla \cdot (\rho \vec{u} \otimes \vec{u}) + \nabla p(\rho)/\varepsilon^2 = 0 \end{cases} \tag{1.27}$$

where $\rho$ is the density of the fluid, $\vec{m} = \rho \vec{u}$ is the momentum of the fluid, and $p(\rho)$ is the pressure. Here we consider a polytropic gas, for which the equation of state takes the form: $p(\rho) = C\rho^\gamma$ where $C$ depends on the entropy (which is assumed to be constant) and $\gamma = c_p/c_V$ is the polytropic constant. Here $\varepsilon$ is the dimensionless reference Much number. As boundary conditions we set $\vec{u} \cdot \mathbf{n} = 0$ on $\partial\Omega$, or assume $\Omega$ is $\mathbb{T}$, i.e. periodic boundary conditions.

Now we recall the classical formal derivation of the incompressible Euler equations from the isentropic compressible Euler system (1.27). We consider

an asymptotic expansion ansatz for the following variables:

$$\begin{aligned}
\rho(x,t) &= \rho_0(x,t) + \varepsilon^2 \rho_2(x,t) + \cdots, \\
p(x,t) &= p_0(x,t) + \varepsilon^2 p_2(x,t) + \cdots, \\
\vec{u}(x,t) &= \vec{u}_0(x,t) + \varepsilon^2 \vec{u}_2(x,t) + \cdots,
\end{aligned} \tag{1.28}$$

we skip the $\mathcal{O}(\varepsilon)$ term because it does not appear in the system Equations (1.27). Inserting (1.28) in (1.27), to $\mathcal{O}(\varepsilon^{-2})$ one gets, in the momentum conservation Equation (3.6):

$$\nabla p_0 = 0.$$

Therefore, $p_0(x,t) = p_0(t)$, and by $p = p(\rho)$, we have $\rho_0 = \rho_0(t)$, i.e. density and pressure are constant in space, with $\rho(x,t) = \rho_0(t) + \varepsilon^2 \rho_2(x,t) + \cdots$.

Next, by taking the $\mathcal{O}(1)$ terms, we have

$$\partial_t \rho_0 + \nabla \cdot (\rho_0 \vec{u}_0) = 0 \tag{1.29}$$

$$\partial_t (\rho_0 \vec{u}_0) + \nabla \cdot (\rho_0 \vec{u}_0 \otimes \vec{u}_0) + \nabla p_2 = 0. \tag{1.30}$$

where

$$p_2 = \lim_{\varepsilon \to 0} \varepsilon^{-2}(p(\rho) - p_0)$$

is the hydrostatic pressure. Now, the incompressibility is forced by using the boundary conditions to solve system (1.27) on the domain $\Omega$ with $\vec{u} \cdot \mathbf{n} = 0$ on $S = \partial\Omega$ or using periodic boundary conditions. Now from $\rho_0 = \rho_0(t)$ one has:

$$\frac{\partial \rho}{\partial t} + \rho_0 \nabla \vec{u}_0 = 0,$$

and

$$\nabla \cdot \vec{u}_0 = -\frac{1}{\rho_0} \frac{d\rho_0}{dt}.$$

Integrating in $\Omega$ one has:

$$-|\Omega| \frac{1}{\rho_0} \frac{d\rho_0}{dt} = \int_\Omega \nabla \cdot \vec{u}_0 d\Omega = \int_{\partial\Omega} \vec{u}_0 \cdot \mathbf{n} dS = 0,$$

because of the boundary conditions, therefore $\rho_0 = Const$ (for details for example see [8, 12]).

This means that the density is also independent of time and then we have: $\rho(x,t) = \rho_0 + \varepsilon^2 \rho_2(x,t) + \cdots$, where $\rho_0$ is a constant of order 1, and then one obtaines $\nabla \cdot \vec{u}_0 = 0$. We finally obtain that, for low Mach number, i.e. $\varepsilon \ll 1$, by considering *well-prepared* initial conditions in the sense:

$$\begin{aligned}
\rho(x,0) &= \rho_0 + \varepsilon^2 \rho_2(x) + \cdots, \\
\nabla \cdot \vec{u}(x,0) &= \vec{u}_0(x) + \mathcal{O}(\varepsilon).
\end{aligned} \tag{1.31}$$

where $|\vec{u_0}|$ is of order 1, such that $\nabla \cdot \vec{u}_0 = 0$, the solution $(\rho, \vec{m})$ with $p = p(\rho)$ of the isentropic Euler system (1.27) will be close to the solution of the the incompressible Euler system,

$$
\begin{aligned}
&\rho_0 = Const, \\
&\nabla \cdot \vec{u}_0 = 0 \\
&\partial_t \vec{u}_0 + (\vec{u}_0 \cdot \nabla)\,\vec{u}_0 + \frac{\nabla p_2}{\rho_0} = 0.
\end{aligned}
\tag{1.32}
$$

We note that, in the low-Mach number model, $p_2$ is the Lagrange multiplier of the divergence free constraint: $\nabla \cdot \vec{u} = 0$. Then, taking the divergence of the last equation and using the incompressibility, one obtains

$$
-\Delta p_2 = \nabla \cdot (\rho_0 \vec{u}_0 \cdot \nabla \vec{u}_0) = \nabla^2 : (\rho_0 \vec{u}_0 \otimes \vec{u}_0).
\tag{1.33}
$$

Furthermore, it is possible to derive the pressure wave equation by (1.27); indeed, if we differentiate with respect the time the density equation and subtract it from the divergence of the momentum equation, we obtain

$$
\partial_{tt}\rho - \frac{\Delta p(\rho)}{\varepsilon^2} = \nabla^2 : (\rho \vec{u} \otimes \vec{u}),
$$

and at the $\mathcal{O}(\varepsilon^0)$, we get (1.33).

**Full Euler Case:**

The rescaled (non-dimensionalised) compressible full Euler equations for an ideal gas in d-dimensions, $x \in \Omega \subset \mathbb{R}^d$, $t \geq 0$, are given by:

$$
\begin{cases}
\rho_t + \nabla \cdot (\rho \vec{u}) = 0 \\[2mm]
(\rho \vec{u})_t + \nabla \cdot (\rho \vec{u} \otimes \vec{u}) + \nabla p / \varepsilon^2 = 0 \\[2mm]
E_t + \nabla \cdot [(E + p)\vec{u}] = 0
\end{cases}
\tag{1.34}
$$

with the (suitably scaled) equation of state:

$$
p = (\gamma - 1)\left(E - \frac{\varepsilon^2}{2}\rho u^2\right)
\tag{1.35}
$$

where $\rho$ is the density of the fluid, $\vec{m} = \rho \vec{u}$ is the momentum of the fluid, $p$ is the pressure and $E$ is the total energy. For simplicity we assume a polytropic

gas with constant $\gamma \geqslant 1$ that is the ratio of the specific heats.

As in the isentropic case, here we provide well prepared initial condition to the low-Much number regime. We assume the following asymptotic expansion:

$$
\begin{aligned}
p(x,t) &= p_0(x,t) + \varepsilon p_1(x,t) + \varepsilon^2 p_2(x,t) + \cdots \\
\vec{u}(x,t) &= \vec{u}_0(x,t) + \varepsilon \vec{u}_1(x,t) + \cdots \\
E(x,t) &= E_0(x,t) + \varepsilon E_1(x,t) + \cdots
\end{aligned}
\tag{1.36}
$$

Inserting (1.36) in the momentum equation in (1.34) and considering terms with $\mathcal{O}(\varepsilon^{-1})$ and $\mathcal{O}(\varepsilon^{-2})$, we formally find that $\nabla p_0 = \nabla p_1 = 0$, thus, the pressure must be constant in space up to order $\varepsilon$, so that from (1.36) we have

$$
p(x,t) = p_0(t) + \varepsilon^2 p_2(x,t) + \cdots
\tag{1.37}
$$

that allows only temporal variations. The expansion in Mach number is also applied to the equation of state, thus from (1.36), $p_0$ is a thermodynamic variable satisfying the equation,

$$
p_0 = (\gamma - 1)E_0
\tag{1.38}
$$

Inserting $\nabla p_0 = \nabla p_1 = 0$ and (1.38) into the energy equation in (1.34), and by taking the $\mathcal{O}(1)$ terms, we get

$$
\begin{cases}
\rho_t + \nabla \cdot (\rho \vec{u}_0) & = 0 \\
(\rho \vec{u}_0)_t + \nabla \cdot (\rho \vec{u}_0 \otimes \vec{u}_0) + \nabla p_2 & = 0 \\
\nabla \cdot \vec{u}_0 = -\dfrac{1}{\gamma p_0(t)} \dfrac{dp_0}{dt}
\end{cases}
\tag{1.39}
$$

We note that if we solve system (1.34) with (1.35) in a domain $\Omega$ with periodic boundary condition we have $\displaystyle\int_\Omega \nabla \cdot u_0 \, dx = 0$, thus by integrating the last equation in (1.39) in $\Omega$ we find that $dp_0/dt = 0$ and this means that the pressure $p_0$ is a constant, i.e., $p_0 := p_* = \text{Const}$. This gives: $\nabla \cdot \vec{u}_0 = 0$. Then for the density equation we obtain

$$
\rho_t + \vec{u}_0 \cdot \nabla \rho = 0,
\tag{1.40}
$$

i.e., the density, in the limit case $\varepsilon = 0$, will be simply advected along the particle paths. Thus, if $\rho$ is constant at the initial time, it should remain constant at any time. Thus by imposing that $\rho(x, t = 0) = \rho_*(x)$, where $\rho_*$

is a strictly positive function such that $\rho_* = \mathcal{O}(1)$, we get that, at low Mach number ($\varepsilon \to 0$), with *well-prepared* initial conditions, i.e.,

$$
\begin{aligned}
\rho(x, t=0) &= \rho_*(x) + \varepsilon^2 \rho_2(x) \\
p(x, t=0) &= p_* + \varepsilon^2 p_2(x) \\
u(x, t=0) &= \hat{u}_0(x) + \mathcal{O}(\varepsilon)
\end{aligned}
\tag{1.41}
$$

with: $\nabla \cdot \hat{u}_0 = 0$, the solution $(\rho, \vec{u}, p)$ of the compressible Euler system (1.34) converges to the solution of the incompressible Euler system

$$
\begin{cases}
\rho_t + \vec{u} \cdot \nabla \rho &= 0 \\
\rho(\vec{u}_t + (\vec{u} \cdot \nabla)\vec{u}) + \nabla p_2 &= 0 \\
\nabla \cdot \vec{u} &= 0 \\
p = (\gamma - 1)E &= p_*
\end{cases}
\tag{1.42}
$$

where

$$
p_2 = \lim_{\varepsilon \to 0} \frac{1}{\varepsilon^2}(p - p_*)
$$

is implicitly defined by the constraint $\nabla \cdot \vec{u} = 0$ and explicitly given by the equation $-\Delta p_2 = \rho_0 \nabla^2 : (\vec{u} \otimes \vec{u})$.

Then in order to prove the asymptotic preserving property of our scheme we consider initial data of the form (1.41). In order to solve (1.34) numerically, the idea is that as $\varepsilon \ll 1$, the first equation becomes less and less relevant, while the total energy is essentially proportional to the pressure. Therefore we write an implicit system using the last two equations, and then compute $\rho^{n+1}$ by post processing.

Now, we rewrite system (1.34) in an equivalent way. We substitute the pressure (1.35) in the equation for the momentum $\vec{m} = (\rho \vec{u})$, with $m = \rho u$, $n = \rho v$ and $\vec{u} = (u, v)$, then we get

$$
\begin{cases}
\rho_t + \nabla \cdot \vec{m} &= 0 \\
\vec{m}_t - (\gamma - 2)\nabla \cdot \left(\dfrac{\vec{m} \otimes \vec{m}}{\rho}\right) + \nabla h + \dfrac{\gamma - 1}{\varepsilon^2}\nabla E &= 0 \\
E_t - \dfrac{\gamma - 1}{2}\varepsilon^2 \nabla \cdot \left(\dfrac{|\vec{m}|^2 \vec{m}}{\rho^2}\right) + \gamma \nabla \cdot \left(E\dfrac{\vec{m}}{\rho}\right) &= 0,
\end{cases}
\tag{1.43}
$$

Now in order to determine the asymptotic behaviour of system (1.43) as $\varepsilon \to 0$, we take the asymptotic ansatz (1.36) and to $\mathcal{O}(\varepsilon^{-2})$ we have

$$
\nabla E_0 = 0 \to E_0(x, t) = E_0(t) \to (\text{by } (1.38)), \quad p_0 = p_0(t),
$$

i.e., the leading order energy (and hence pressure) are constant in space. Using (1.38), from the energy equation in (3.2), we get

$$\nabla \cdot \vec{u}_0 = \frac{1}{\gamma p_0} \frac{dp_0}{dt}. \tag{1.44}$$

and as previously done, with fixed or periodic boundary conditions, we get $\nabla \cdot \vec{u}_0 = 0$ and it follows $p_0 = p_*$.

Now for the equation of the momentum at $\mathcal{O}(1)$ we obtain:

$$\partial_t(\rho_0 \vec{u}_0) - (\gamma - 2)\nabla \cdot (\rho_0 \vec{u}_0 \otimes \vec{u}_0) + \nabla(\rho_0 u_0 v_0) + \frac{(\gamma - 1)}{\varepsilon^2}\nabla E_2 = 0, \tag{1.45}$$

and by (1.37) for the $\mathcal{O}(1)$ order pressure one has

$$p_2 = (\gamma - 1)E_2 - \frac{(\gamma - 1)}{2}(\rho_2 u_0^2),$$

then the $\mathcal{O}(1)$ equations are

$$\begin{cases} \partial_t \rho_0 + \vec{u}_0 \cdot \nabla(\rho_0) &= 0, \\ \partial_t(\rho_0 \vec{u})_0 + \nabla \cdot (\rho_0 \vec{u}_0 \otimes \vec{u}_0) + \nabla p_2 &= 0, \end{cases} \tag{1.46}$$

with $\nabla \cdot \vec{u}_0 = 0$ and $p_0$ constant, i.e. the incompressible Euler Equation (1.42).

Next we propose a numerical scheme that is applicable for all ranges of the Mach number.

# Chapter 2

# Numerical Methods

In this chapter we discretize system (1) by using a central scheme in a *staggered* grid, and in particular we consider the Nessyahu-Tadmor (NT) central scheme in one space dimension [22] and Jiang-Tadmor (JT) central scheme in 2D [15], that is a natural extensions of the first order Lax Friedrichs scheme in order to simplify the treatment of the numerical flux. This approach is extremely simple because it has the advantage of not requiring approximate Riemann solvers which, on the other hand, are essential for the high-resolution upwind schemes.

## 2.1 Central Scheme

This central scheme is obtained integrating the conservation law in space and time on control volumes: $V_{j+\frac{1}{2}}^n = [x_j, x_{j+1}] \times [t^n, t^n + \Delta t]$ which are staggered with respect to the cell on which the cell averages are based. In this faction, the discontinuities in the pointwise solution, produced by the reconstruction algorithm are located at the center of the staggered control volumes. As a consequence, the solution is smooth at the edges of the control volumes, and this guarantees a simple treatment of the numerical fluxes.

### 2.1.1 Nessyahu-Tadmor 1D model

We consider a system of $m$ conservation laws dimensional

$$u_t + f(u)_x = 0, \tag{2.1}$$

where $u \in \mathbb{R}^m$ and $f(u)$ is the flux $m$-vector. We suppose that the Jacobian matrix $A$ of $f$

$$A_{pq}(u) = \left(\frac{\partial f_p}{\partial u_q}\right) \quad p, q = 1, \ldots, m.$$

has real eigenvalues and a complete set of eigenvectors. To evolve in time, from the cell averages $\{\bar{u}^n\}$, it is necessary to perform a reconstruction of $u^n(x)$

$$u^n(x) = \sum_j P_j(x, t)\chi_j(x) \tag{2.2}$$

where the $P_j(x, t)$ is a polynomial of degree 1

$$P_j(x, t) = u_j(t) + u'_j\left(\frac{x - x_j}{\Delta x}\right), \quad x_{j-\frac{1}{2}} \leqslant x < x_{j+\frac{1}{2}} \tag{2.3}$$

$\chi_j(x)$ is the characteristic function of interval $[x_j, x_{j+1}]$, and $u'_j$ is an approximate slope at the grid point $x_j$ and can be approximated

$$u'_j = \left.\frac{\partial u}{\partial x}\right|_{x_j} + \mathcal{O}(\Delta x).$$

Integrating (2.1) on the staggered control volume $V^n_{j+\frac{1}{2}}$
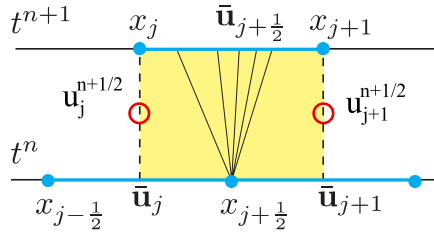


Figure 2.1

where $V^n_{j+\frac{1}{2}} = [x_j, x_{j+1}] \times [t^n, t^n + \Delta t]$ and dividing by $\Delta x$, we find:

$$\bar{u}^{n+1}_{j+\frac{1}{2}} = \bar{u}^n_{j+\frac{1}{2}} - \frac{1}{\Delta x}\left[\int_{t^n}^{t^n+\Delta t} f(u(x_{j+1}, \tau))d\tau - \int_{t^n}^{t^n+\Delta t} f(u(x_j, \tau))d\tau\right]. \tag{2.4}$$

where $\bar{u}^n_{j+\frac{1}{2}}$ is evaluated integrating the reconstruction on $[x_j, x_{j+1}]$

$$\begin{aligned}\bar{u}^n_{j+\frac{1}{2}} &= \frac{1}{\Delta x}\left[\int_{x_j}^{x_{j+\frac{1}{2}}} P_j(x, t)dx + \int_{x_{j+\frac{1}{2}}}^{x_{j+1}} P_{j+1}(x, t)dx\right] = \\ &= \frac{1}{2}(\bar{u}^n_j + \bar{u}^n_{j+1}) - \frac{1}{8}(u'_{j+1} - u'_j).\end{aligned} \tag{2.5}$$

27

The linear integrals of the polynomials $P_j(x,t)$ and $P_{j+1}(x,t)$ can be evaluated exactly, while the integrals on $f(u(x_{j+1}, \tau))$ and $f(u(x_j, \tau))$ of the (2.4), since they are smooth functions of $\tau$ if the time step is small enough, can be evaluated approximately by a quadrature formula such as midpoint rule for example. Thus we have

$$\bar{u}_{j+\frac{1}{2}}^{n+1} = \bar{u}_{j+\frac{1}{2}}^{n} - \frac{\Delta t}{\Delta x}[f(u_{j+1}^{n+\frac{1}{2}}) - f(u_j^{n+\frac{1}{2}})]. \tag{2.6}$$

where by Taylor expansion and the conservation law (2.1)

$$u_j^{n+\frac{1}{2}} = \bar{u}_j^n - \frac{\Delta t}{2\Delta x}f_j'. \tag{2.7}$$

Here $f_j'$ is the numerical derivative of the flux $f(u(x_j, t))$.

$$f_j' = \left.\frac{\partial f}{\partial x}\right|_{x_j} + \mathcal{O}(\Delta x) \tag{2.8}$$

These constraints, given by (2.8), guarantee the **second-order** accuracy of the central difference schemes (2.6).

At the end, just to ensure also that the scheme is "*non-oscillatory*" it is sufficient to use a suitable slope limiter, such as *MinMod* (see for details, [21]) or *UNO* (Uniformly Non Oscillatory, [14]), where the *MinMod* function is defined by

$$MinMod(a,b) = \begin{cases} a & \text{if } |a| < |b| \text{ and } ab > 0 \\ b & \text{if } |b| < |a| \text{ and } ab > 0 \\ 0 & \text{if } ab \leqslant 0 \end{cases} \tag{2.9}$$

$$= \frac{1}{2}(sgn(a) + sgn(b))\min(|a|, |b|).$$

### 2.1.2 Jiang-Tadmor 2D model

We consider the two dimensional system of equations

$$u_t + f(u)_x + g(u)_y = 0 \tag{2.10}$$

with initial data $u(x, y, 0) = u_0(x, y)$. To approximate (2.10) by a central scheme a key point is the reconstruction step. Then starting from

$u^n(x, y) := u(x, y, t^n)$ we compute a piecewise-linear approximation of the form

$$u^n(x, y) = \sum_{pq} \left( \bar{u}^n_{pq} + u'_{pq} \left( \frac{x - x_p}{\Delta x} \right) + u\grave{}_{pq} \left( \frac{y - y_q}{\Delta y} \right) \right) \chi_{pq}(x, y). \qquad (2.11)$$

where here $\bar{u}$ is the approximate cell average at $t = t^n$, associated with the cell $C_{pq} = I_p \times J_q$ centered around $(x_p = p\Delta x, y_q = q\Delta y)$, i.e.,

$$C_{pq} := \left( (\xi, \eta) \,\middle|\, |\xi - x_p| \leq \frac{\Delta x}{2}, |\eta - y_q| \leq \frac{\Delta y}{2} \right).$$

Here, $u'_{pq}$ and $u\grave{}_{pq}$ are discrete slopes in $x$- and $y$-directions, respectively, that are reconstructed from the given cell averages.
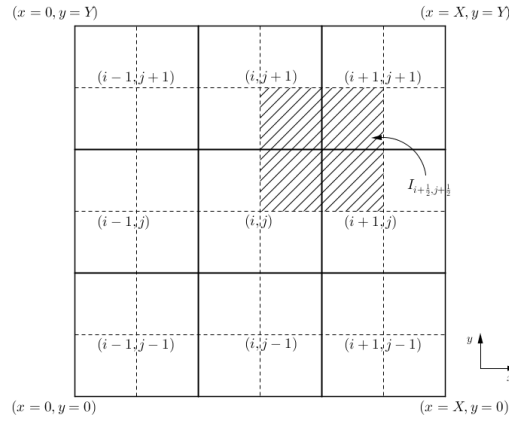


Figure 2.2

System (2.10) is integrated on the staggered control volume:

$C_{i+\frac{1}{2},j+\frac{1}{2}} \times [t^n, t^{n+1})$ with $C_{i+\frac{1}{2},j+\frac{1}{2}} := I_{i+\frac{1}{2}} \times J_{j+\frac{1}{2}}$ centered around $(x_{i+\frac{1}{2}}, y_{j+\frac{1}{2}})$, with $I_{i+\frac{1}{2}} = [x_i, x_{i+1}]$ and $J_{j+\frac{1}{2}} = [y_j, y_{j+1}]$.

Integrating (2.10) in space and time on $C_{i+\frac{1}{2},j+\frac{1}{2}}$, one finds:

$$
\begin{aligned}
\bar{u}^{n+1}_{i+\frac{1}{2},j+\frac{1}{2}} = \bar{u}^n_{i+\frac{1}{2},j+\frac{1}{2}} \quad &- \quad \frac{\Delta t}{\Delta x} \left( \int_{t^n}^{t^{n+1}} \int_{y \in J_{j+\frac{1}{2}}} [f(u(x_{i+1}, y, \tau)) - f(u(x_i, y, \tau))] dy d\tau \right) \\
&- \frac{\Delta t}{\Delta y} \left( \int_{t^n}^{t^{n+1}} \int_{x \in I_{j+\frac{1}{2}}} [g(u(x, y_{i+1}, \tau)) - f(u(x, y_j, \tau))] dx d\tau \right)
\end{aligned}
$$

$(2.12)$

with $\bar{u}^n_{i+\frac{1}{2},j+\frac{1}{2}} = \frac{1}{\Delta x \Delta y} \int_{C_{i+\frac{1}{2},j+\frac{1}{2}}} u(x,y,t^n)dxdy.$

The first term on the right-hand side $\bar{u}^n_{i+\frac{1}{2},j+\frac{1}{2}}$ is evaluated integrating exactly the reconstruction (2.11) on the four intersecting cell $C_{ij}$, $C_{i+1,j}$, $C_{i+1,j+1}$, and $C_{i,j+1}$.

Then, computing the four integrals we find the exact staggered averages of the reconstructed solution at $t = t^n$ (see in details [15]):

$$
\begin{aligned}
\bar{u}_{i+\frac{1}{2},j+\frac{1}{2}} &= \frac{1}{\Delta x \Delta y} \int_{C_{i+\frac{1}{2},j+\frac{1}{2}}} u^n(x,y)dxdy \\
&= \frac{1}{4}(\bar{u}^n_{ij} + \bar{u}^n_{i+1,j} + \bar{u}^n_{i,j+1} + \bar{u}^n_{i+1,j+1}) \\
&+ \frac{1}{16}\left\{(u'_{i,j} - u'_{i+1,j}) + (u'_{i,j+1} - u'_{i+1,j+1})\right. \\
&+ \left.(u^{\backprime}_{ij} - u^{\backprime}_{i,j+1}) + (u^{\backprime}_{i+1,j} - u^{\backprime}_{i+1,j+1})\right\}
\end{aligned}
\tag{2.13}
$$

In order to approximate the four fluxes on the right of (2.12), they are integrated with the midpoint quadrature rule for second order approximation of the temporal integral, and the second-order trapezoidal quadrature rule for the spatial integration across the $x - axis$ and $y - axis$, and the value of $u$ at the midpoint $u^{n+\frac{1}{2}}_{ij} = u(x_i, x_j, t^{n+\frac{1}{2}})$ is predicted with Taylor expansion. Then the scheme has a predictor-corrector structure:

- we start with the cell averages $\bar{u}^n_{ij}$, and we use **the predictor step** for the evaluation of the midpoint values:

$$
u^{n+\frac{1}{2}}_{ij} = \bar{u}^n_{ij} - \frac{\Delta t}{2\Delta x}f(u)'_{ij} - \frac{\Delta t}{2\Delta y}g(u)^{\backprime}_{ij}.
\tag{2.14}
$$

- Then we compute the new cell averages by **the corrector step**:

$$
\begin{aligned}
\bar{u}^{n+1}_{i+\frac{1}{2},j+\frac{1}{2}} = \bar{u}^n_{i+\frac{1}{2},j+\frac{1}{2}} &- \frac{\Delta t}{2\Delta x}\left(f(u^{n+\frac{1}{2}}_{i+1,j}) - f(u^{n+\frac{1}{2}}_{i,j}) + f(u^{n+\frac{1}{2}}_{i+1,j+1}) - f(u^{n+\frac{1}{2}}_{i,j+1})\right) \\
&- \frac{\Delta t}{2\Delta y}\left(g(u^{n+\frac{1}{2}}_{i,j+1}) - g(u^{n+\frac{1}{2}}_{i,j}) + g(u^{n+\frac{1}{2}}_{i+1,j+1}) - g(u^{n+\frac{1}{2}}_{i+1,j})\right).
\end{aligned}
\tag{2.15}
$$

We note that in (2.14)

$$
f'(u)_{ij} \approx f_x(\bar{u}^n(x_i, y_j))\Delta x \quad , \quad g^{\backprime}(u)_{ij} \approx g_y(\bar{u}^n(x_i, y_j))\Delta y
$$

are one dimensional discrete slopes in the $x$- and $y$-directions. For example an approximation of the these space derivatives can be computed by using a suitable slope limiter, such as MinMod (2.9) or UNO (Uniformly Non Oscillatory, [14]).

These two steps produce a second-order accurate non-oscillatory scheme. Of course the non oscillatory behaviour of the scheme depends on the reconstructed discrete slopes $u'$, $u$`, $f(u)'$, and $g(u)$`.

Then, we apply the proposed JT central scheme based on the predictor-corrector steps (2.14)-(2.15) to the two-dimensional Euler Equations (3.18):

$$\frac{\partial}{\partial t}\begin{pmatrix}\rho \\ u \\ v \\ E\end{pmatrix} + \frac{\partial}{\partial x}\begin{pmatrix}\rho u \\ \rho u^2 + \frac{p}{\varepsilon^2} \\ \rho uv \\ u(E+p)\end{pmatrix} + \frac{\partial}{\partial y}\begin{pmatrix}\rho v \\ \rho uv \\ \rho v^2 + \frac{p}{\varepsilon^2} \\ v(E+p)\end{pmatrix} = 0$$

where $\rho$ is the density, $u$ and $v$ are $x$- and $y$-velocities, $E$ the total energy and $p = (\gamma - 1)(E - \varepsilon^2 \rho(u^2 + v^2)/2)$ the pressure.

This scheme guarantees a simple and robust space discretization and, in particular, simplifies flux computation and guarantees a natural central discretization in the low Mach limit, thus dramatically reducing the excessive numerical diffusion of the classical upwind discretizations. Furthermore second order in space is automatically guaranteed.

## 2.2   S-IMEX R-K scheme

Two systems are considered, isentropic and complete Euler systems. Two implicit strategies are tested: one resulting in a non-linear system solved by Newton's iteration, and the other one is obtained by linearization.

The semi-implicit approach uses explicit-implicit Runge-Kutta methods (IMEX R-K) and the proposed schemes result stable, linearly implicit, and can be designed up to *any order of accuracy.*

Furthermore, a great advantage of the semi-implicit approach for computing the numerical solution for isentropic or full Euler equations is that we do not require solutions of nonlinear system that usually one has when try to solve implicitly the pressure term (stiff term) in the system (1.34).

Let us consider an autonomous system of the form

$$\frac{d\mathbf{U}}{dt} = \mathcal{H}(\mathbf{U}^*, \mathbf{U}). \tag{2.16}$$

with $\mathcal{H} : \mathbb{R}^m \times \mathbb{R}^m \to \mathbb{R}^m$ is supposed to be sufficiently differentiable. Suppose that the dependence on the first argument of $\mathcal{H}$ is non-stiff, while that on the second argument is stiff.

Such a system can be rewritten in the partitioned form [13]:

$$\frac{\partial \mathbf{U}^*}{\partial t} = \mathcal{H}(\mathbf{U}^*, \mathbf{U}), \quad \frac{\partial \mathbf{U}}{\partial t} = \mathcal{H}(\mathbf{U}^*, \mathbf{U}) \tag{2.17}$$

with $\mathbf{U}^*(t_0) = \mathbf{U}(t_0) = \mathbf{U_0}$. Then a natural way to discretize in time this system is to treat the variable $\mathbf{U}$ implicitly while the variable $\mathbf{U}^*$ explicitly. Implicit-explicit (IMEX) Runge-Kutta (RK) methods are suitable for the solution of this kind of problems.

Usually IMEX RK scheme can be represented by a pair Butcher tables given by:

$$\begin{array}{c|c} \tilde{c} & \tilde{A} \\ \hline & \tilde{b}^T \end{array}, \quad \begin{array}{c|c} c & A \\ \hline & b^T \end{array}$$

where the $s \times s$ low triangular matrices $\tilde{A} = (\tilde{a}_{ij})$ $(\tilde{a}_{ij} = 0$ for all $j \geq i)$, and $A = (a_{ij})$ $(a_{ij} = 0$ for all $j > i)$ are the matrices of the explicit and implicit parts of the scheme, respectively, while the vectors $\tilde{b} = (\tilde{b}_1, \cdots, \tilde{b}_s)$, $b = (b_1, \cdots, b_s)$, $\tilde{c} = (\tilde{c}_1, \cdots, \tilde{c}_s)$, and $c = (c_1, \cdots, c_s)$, are $s$-dimensional vectors or real coefficients, which $\tilde{c}$ and $c$ given by the usual relations

$$\tilde{c}_i = \sum_{j=1}^{i-1} \tilde{a}_{ij}, \quad c_i = \sum_{j=1}^{i} a_{ij}, \quad i = 1, \cdots, s.$$

Then a semi-implicit Runge-Kutta method applied to (2.16) is implemented as follows, (see [3] for details). First we set $\overline{\mathbf{U}}_1 = \mathbf{U}_1^* = \mathbf{U}^n$. Then we compute the stage values:

$$\mathbf{U}_i^* = \mathbf{U}^n + \Delta t \sum_{j=1}^{i-1} \tilde{a}_{ij} \mathbf{K}_j, \qquad \overline{\mathbf{U}}_i = \mathbf{U}^n + \Delta t \sum_{j=1}^{i-1} a_{ij} \mathbf{K}_j, \tag{2.18}$$

for $2 \leq i \leq s$, and the stage fluxes

$$\mathbf{K}_i = \mathcal{H}(\mathbf{U}_i^*, \overline{\mathbf{U}}_i + \Delta t a_{ii} \mathbf{K}_i), \quad 1 \leq i \leq s \tag{2.19}$$

and finally update the numerical solution by

$$\mathbf{U}^{*,n+1} = \mathbf{U}^{*,n} + \Delta t \sum_{i=1}^{s} \tilde{b}_i K_i, \quad \mathbf{U}^{n+1} = \mathbf{U}^n + \Delta t \sum_{i=1}^{s} b_i K_i. \tag{2.20}$$

Now, we give an important property for our scheme, the *globally stiffly accurate* property, [4, 5].

**Definition.** *We say that an IMEX R-K scheme satisfies the **globally stiffly accurate** (GSA) property if $b^T = e_s^T A$ and $\tilde{b}^T = e_s^T \tilde{A}$, with $e_s = (0, \ldots, 0, 1)^T$, and $c_s = \tilde{c}_s = 1$, i.e. the numerical solution is identical to the last internal stage value of the scheme.*

In our numerical tests, we consider some GSA IMEX R-K scheme, just presented in the literature. Below we give as example the Butcher tables of two GSA IMEX schemes.

- Fist order Euler IMEX scheme [1]:

$$
\begin{array}{c|cc}
0 & 0 & 0 \\
1 & 1 & 0 \\
\hline
 & 1 & 0
\end{array}
\qquad
\begin{array}{c|cc}
0 & 0 & 0 \\
1 & 0 & 1 \\
\hline
 & 0 & 1
\end{array}
\tag{2.21}
$$

- Second order IMEX R-K scheme, [1]:

$$
\begin{array}{c|ccc}
0 & 0 & 0 & 0 \\
\gamma & \gamma & 0 & 0 \\
1 & \delta & 1-\delta & 0 \\
\hline
 & \delta & 1-\delta & 0
\end{array}
\qquad
\begin{array}{c|ccc}
0 & 0 & 0 & 0 \\
\gamma & 0 & \gamma & 0 \\
1 & 0 & 1-\gamma & \gamma \\
\hline
 & 0 & 1-\gamma & \gamma
\end{array}
\tag{2.22}
$$

  with $\delta = 1 - 1/(2\gamma)$ and we chose $\gamma > 1/2$.

- Second order IMEX R-K scheme with $a_{11} = 0$:

$$
\begin{array}{c|ccc}
0 & 0 & 0 & 0 \\
c & c & 0 & 0 \\
1 & 1-1/(2c) & 1/(2c) & 0 \\
\hline
 & 1-1/(2c) & 1/(2c) & 0
\end{array}
\qquad
\begin{array}{c|ccc}
0 & 0 & 0 & 0 \\
c & c-a_{22} & a_{22} & 0 \\
1 & 1-b_2-\gamma & b_2 & \gamma \\
\hline
 & 1-b_2-\gamma & b_2 & \gamma
\end{array}
\tag{2.23}
$$

  where $c = 2.1$, $\gamma = (1/2)(2c-1)/(-1+c)$, $b_2 = (1/2-\gamma)/c$ and $a_{22} = c$.

**Remark 8.** *We note that the NT central scheme is already second order in space. Then in order to make it second order in time we proceed as follows. First we compute the semi-implicit predictor (non necessarily conservative) at location $(x_j, t^{n+\frac{1}{2}})$ for the evaluation of $u_j^{n+\frac{1}{2}}$, and finally we compute a conservative correction for $\bar{u}_{j+\frac{1}{2}}^{n+1}$ (see figure 2.1).*

This technique can in principle be extended to a $s$-stage Runge-Kutta methods. Indeed, first we compute a semi-implicit predictor at location $(x_j, t^n + c_i \Delta t)$ for the (non conservative) stage values $\mathbf{U_i}$, $i = 1, \ldots, s-1$, and next we evaluate a conservative correction for the numerical solution $\bar{u}_{j+\frac{1}{2}}^{n+1}$.

# Chapter 3

# FV Scheme: 1D problem

In this thesis, an all speed method that is second order in both space and time is developed. Here the word "all speed" indicates that the scheme is applicable for all Mach numbers, ranging from very small to order one values, and its stability and accuracy are independent of $\varepsilon$.

The design of an "all speed" scheme is mainly a mathematical and numerical issue. Though isentropic flows occur only when the changes of flow variables are small and gradual, numerically the equations themselves carry similar mathematical difficulties and properties as the full Euler system. They are able to treat both finite and small Mach number regimes, exhibit shocks involved when the Mach number is not too small and possess the incompressible limit.

## 3.1  Isentropic Case

We start using this simplified model to explain and test the basic ideas, both to slow AP property and for second order convergence, even at the price of a less physically realistic description. This framework is not restricted to the isentropic Euler equations. Its extension to the full Navier-Stokes equations for practical simulations is on going. Mathematically the basic ideas of scheme designing for achieving AP and second-order properties are similar, but they involves more equations and complexity.

### 3.1.1   Structure of the system

The isentropic Euler equations in general spatial dimension are given by

$$
\begin{cases}
\rho_t + \nabla \cdot (\rho \vec{u}) = 0, \\
(\rho \vec{u})_t + \nabla \cdot (\rho \vec{u} \otimes \vec{u}) + \nabla p(\rho) = 0.
\end{cases}
\tag{3.1}
$$

For standard applications, the **equation of state** takes the form

$$
p = p_0 \left( \frac{\rho}{\rho_0} \right)^{\gamma},
$$

where $\rho$ is the density of the fluid, $\vec{m} = \rho \vec{u}$ is the momentum of the fluid, $p(\rho)$ is the pressure. Typically air is composed of $N_2$ and $O_2$, which gives $\gamma = 1.4$.

To describe the low Mach number (incompressible) limit, we rescale the variables in the following way. Let $x_0$, $t_0$, $\rho_0$, $p_0$, $u_0$ be a set of characteristic scales for the variables in the equations. Inserting these into the equations, we get the nondimensionalized equations

$$
\begin{cases}
\dfrac{\rho_0}{t_0} \tilde{\rho}_{\tilde{t}} + \dfrac{\rho_0 u_0}{x_0} \nabla_{\tilde{x}} \cdot (\tilde{\rho} \tilde{\vec{u}}) = 0, \\[2mm]
\dfrac{\rho_0 u_0}{t_0} (\tilde{\rho} \tilde{\vec{u}})_{\tilde{t}} + \dfrac{u_0^2 \rho_0}{x_0} \nabla_{\tilde{x}} \cdot (\tilde{\rho} \tilde{\vec{u}} \otimes \tilde{\vec{u}}) + \dfrac{p_0}{x_0} \nabla \tilde{p} = 0, \\[2mm]
\tilde{p} = \tilde{\rho}^{\gamma}.
\end{cases}
\tag{3.2}
$$

Note that $u_0 = x_0/t_0$, we have

$$
\begin{cases}
\rho_t + \nabla \cdot (\rho \vec{u}) = 0, \\[2mm]
(\rho \vec{u})_t + \nabla \cdot (\rho \vec{u} \otimes \vec{u}) + \dfrac{p_0}{\rho_0 u_0^2} \nabla p = 0, \\[2mm]
p(\rho) = \rho^{\gamma},
\end{cases}
\tag{3.3}
$$

where we removed the $\sim$ on the dimensionless variables. What remains to be determined is the term in front of the pressure. Since unperturbed speed of sound is given by $c_0^2 = \gamma p_0/\rho_0$, one defines the parameter $\varepsilon$ as $\varepsilon^2 = \rho_0 u_0^2/p_0 = \gamma \mathcal{M}^2$ where $\mathcal{M} = u_0/c_0$ is the Mach number. The nondimensionalized equations then take the form

$$\begin{cases} \rho_t + \nabla \cdot (\rho \vec{u}) = 0, \\[2mm] (\rho \vec{u})_t + \nabla \cdot (\rho \vec{u} \otimes \vec{u}) + \nabla p(\rho)/\varepsilon^2 = 0, \\[2mm] p(\rho) = \rho^\gamma. \end{cases} \tag{3.4}$$

This is one of the most studied nonlinear hyperbolic systems. It is rigorously proved by Klainerman and Majda [18, 19] that when $\varepsilon \to 0$, i.e., when the fluid velocity is small compared with the speed of sound, the solution of (3.4) converges to its incompressible counterpart.

## 3.1.2   Discretization

Next we propose a numerical scheme that is applicable for all ranges of the Mach numbers.

For simplicity, we consider the domain $\Omega = [0, 1]$, we use a uniform spatial mesh with $\Delta x = 1/N$, where $N$ is an positive integer and the grid points are defined as $x_j = j\Delta x$, $j = 0, 1, \cdots, N$. Here $\rho$, $u$ and $m = \rho u$ denote respectively the density, the velocity and the momentum of the gas in one dimension. Then (3.4) becomes

$$\rho_t + m_x = 0$$

$$m_t + \left( \frac{m^2}{\rho} + \frac{p}{\varepsilon^2} \right)_x = 0 \tag{3.5}$$

The system is closed by $p = \rho^\gamma$. We shall discretize space in a way similar to the NT central scheme (see [22]), while we discretize time by a first order semi-implicit Euler (2.21): stiff terms will be evaluated at time $t^{n+1}$, while non-stiff terms will be evaluated at time $t^n$.

Then integrating the equation on a staggered grid, from time $t^n = n\Delta t$, (see Figure 3.1) we obtain the first order semi-implicit scheme:
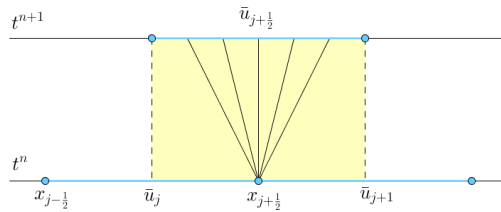


Figure 3.1: Staggered grid form $t^n$ to $t^{n+1}$.

$$\overline{\rho}_{j+\frac{1}{2}}^{n+1} = \overline{\rho}_{j+\frac{1}{2}}^n - \frac{\Delta t}{\Delta x}(m_{j+1}^{n+1} - m_j^{n+1})$$

$$\overline{m}_{j+1/2}^{n+1} = \overline{m}_{j+1/2}^n - \frac{\Delta t}{\Delta x}(f_{j+1}^n - f_j^n) - \frac{\Delta t}{\varepsilon^2 \Delta x}(p_{j+1}^{n+1} - p_j^{n+1})$$

(3.6)

where $f_j^n = (\overline{m}_j^n)^2/\overline{\rho}_j^n$. We note that second order in space is obtained by standard reconstruction adopted in Nessyahu-Tadmor scheme (see for details [22]), es.

$$\overline{\rho}_{j+\frac{1}{2}} = \frac{1}{2}(\overline{\rho}_j + \overline{\rho}_{j+1}) - \frac{1}{8}(\rho'_{j+1} - \rho'_j)$$

with $\rho'_j$ a first order approximation of the first derivative on cell $j$, we use *MinMod* slope limiter in most cases (2.9).

A similar equation can be written for $m_j^{n+1}$:

$$m_j^{n+1} = m_j^n - \frac{\Delta t}{\Delta x}\mathcal{D}_x f_j^n - \frac{\Delta t}{\varepsilon^2 \Delta x}\mathcal{D}_x p_j^{n+1}$$

with $\mathcal{D}_x f_j^n = (f_{j+\frac{1}{2}}^n - f_{j-\frac{1}{2}}^n)$ and $\mathcal{D}_x p_j^{n+1} = (p_{j+\frac{1}{2}}^{n+1} - p_{j-\frac{1}{2}}^{n+1})$.

Using such equation, and substituting it into the density equation for $\overline{\rho}_{j+\frac{1}{2}}^{n+1}$ one gets an equation of the form:

$$\overline{\rho}_{j+\frac{1}{2}}^{n+1} - \frac{\Delta t^2}{\varepsilon^2 \Delta x^2}\mathcal{D}_x^2 p_{j+\frac{1}{2}}^{n+1} = \phi_{j+\frac{1}{2}}^n$$

(3.7)

which is an elliptic equation with

$$\phi_{j+\frac{1}{2}}^n = \overline{\rho}_{j+\frac{1}{2}}^n - \frac{\Delta t}{\Delta x}\mathcal{D}_x m_{j+\frac{1}{2}}^n + \frac{\Delta t^2}{\Delta x^2}\mathcal{D}_x^2 f_{j+\frac{1}{2}}^n$$

that denotes quantities that can be computed explicitly (in a conservative way), where $\forall h$,

$$\mathcal{D}_x^2 h_j \equiv h_{j+1} - 2h_j + h_{j-1}.$$

To obtain $\overline{\rho}_{j+\frac{1}{2}}^{n+1}$ in (3.7), where $p_{j+1/2}^{n+1} = (\overline{\rho}_{j+\frac{1}{2}}^{n+1})^\gamma$, a nonlinear system of equations needs to be solved. There are two possibilities:

1. **Non-linear approach**: One possible way to simplify it is to use $p$ as unknown and considering $\rho = \rho(p)$, then we get $\overline{\rho}_{j+\frac{1}{2}}^{n+1} = (p_{j+1/2}^{n+1})^{1/\gamma}$. In this case the nonlinearity is in the diagonal of the system, and we get a non linear equation that has to be solved for each time step for the unknown $\overline{\rho}_{j+\frac{1}{2}}^{n+1}$. For example if we use Newton's method we need few iterations.

2. **Linearized approach**: On the other hand, if we approximate the Laplace operator $(p^{n+1})_{xx}$ discretized in (3.7) by the approximation

$$\frac{\partial^2}{\partial x^2}\left(p(\rho^{n+1})\right) \approx \frac{\partial}{\partial x}\left(p'(\rho^n)\rho_x^{n+1}\right)$$

a semi-implicit approach is obtained and then this implies to solve a linear system in (3.7). Then $\overline{m}_{j+1/2}^{n+1}$ are computed, from the second equation of (3.6).

### 3.1.3 Asymptotic Preserving Property

Now we show that the scheme (3.6) is asymptotic preserving. In order to show that the scheme (3.6) satisfies the AP property for the original model (3.4), we should demonstrate that such a scheme (3.6) applied to (3.4) is AP if in the low Mach number limit, i.e. as $\varepsilon \to 0$, such scheme provides a consistent discretization of the incompressible Euler equation, (1.32) with spatial and temporal steps fixed.

To investigate the AP property, we consider 1D problem (3.6). We note that in one dimension with periodic boundary conditions, the solution of (1.32) is such that $\rho_0$ and $m_0$ are constants in both space and time. Then we prove the AP property by considering the asymptotic expansions:

$$\begin{aligned}
\rho_j^n &= \rho_{0,j}^n + \varepsilon^2 \rho_{2,j}^n + \cdots, \\
m_j^n &= (\rho u)_j^n = (\rho u)_{0,j}^n + \varepsilon^2 (\rho u)_{2,j}^n + \cdots.
\end{aligned} \tag{3.8}$$

By replacing the following expansion into (3.6), to the $\mathcal{O}(\varepsilon^{-2})$ term, we have

$$\frac{\Delta t}{\Delta x}(p_{0,j+1}^{n+1} - p_{0,j}^{n+1}) = 0.$$

Relation $p(\rho) = \rho^\gamma$, implies $\rho_{0,j+1}^{n+1} = \rho_{0,j}^{n+1}$ for all $j$, and this means that the density is constant in space and it is consistent with the initial condition (1.31) where $\rho_0$ is a quantity independent of space, then we get: $\rho_{0,j}^{n+1} = \rho_0^{n+1}$ for all $j$, then it is constant in space but not necessarily in time. Now considering here periodic boundary conditions, summing the first equation in (3.6) over all the grid points $j$, and by the fact that $\rho_{0,j}^{n+1} = \rho_0^{n+1}$ for all $j$, we get

$$\overline{\rho}_0^{n+1} = \frac{1}{N} \sum_j \overline{\rho}_{0,j+\frac{1}{2}}^n, \tag{3.9}$$

where $N$ is the total number of the grid points, this means that the density in the new step is constant and it is equal to the average value of the density to the previous time step. Furthermore, as the leading order term $\rho_{0,j}^n$ of the density in the previous time step is constant in space, so this says that the quantities in (3.9) coincide, then the density is also constant in time, as in the continuous case, i.e,

$$\overline{\rho}_{0,j+\frac{1}{2}}^{n+1} = \overline{\rho}_{0,j+\frac{1}{2}}^{n} = \overline{\rho}_0^n = \rho_0. \tag{3.10}$$

Furthermore, from (3.6), the $\mathcal{O}(1)$ equation for the density is given by

$$\overline{\rho}_{0,j+\frac{1}{2}}^{n+1} = \overline{\rho}_{0,j+\frac{1}{2}}^{n} - \frac{\Delta t}{\Delta x}(m_{0,j+1}^{n+1} - m_{0,j}^{n+1})$$

and using (3.10), we cancel the density terms so to get

$$\rho_0 \frac{\Delta t}{\Delta x}(u_{0,j+1}^{n+1} - u_{0,j}^{n+1}) = 0. \tag{3.11}$$

We note that in 1D, $\nabla \cdot u_0(x) = 0$ is equivalent to $u_0(x) = Const$, and from (3.8) this means that $m_{0,j}^n = (\rho_0 u_0)_{0,j}^n$ is a constant in space. Then by (3.11), we get $u_{0,j+1}^{n+1} = u_{0,j}^{n+1}$ for all $j$, i.e., the $\mathcal{O}(1)$ term of the velocity $(u_0^{n+1})$ is also constant in space. Then we obtain the discrete incompressibility condition for the velocity $u_0^{n+1}$.

Finally, by (3.7) and using that $\rho_0^n$, $m_0^n$ are constants and $\overline{\rho}_{0,j+\frac{1}{2}}^{n+1} = \overline{\rho}_{0,j+\frac{1}{2}}^{n}$, we get $\frac{\Delta t}{\Delta x}\mathcal{D}_x m_{j+\frac{1}{2}}^n + \frac{\Delta t^2}{\Delta x^2}\mathcal{D}_x^2 f_{j+\frac{1}{2}}^n = 0$, then the $\mathcal{O}(1)$ term of (3.7) is:

$$p_{2,j+\frac{3}{2}}^{n+1} - 2p_{2,j+\frac{1}{2}}^{n+1} + p_{2,j-\frac{1}{2}}^{n+1} = 0,$$

or

$$p_{2,j+\frac{3}{2}}^{n+1} - p_{2,j+\frac{1}{2}}^{n+1} = p_{2,j+\frac{1}{2}}^{n+1} - p_{2,j-\frac{1}{2}}^{n+1}$$

for all $j$, then by the periodic boundary condition we get $p_{2,j+\frac{1}{2}}^{n+1} = p_2^{n+1}$, and then $\rho_2^{n+1}$ is independent of space. Now replacing (3.8) into the momentum equation in (3.6) and equate the $\mathcal{O}(1)$ terms in the momentum equation, we have:

$$m_{0,j+\frac{1}{2}}^{n+1} = m_{0,j+\frac{1}{2}}^{n} = m_0^n, \tag{3.12}$$

Then, by the periodic boundary conditions, when $\varepsilon \to 0$, the scheme (3.6) relaxes to (3.10) and (3.12), i.e., a consistent discretization of (1.32) in one space dimension. Then the scheme here proposed is AP.

## 3.2 Numerical Tests

In this section we present the performances of the proposed globally first and second IMEX(R-K)-NT scheme. We test our new schemes presenting several numerical test cases in one and two space dimensions and show that the schemes are accurate for a wide range of values of Mach numbers. The schemes run for different value of the parameter $\varepsilon$ ranging from compressible to incompressible flows. For all the numerical tests we give well prepared initial and boundary conditions. Finally several convergence tests allow to observe the correct second order accuracy of our scheme both in compressible and incompressible regimes.

**Note:** In all our tests, we used a second order reconstruction in space, based on the following $\theta$-limiters, with $\theta = 1.5$, (see for example [15])

$$U_i' = MinMod\left(\theta\frac{U_i - U_{i-1}}{\Delta x}, \frac{U_{i+1} - U_{i-1}}{2\Delta x}, \theta\frac{U_{i+1} - U_i}{\Delta x}\right)$$

### 3.2.1 Example 1: Riemann problem

We consider the following initial data, [9]

$$\begin{cases} \rho(x,0) = 1.0, & m(x,0) = 1 - \frac{\varepsilon^2}{2}, & x \in [0, 0.2]\bigcup[0.8, 1], \\ \rho(x,0) = 1 + \varepsilon^2, & m(x,0) = 1, & x \in (0.2, 0.3], \\ \rho(x,0) = 1, & m(x,0) = 1 + \frac{\varepsilon^2}{2}, & x \in (0.3, 0.7], \\ \rho(x,0) = 1 - \varepsilon^2, & m(x,0) = 1, & x \in (0.7, 0.8], \end{cases} \tag{3.13}$$

This example consists of several Riemann problems. We choose $p(\rho) = \rho^2$, final time $T = 0.05$ and periodic boundary conditions.
In Figure 3.2 we report the solutions for the density on the left and for the momentum on the right. In this example we choose $\varepsilon = 0.8$, 0.3, 0.05 and $\varepsilon = 10^{-4}$. We note that for large $\varepsilon$, shocks and contact discontinuities appear. Here we choose the same values of $\Delta t$ as in [9], in order to make the schemes stable. A reference solution is also computed with $\Delta x = 1/500$, and $\Delta t = 1/20000$. We note that we determine $\Delta t$ by the formula:

$$\Delta t = CFL_{Imp}\frac{\Delta x}{\max|u| + c_s} \tag{3.14}$$

with $c_s = \sqrt{\gamma p/\rho}$. The value of $CFL_{Imp}$ are shown. Note that this is not the classical CFL number that one has to adopt for explicit schemes. Indeed, for

explicit schemes one has to choose

$$\Delta t = CFL_{Exp} \frac{\Delta x}{\max |u| + c_s/\varepsilon},$$

with $CFL_{Exp} < 1$. The equivalent $CFL$ considering to the time step that we adopt is

$$CFL = CFL_{Imp} \frac{\max |u| + c_s/\varepsilon}{\max |u| + c_s}$$
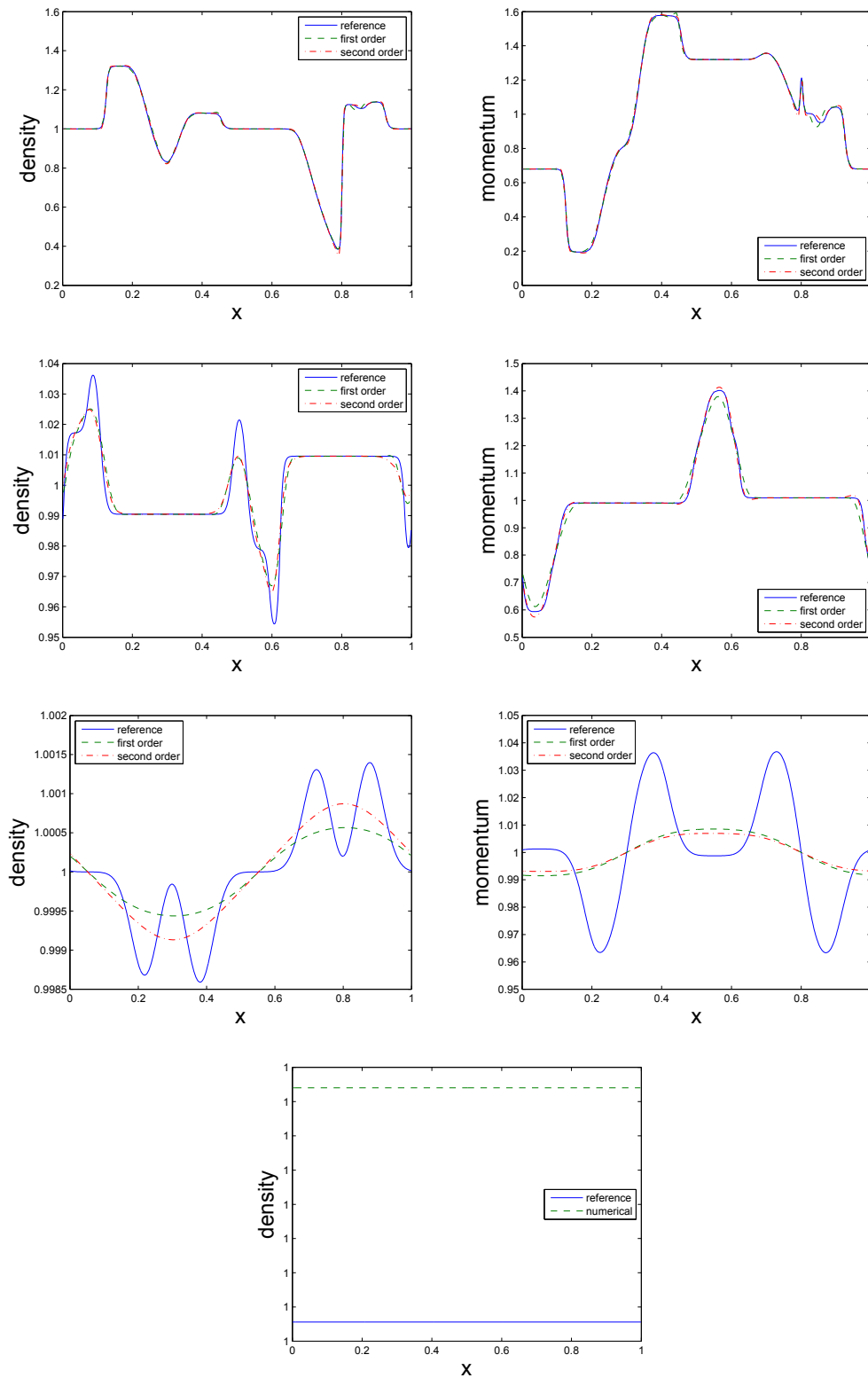
and it is reported in the figures.

Figure 3.2: Numerical results of the Riemann problem at final time $T = 0.05$ with $\Delta x = 1/200$, $\Delta t = 1/2000$, for the density (left) and momentum (right) for the isentropic Euler equations, when $\varepsilon = 0.8$, $0.3$ and $0.05$, while when $\varepsilon = 10^{-4}$ we desplay the density that is constant. The solid line is the reference solution calculated with $\Delta x = 1/500$ and $\Delta t = 1/20000$. We have three different lines:"—","- -","· - ·" that rapresent respectively the reference solution, the first order and the second order of accuracy of the numerical solution.

We observe that our scheme is able to reproduce the same results of the reference solution at different values of the parameter $\varepsilon$. In the case when the Mach number is small $\varepsilon = 0.05$, which gives $\varepsilon^2 = 2.5 \times 10^{-3}$, the scheme projects the solution to the limit incompressible solution faster than an explicit scheme. The aim of our scheme, is to avoid to capture the microstructures (acoustic waves) of the solution, and to get the solution, when $\varepsilon$ becomes small, at reasonable cost and using an unresolved mesh.

### 3.2.2  Example 2: Convergence test

Here we verify the temporal and spatial order of accuracy of the scheme in compressible and incompressible regimes in one dimension. In order to do that we consider the Equations (3.5), taking as computational domain $\Omega = [-2.5, 2.5]$ with initial conditions

$$u_0 = \sin\left(\frac{2\pi x}{L}\right), \quad \rho_0 = \left(1 + \frac{(\gamma - 1)u_0}{2c}\right)^{\frac{2}{\gamma - 1}}, \quad p_0 = \rho_0^{\gamma}$$

where $\gamma = 2$, $c = \frac{1}{\varepsilon}\sqrt{\gamma}$, $L = 5$ and final time $T = 0.3$.

To verify the order, we perform several run at various $\Delta x$, and $\Delta t$ is given by (3.14) with CFL $= 0.45$. We start with $\Delta x = 1/10$ and refine the grid in the simulations starting with $N = 10$ and doubling up it to $N = 2560$. The results for the density for different values of the Mach numbers are listed in Table below. We obtain similar results for velocity and pressure. In the following table, since we used a staggered grid, we compute the experimental order of convergence (EOC) by the formula (3.15) considering the $L^1$ norm of the relative error between the numerical solution at $N$ grid points and the numerical solution at $2N$ grid points. Then, denoting $U$ the numerical solution, in the table, we report the quantities

$$EOC := log_2\left(\frac{e_N}{e_{2N}}\right) \tag{3.15}$$

with

$$e_N = \frac{\left\|U(N) - \overline{U}(N)\right\|_{L^1}}{\left\|\overline{U}(N)\right\|_{L^1}}$$

where the components of the vector $\overline{U}(N)$ are computed as follows

$$\overline{U}_i(N) = \frac{U_{2i-1}(2N) + U_{2i}(2N)}{2}.$$

The results show second-order convergence for large values of $\varepsilon = 1, 0.3$ and small one $\varepsilon = 0.05$, as expected. We can get similar results for the other variables, namely, for the velocity and pressure of the fluid.

| Density error with CFL = 0.45 and T = 0.3 | | | | | |
|---|---|---|---|---|---|
| | $\varepsilon = 0.8$ | | $\varepsilon = 0.3$ | | $\varepsilon = 0.05$ |
| N | $L^1$ error | $L^1$ order | $L^1$ error | $L^1$ order | $L^1$ error | $L^1$ order |
| 10 | 1.123e-02 | – | 1.209e-02 | – | 1.416e-04 | – |
| 20 | 1.985e-03 | 2.4994 | 6.837e-03 | 0.8227 | 2.110e-04 | -0.5757 |
| 40 | 9.634e-04 | 1.0433 | 2.690e-03 | 1.3460 | 1.282e-03 | -2.6035 |
| 80 | 2.241e-04 | 2.1040 | 8.552e-04 | 1.6530 | 6.219e-03 | -2.2782 |
| 160 | 5.561e-05 | 2.0106 | 2.373e-04 | 1.8494 | 4.551e-03 | 0.4507 |
| 320 | 1.353e-05 | 2.0397 | 6.023e-05 | 1.9783 | 1.597e-03 | 1.5111 |
| 640 | 3.269e-06 | 2.0489 | 1.509e-05 | 1.9971 | 4.993e-04 | 1.6771 |
| 1280 | 7.868e-07 | 2.0547 | 3.774e-06 | 1.9993 | 1.358e-04 | 1.8789 |
| 2560 | 1.898e-07 | 2.0517 | 9.420e-07 | 2.0023 | 3.405e-05 | 1.9951 |

We observe that because of the acoustic waves, when the Mach number $\varepsilon$ goes to zero, in order to get the second order of accuracy, we need to refine the grid.

### 3.2.3   Example 3: Two collision acoustic waves:

Consider the evolution of two collision acoustic waves, with the following well prepared initial data (see fig. 3.3), i.e. when $\varepsilon$ goes to 0, the density and momentum are consistent with the incompressible limit:

$$p(\rho_\varepsilon) = \rho_\varepsilon^\gamma, \quad \text{for} \quad x \in [-1, 1], \quad \text{with} \ \gamma = 1.4$$
$$\rho_\varepsilon(x, 0) = 0.955 + \tfrac{\varepsilon}{2}(1 - \cos(2\pi x)) \quad , \quad u_\varepsilon(x, 0) = -\text{sign}(x)\sqrt{\gamma}(1 - \cos(2\pi x)).$$

(3.16)



a)

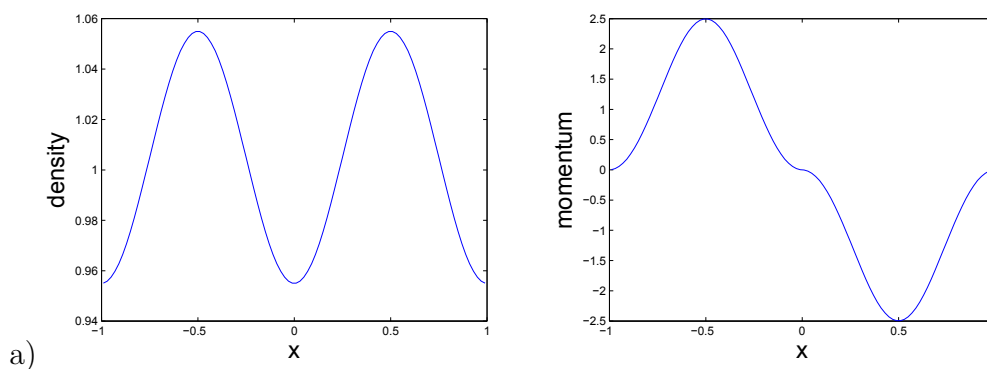Figure 3.3: a) The initial density (left) and momentum (right) when $\varepsilon = 0.1$

These acoustic pulses, one right-running and one left-runnig, collide and superpose and then separate again and during the whole procedure no shock forms. Now, as done in [8], we choose as spatial step $\Delta x = 1/50$ and and time $\Delta t = 1/1000$ in order to keep the scheme stable, final time $T = 0.05$, $\varepsilon = 0.1$ and periodic boundary conditions.
Below are displayed the numerical results of the density and the momentum of the fluid to different final times $T$.

b)



c)



d)



e)

f)
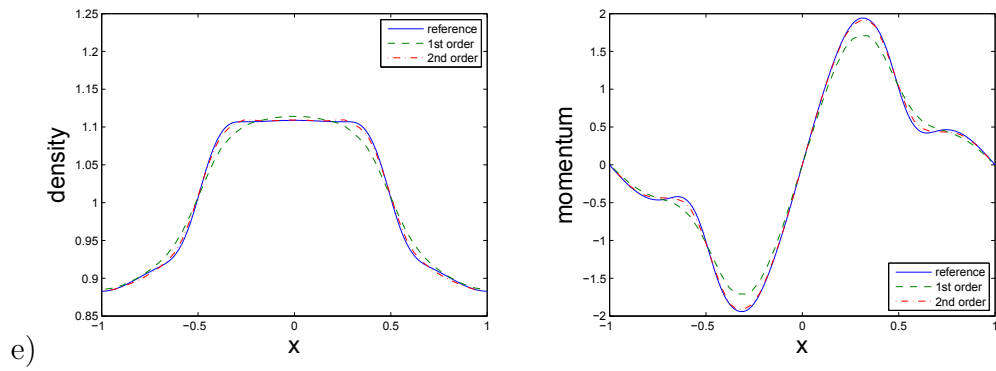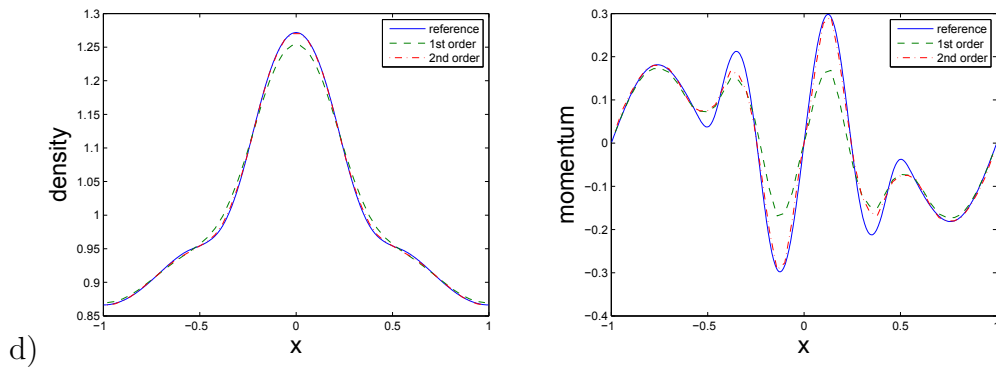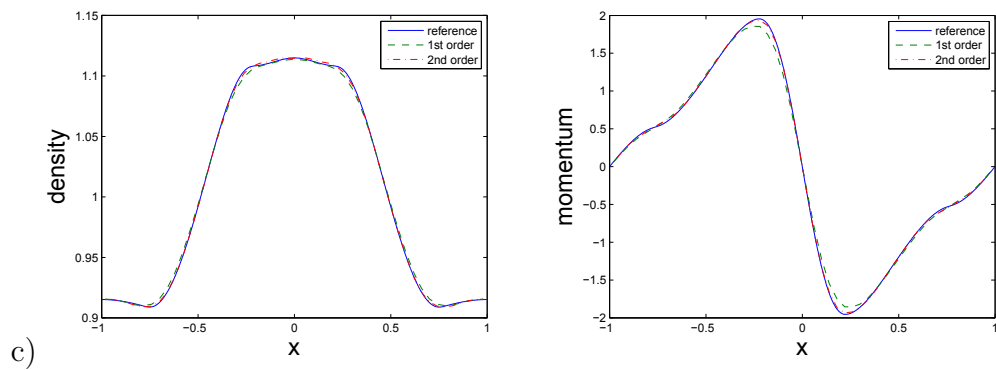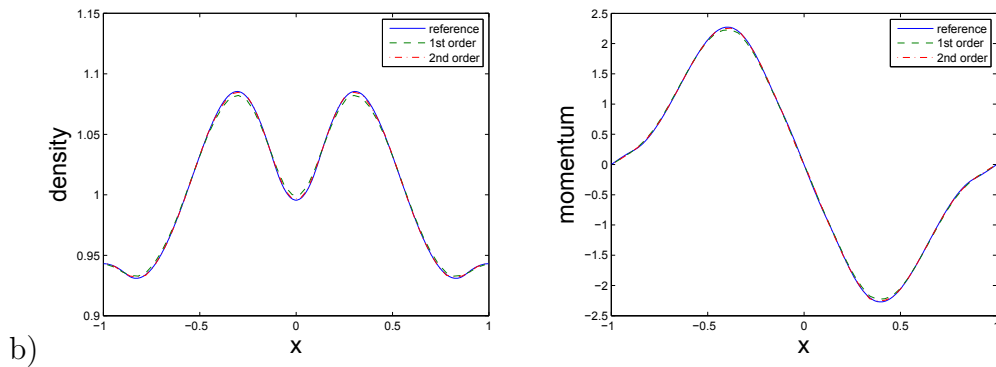
Figure 3.4: $\varepsilon = 0.1$, b) $T = 0.01$; c) $T = 0.02$; d) $T = 0.04$; e) $T = 0.06$; f) $T = 0.08$.

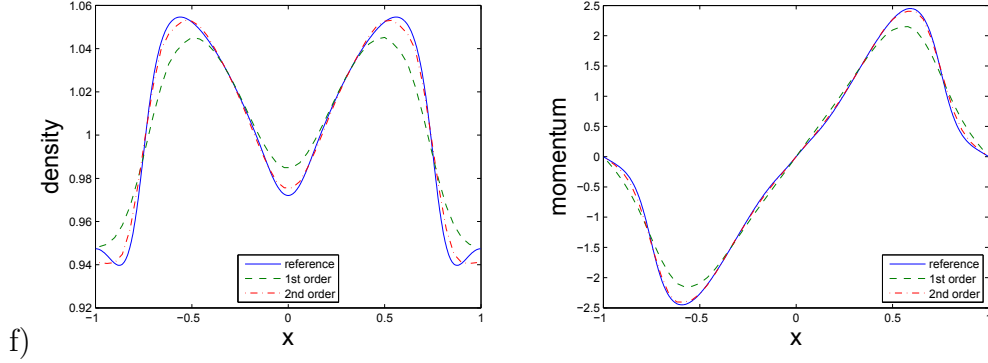In Figure (3.4), we report the results of the first order scheme "- -" and the second order one "$\cdot$-$\cdot$" simulated with $\Delta x = 1/50$ and $\Delta t = 1/1000$ with respect to the reference solution "—" simulated with $\Delta x = 1/500$ and $\Delta t = 1/10000$.

## 3.3    Full Euler case

Here we introduce an asymptotic preserving, all Mach number, finite volume scheme for the numerical solution of the compressible Euler equations of gas dynamics. We employ an semi-implicit time discretization without splitting the fluxes, solving a linearized elliptic equation avoiding to use an iterative method to solve it.

### 3.3.1    Structure of the system

We consider the compressible Euler equations for an ideal gas:

$$\begin{cases} \rho_t + \nabla \cdot (\rho \vec{u}) = 0 \\ (\rho \vec{u})_t + \nabla \cdot (\rho \vec{u} \otimes \vec{u}) + \nabla p = 0 \\ E_t + \nabla \cdot [(E + p)\vec{u}] = 0 \end{cases} \tag{3.17}$$

where $\rho$ is the density, $\vec{u}$ the velocity of the fluid, $E$ the total energy and $p$ the pressure. The System (3.17) is closed by equation of state (EOS):

$$p = (\gamma - 1)\left( E - \frac{1}{2}\rho u^2 \right)$$

for simplicity we assume a polytropic gas with constant $\gamma = c_p/c_V > 1$.

We rescale the equations to emphasize the (possibly) small Mach number $\varepsilon$, the scaling parameters are: $\rho_0, u_0, p_0, x_0, t_0$, where the dimensionless variables are then given by

$$\hat{\rho} = \rho/\rho_0, \quad \hat{u} = u/u_0, \quad \hat{p} = p/p_0, \quad \hat{E} = E/E_0, \quad \hat{x} = x/x_0, \quad \hat{t} = t/t_0.$$

Now considering the fact that $u_0 = x_0/t_0$ and inserting these into the Equations (3.17) (and omitting the hat) one obtains the rescaled (non-dimensionalised) compressible Euler equations:

$$\begin{cases} \rho_t + \nabla \cdot (\rho\vec{u}) = 0 \\ (\rho\vec{u})_t + \nabla \cdot (\rho\vec{u} \otimes \vec{u}) + \frac{1}{\varepsilon^2}\nabla p = 0 \\ E_t + \nabla \cdot [(E + p)\vec{u}] = 0, \end{cases} \qquad (3.18)$$

with the equation of state

$$p = (\gamma - 1)\left(E - \frac{\varepsilon^2}{2}\rho u^2\right)$$

where the dimensionless reference Mach number is $\varepsilon^2 = \rho_0 u_0^2/p_0$. This parameter $\varepsilon$ represents a global Mach number characterizing the non dimensionalization but not the local Mach number.

The system (3.18) is *hyperbolic* and the eigenvalues in direction $\mathbf{n}$ are:

$$\lambda_1 = \vec{u} \cdot \mathbf{n} - \frac{c_s}{\varepsilon}, \quad \lambda_2 = \vec{u} \cdot \mathbf{n}, \quad \lambda_3 = \vec{u} \cdot \mathbf{n} + \frac{c_s}{\varepsilon}$$

where $c_s = \sqrt{(\partial p/\partial\rho)_s}$ where the derivative is taken at constant entropy $S$.

The aim of this thesis is the numerical simulation of unsteady compressible flows when the Mach number $\varepsilon$ spans by orders of magnitude. Compressible flow equations converge to incompressible equations when the Mach number vanishes. This convergence has been rigorously studied mathematically by Klainerman and Majda [18, 19]. When the Mach number is of $\mathcal{O}(1)$, modern shock capturing methods are able to capture shocks and other complex structures with high numerical resolutions at a reasonable cost.

On the other hand, when we are near the incompressible regime, and Mach number is very small, flows are slow compared with the speed of sound and in such a situation, pressure waves become very fast compared to material waves. In several cases, acoustic waves possess very small energy and they are unimportant in the incompressible regime, then one is not interested in resolving them.

From a numerical point of view, when the Mach number is very small, standard explicit shock-capturing methods require a CFL time restriction dictated by the sound speed $c_s/\varepsilon$ to integrate the system. This leads to the stiffness in time, [8, 9, 11] , where the time discretization is constrained by a stability condition given by

$$\Delta t < \Delta x/\lambda_{\max} \approx \mathcal{O}(\varepsilon\Delta x)$$

for small $\varepsilon$ where $\Delta t$ is the time-step, $\Delta x$ the space step and

$$\lambda_{\max} = \max_{\Omega}(|\vec{u}| + c_s/\varepsilon)$$

This means that it is required for the integration on time an increasingly large computational time for smaller and smaller $\varepsilon$. The second drawback is due to the excessive numerical viscosity of standard upwind schemes, that scales as $\varepsilon^{-1}$, leading to highly inaccurate solutions. Thus, it is also crucial how the space derivatives are discretized in order to get stability and consistency for the scheme in the incompressible limit (*asymptotic preserving property*).

In this thesis we want to develop an original numerical scheme that works in all regimes of Mach number for the solution of system (3.18), including both compressible and incompressible regime.
The idea is to design a high order numerical scheme for compressible Euler, whose stability and accuracy are independent of $\varepsilon$, and which is able to capture shocks and discontinuities in the compressible regime, for large $\varepsilon$ and, at the same time, it is a good incompressible solver in the incompressible limit regime. This means that the scheme has to be asymptotic preserving [16, 17], i.e., a numerical scheme which gives a consistent discretization of the compressible Euler equations and in the limit as $\varepsilon \to 0$, with $\Delta x$ and $\Delta t$ fixed, provides a consistent discretization of the incompressible Euler equations.

Finally if the scheme is uniformly stable with respect to the parameter $\varepsilon$, the scheme is called *asymptotic stable* (AS). Of course, if a scheme is AP and AS, an uniform accuracy for all range of the parameter $\varepsilon$ is expected.
The features of the our scheme is the combination of a specific semi-implicit time strategy by using IMEX R-K schemes for the time [1, 3, 6, 24] in which, in (3.18), the low Mach number stiff term (pressure term) is treated implicitly and the flux is treated explicitly. For the space discretization, shock capturing methods are employed. In particular, following the approach of Nessyahu and Tadmor [22], we consider second-order, non-oscillatory central scheme on a staggered grid.

### 3.3.2   Discretization first-order in time

Consider the compressible Euler equations in 1D. We rescale the equations to emphasize the (possibly) small Mach number $\varepsilon$. For simplicity we assume a polytropic gas with constant $\gamma$.

$$\rho_t + m_x = 0$$
$$m_t + (\rho u^2 + p/\varepsilon^2)_x = 0$$
$$E_t + ((E + p)u)_x = 0$$

where $u = m/\rho$ is the fluid velocity.
The closure relation is

$$p = (\gamma - 1)\left(E - \frac{\varepsilon^2}{2}\rho u^2\right).$$

The idea is now that as $\varepsilon \ll 1$, the first equation becomes less and less relevant, while the total energy is essentially proportional to the pressure. Therefore we write an implicit system using the last two equations, and then compute $\rho^{n+1}$ by post processing. Discretize equations on a staggered grid from $t^n$ to $t^{n+1}$, using the NT central scheme, with a first order S-IMEX method in time, obtaining:

$$
\begin{aligned}
\overline{\rho}_{j+\frac{1}{2}}^{n+1} &= \overline{\rho}_{j+\frac{1}{2}}^{n} && && -\frac{\Delta t}{\Delta x}(m_{j+1}^{n+1} - m_j^{n+1}) \\[2mm]
\overline{m}_{j+1/2}^{n+1} &= \overline{m}_{j+1/2}^{n} & -\frac{\Delta t}{\Delta x}\frac{3-\gamma}{2}(f_{j+1}^n - f_j^n) & -\frac{\Delta t}{\Delta x}\frac{\gamma-1}{\varepsilon^2}(E_{j+1}^{n+1} - E_j^{n+1}) \\[2mm]
\overline{E}_{j+\frac{1}{2}}^{n+1} &= \overline{E}_{j+\frac{1}{2}}^{n} & +\frac{\Delta t}{\Delta x}\frac{\gamma-1}{2}(g_{j+1}^n - g_j^n) & -\gamma\frac{\Delta t}{\Delta x}\left(\frac{E_{j+1}^n m_{j+1}^{n+1}}{\rho_{j+1}^n} - \frac{E_j^n m_j^{n+1}}{\rho_j^n}\right)
\end{aligned}
$$

$$(3.19)$$

Here for short we denoted $f = m^2/\rho$ and $g = m^3/\rho^2$.
Just as in the case of isentropic gas dynamics, an equation for $m_j^{n+1}$ is adopted

$$m_j^{n+1} = m_j^n - \frac{\Delta t}{\Delta x}\frac{3-\gamma}{2}\mathcal{D}_x f_j^n - \frac{\Delta t}{\Delta x}\frac{\gamma-1}{\varepsilon^2}\mathcal{D}_x E_j^{n+1} \qquad (3.20)$$

and by replacing $m_j^{n+1}$ in the energy equation, we get:

$$
\begin{aligned}
E_{j+\frac{1}{2}}^{n+1} =\ & \phi_{j+\frac{1}{2}}^n + \gamma(\gamma-1)\frac{\Delta t^2}{\varepsilon^2 \Delta x^2}\cdots \\[2mm]
& \cdots\left(\frac{E_{j+1}^n}{\rho_{j+1}^n}E_{j+\frac{3}{2}}^{n+1} - \left(\frac{E_{j+1}^n}{\rho_{j+1}^n} + \frac{E_j^n}{\rho_j^n}\right)E_{j+\frac{1}{2}}^{n+1} + \frac{E_j^n}{\rho_j^n}E_{j-\frac{1}{2}}^{n+1}\right)
\end{aligned}
$$

$$(3.21)$$

with

$$\phi_{j+\frac{1}{2}}^n = E_{j+\frac{1}{2}}^* - \gamma \frac{\Delta t}{\Delta x} \mathcal{D}_x \left[ \left( \frac{E}{\rho} \right)_{j+\frac{1}{2}}^n m_j^n \right] + \gamma \frac{3-\gamma}{2} \frac{\Delta t^2}{\Delta x^2} \mathcal{D}_x \left[ \frac{E_{j+\frac{1}{2}}^n}{\rho_{j+\frac{1}{2}}^n} \mathcal{D}_x f_j^n \right]$$
(3.22)

where

$$E_{j+\frac{1}{2}}^* = \overline{E}_{j+\frac{1}{2}}^n + \frac{\gamma-1}{2} \frac{\Delta t}{\Delta x} \mathcal{D}_x g_{j+\frac{1}{2}}^n \qquad (3.23)$$

The quantity $\phi_{j+\frac{1}{2}}^n$ contains something that can be computed explicitly.

Solving the triangular system (3.21), we get $\overline{E}_{j+\frac{1}{2}}^{n+1}$, which is then used in the second and third equation of (3.19), and at the end the density $\overline{\rho}_{j+\frac{1}{2}}^{n+1}$ is computed from the first equation.

## 3.4 Numerical Tests

We present several numerical test cases to illustrate the correct behaviour of our new second order scheme applied to the full Euler system in one dimension.

### 3.4.1 Example 1: Convergence test

Similarly to the isentropic case, we consider in the one dimensional full Euler system a simple wave test to study the experimental order of convergence (EOC). Instead of comparing the numerical solution $U$ with exact solution, the EOC can be computed using numerical solutions on each grid of sizes $N_{j+1} = 2N_j$, with $j = 1, 2, 3$ namely, since we adopted a staggered grid then the EOC can be written in the following way:

$$\text{EOC} := \log_2 \left( \frac{\text{err}_{N_j}}{\text{err}_{N_{j+1}}} \right)$$

where

$$\text{err}_{N_j} = \frac{\sum_{i=1}^{N_j} \left| U_i(N_j) - \frac{U_{2i-1}(N_{j+1}) + U_{2i}(N_{j+1})}{2} \right|}{\sum_{i=1}^{N_j} |U_i(N_j)|}$$

The computational domain is $\Omega = [-2.5, 2.5]$ the final time is $T = 0.3$ and the CFL condition was imposed at $0.45$:

$$\begin{cases} u = \sin\left(\frac{2\pi x}{L}\right) \\ \rho = \left(1 + \frac{(\gamma-1)u}{2c}\right)^{\frac{2}{\gamma-1}} \\ p = \rho^\gamma \end{cases}$$

with $\gamma = 1.4$, $c = \frac{1}{\varepsilon}\sqrt{\gamma}$, $L = 5$. Below we report the following table of convergence for the density, momentum and energy for different values of the Mach number. In this example we used $\theta - MinMod$ limiter, taking $\theta = 1.5$:

$$U_i' = MinMod\left(\theta \frac{U_i - U_{i-1}}{\Delta x}, \frac{U_{i+1} - U_{i-1}}{2\Delta x}, \theta \frac{U_{i+1} - U_i}{\Delta x}\right)$$

| CFL = 0.45, T = 0.3 and $\varepsilon = 0.8$ | | | | | |
|---|---|---|---|---|---|
| $N$ | $L^1$-error $\rho$ | EOC $\rho$ | $L^1$-error $m$ | EOC $m$ | $L^1$-error $E$ | EOC $E$ |
| 20 | 5.472e-03 | – | 1.347e-02 | – | 6.990e-03 | – |
| 40 | 1.602e-03 | 1.7727 | 4.047e-03 | 1.7352 | 2.603e-03 | 1.4251 |
| 80 | 4.792e-04 | 1.7408 | 1.302e-03 | 1.6361 | 7.481e-04 | 1.7990 |
| 160 | 1.237e-04 | 1.9536 | 3.639e-04 | 1.8392 | 2.018e-04 | 1.8900 |
| 320 | 3.120e-05 | 1.9874 | 9.381e-05 | 1.9556 | 5.146e-05 | 1.9715 |
| 640 | 7.732e-06 | 2.0126 | 2.353e-05 | 1.9955 | 1.286e-05 | 2.0002 |

| CFL = 0.45, T = 0.3 and $\varepsilon = 0.1$ | | | | | |
|---|---|---|---|---|---|
| $N$ | $L^1$-error $\rho$ | EOC $\rho$ | $L^1$-error $m$ | EOC $m$ | $L^1$-error $E$ | EOC $E$ |
| 20 | 1.988e-03 | – | 3.894e-02 | – | 2.708e-03 | – |
| 40 | 3.959e-04 | 2.3281 | 7.445e-03 | 2.3870 | 5.501e-04 | 2.2998 |
| 80 | 1.202e-04 | 1.7199 | 2.241e-03 | 1.7319 | 1.676e-04 | 1.7145 |
| 160 | 3.036e-05 | 1.9850 | 5.641e-04 | 1.9904 | 4.266e-05 | 1.9742 |
| 320 | 7.628e-06 | 1.9929 | 1.400e-04 | 2.0100 | 1.077e-05 | 1.9863 |
| 640 | 1.895e-06 | 2.0090 | 3.501e-05 | 2.0000 | 2.682e-06 | 2.0051 |

We can see the second order of accuracy also for very small Mach number as $10^{-4}$, setting the final time step $T = 0.01$.

| CFL = 0.45, T = 0.01 and $\varepsilon = 10^{-4}$ | | | | | |
|---|---|---|---|---|---|
| $N$ | $L^1$-error $\rho$ | EOC $\rho$ | $L^1$-error $m$ | EOC $m$ | $L^1$-error $E$ | EOC $E$ |
| 20 | 1.844e-05 | – | 4.792e-01 | – | 2.582e-05 | – |
| 40 | 1.084e-05 | 0.7667 | 2.105e-01 | 1.1865 | 1.518e-05 | 0.7667 |
| 80 | 2.929e-06 | 1.8881 | 5.463e-02 | 1.9463 | 4.100e-06 | 1.8881 |
| 160 | 7.332e-07 | 1.9980 | 1.360e-02 | 2.0057 | 1.026e-06 | 1.9980 |
| 320 | 1.831e-07 | 2.0018 | 3.394e-03 | 2.0031 | 2.563e-07 | 2.0018 |
| 640 | 4.582e-08 | 1.9982 | 8.492e-04 | 1.9986 | 6.415e-08 | 1.9982 |

## 3.4.2   Example 2: Two Colliding Acoustic Pulses

We consider again two colliding acoustic pulses in a weakly compressible regime, this test has been taken from [20, 23]. The initial conditions are given by

$$
\begin{aligned}
&p(\rho_\varepsilon) = \rho_\varepsilon^\gamma, \quad \text{for} \quad x \in [-1, 1], \quad \text{with} \quad \gamma = 1.4 \\
&\rho_\varepsilon(x, 0) = \rho_0 + \tfrac{1}{2}\varepsilon\rho_1(1 - \cos(2\pi x)) \quad \rho_0 = 0.955, \quad \rho_1 = 2.0 \\
&u_\varepsilon(x, 0) = \tfrac{1}{2}u_0\text{sign}(x)u_0(1 - \cos(2\pi x)) \quad u_0 = 2\sqrt{\gamma} \\
&p(x, 0) = p_0 + \tfrac{1}{2}\varepsilon p_1(1 - \cos(2\pi x)), \quad p_0 = 1.0, \quad p_1 = 2\gamma
\end{aligned}
\tag{3.24}
$$

The domain is $-L \leq x \leq L = 2/\varepsilon$ the boundary conditions are periodic. We show in the Figure 3.5 the plots of the pressure obtained using the second order globally stiffly accurate NT scheme at different times $t = 0.815$ and $t = 1.63$. We choose $\varepsilon = 1/11$ and we display the initial pressure distributions for comparison. The results show a similar behaviour as in [23].
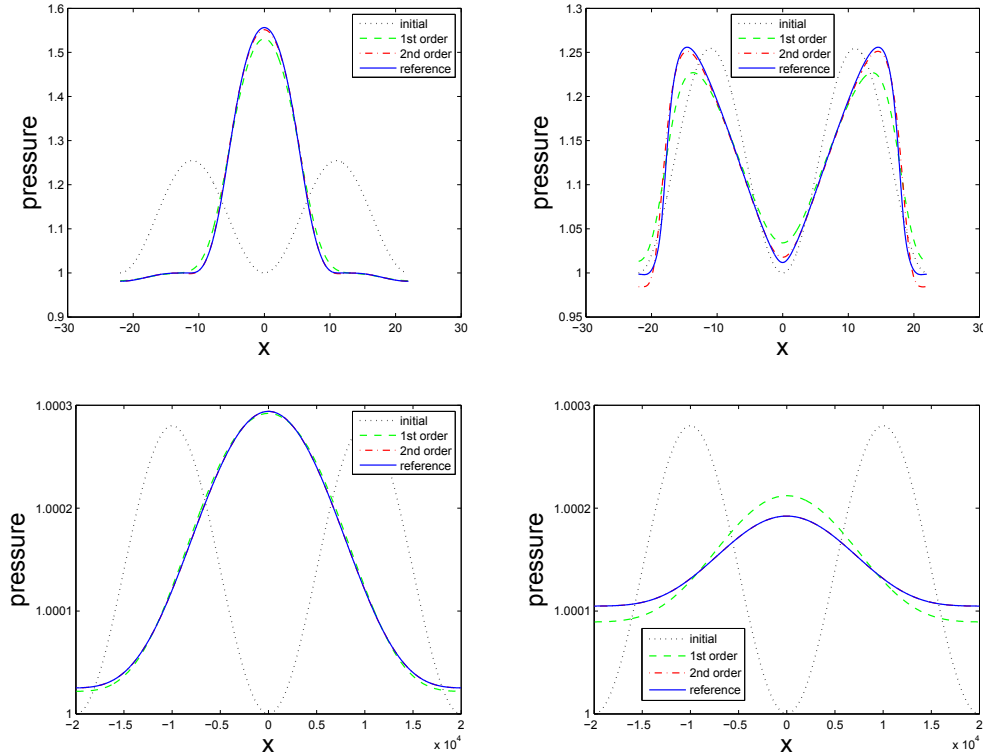


Figure 3.5: Pressure of the fluid when $\varepsilon = 1/11$ (top panel) and $\varepsilon = 10^{-4}$ (bottom panel) with $N = 440$ at time $T = 0.815$ (Left) and at time $T = 1.63$ (Right). We displayed the initial condition "· · ·", the numerical solution to the first "- -" and second order in time "· - ·". The reference solution "—". has been computed with $N = 1500$.

# Chapter 4

# FV Scheme: 2D problem

## 4.1 Isentropic case

We consider the domain $\Omega = [0,1] \times [0,1]$, a uniform spatial mesh with $\Delta x = 1/N$, $\Delta y = 1/N$, with $N$ a positive integer, the grid points defined as $x_i = i\Delta x$, $y_j = j\Delta y$, with $i, j = 0, 1, \cdots, N$. The Euler equations for isentropic case in 2D of the gas dynamics are given by

$$
\begin{aligned}
\rho_t + (\rho u)_x + (\rho v)_y &= 0 \\
(\rho u)_t + \left(\rho u^2\right)_x + (\rho u v)_y + \frac{p_x}{\varepsilon^2} &= 0 \\
(\rho v)_t + (\rho u v)_x + \left(\rho v^2\right)_y + \frac{p_y}{\varepsilon^2} &= 0
\end{aligned}
\tag{4.1}
$$

The system is closed by $p = \rho^\gamma$. In order to discretize this system in space, we used Jiang-Tadmor method introduced in the section 2.1.

### 4.1.1 Discretization

Integrate the equation on staggered grid, from time $t^n$ to time $t^{n+1}$, calling for simplicity of writing: $m = \rho u$ and $\mathfrak{n} = \rho v$, we obtain the follow discretization:

$$
\begin{aligned}
\overline{\rho}^{n+1}_{i+\frac{1}{2},j+\frac{1}{2}} &= \overline{\rho}^n_{i+\frac{1}{2},j+\frac{1}{2}} - \lambda \mathcal{D}_x m^{n+1}_{i+\frac{1}{2},j+\frac{1}{2}} - \mu \mathcal{D}_y \mathfrak{n}^{n+1}_{i+\frac{1}{2},j+\frac{1}{2}} \\[2ex]
\overline{m}^{n+1}_{i+\frac{1}{2},j+\frac{1}{2}} &= \overline{m}^n_{i+\frac{1}{2},j+\frac{1}{2}} - \lambda \mathcal{D}_x f^n_{i+\frac{1}{2},j+\frac{1}{2}} - \mu \mathcal{D}_y h^n_{i+\frac{1}{2},j+\frac{1}{2}} - \frac{\lambda}{\varepsilon^2} \mathcal{D}_x p^{n+1}_{i+\frac{1}{2},j} \\[2ex]
\overline{\mathfrak{n}}^{n+1}_{i+\frac{1}{2},j+\frac{1}{2}} &= \overline{\mathfrak{n}}^n_{i+\frac{1}{2},j+\frac{1}{2}} - \lambda \mathcal{D}_x h^n_{i+\frac{1}{2},j+\frac{1}{2}} - \mu \mathcal{D}_y g^n_{i+\frac{1}{2},j+\frac{1}{2}} - \frac{\mu}{\varepsilon^2} \mathcal{D}_y p^{n+1}_{i,j+\frac{1}{2}}
\end{aligned}
\tag{4.2}
$$

where $\forall h$:

$$\mathcal{D}_x h_{i+\frac{1}{2},j+\frac{1}{2}} = \frac{1}{2}(\mathcal{D}_x h_{i+\frac{1}{2},j}+\mathcal{D}_x h_{i+\frac{1}{2},j+1}) \quad , \quad \mathcal{D}_y h_{i+\frac{1}{2},j+\frac{1}{2}} = \frac{1}{2}(\mathcal{D}_y h_{i,j+\frac{1}{2}}+\mathcal{D}_y h_{i+1,j+\frac{1}{2}})$$

and

$$\mathcal{D}_x h_{i+\frac{1}{2},j} = h_{i+1,j} - h_{i,j} \quad , \quad \mathcal{D}_x h_{i+\frac{1}{2},j+1} = h_{i+1,j+1} - h_{i,j+1},$$
$$\mathcal{D}_y h_{i,j+\frac{1}{2}} = h_{i,j+1} - h_{i,j} \quad , \quad \mathcal{D}_y h_{i+1,j+\frac{1}{2}} = h_{i+1,j+1} - h_{i+1,j},$$

with $f_{i,j}^n = (m_{i,j}^n)^2/\rho_{i,j}^n$, $g_{i,j}^n = (\mathfrak{n}_{i,j}^n)^2/\rho_{i,j}^n$, $h_{i,j}^n = (\rho u v)_{i,j}^n$ and $\lambda = \frac{\Delta t}{\Delta x}$, $\mu = \frac{\Delta t}{\Delta y}$. Second order in space is obtained by standard reconstruction adopted in Jiang-Tadmor scheme, with

$$\begin{aligned}
\overline{\rho}_{i+\frac{1}{2},j+\frac{1}{2}} &= \tfrac{1}{4}(\overline{\rho}_{i,j} + \overline{\rho}_{i+1,j} + \overline{\rho}_{i,j+1} + \overline{\rho}_{i+1,j+1}) \\[2mm]
&+ \tfrac{1}{16}(\rho'_{i,j} - \rho'_{i+1,j} + \rho'_{i,j+1} - \rho'_{i+1,j+1})\Delta x \\[2mm]
&+ \tfrac{1}{16}(\rho\grave{}_{i,j} - \rho\grave{}_{i,j+1} + \rho\grave{}_{i+1,j} - \rho\grave{}_{i+1,j+1})\Delta y
\end{aligned}$$

where $\rho'_{i,j}$ and $\rho\grave{}_{i,j}$ a first order approximation of the first derivative on cell $(i,j)$ (we use *MinMod* in most cases (2.9)). Similarly for $\overline{m}_{i+\frac{1}{2},j+\frac{1}{2}}^{n+1}$, and $\overline{\mathfrak{n}}_{i+\frac{1}{2},j+\frac{1}{2}}^{n+1}$.

For the prediction step, similar equations can be written for $m_{i,j}^{n+1}$ and $\mathfrak{n}_{i,j}^{n+1}$, i.e.,

$$\begin{aligned}
m_{i,j}^{n+1} &= m_{i,j}^n - \frac{\Delta t}{\Delta x}\mathcal{D}_x f_{i,j}^n - \frac{\Delta t}{\Delta y}\mathcal{D}_y h_{i,j}^n - \frac{\Delta t}{\varepsilon^2 \Delta x}\mathcal{D}_x p_{i,j}^{n+1} \\[2mm]
\mathfrak{n}_{i,j}^{n+1} &= \mathfrak{n}_{i,j}^n - \frac{\Delta t}{\Delta x}\mathcal{D}_x h_{i,j}^n - \frac{\Delta t}{\Delta y}\mathcal{D}_y g_{i,j}^n - \frac{\Delta t}{\varepsilon^2 \Delta y}\mathcal{D}_y p_{i,j}^{n+1}
\end{aligned} \tag{4.3}$$

with $\mathcal{D}_x p_{i,j} = p_{i+\frac{1}{2},j} - p_{i-\frac{1}{2},j}$ and similarly $\mathcal{D}_x f_{i,j}$ and $\mathcal{D}_y h_{i,j}$. Plugging these equations in $\overline{\rho}_{i+\frac{1}{2},j+\frac{1}{2}}^{n+1}$ one obtains an equation of the form:

$$\overline{\rho}_{i+\frac{1}{2},j+\frac{1}{2}}^{n+1} = \phi_{i+\frac{1}{2},j+\frac{1}{2}}^n + \frac{\lambda^2}{\varepsilon^2}\mathcal{D}_x^2 p_{i+\frac{1}{2},j}^{n+1} + \frac{\mu^2}{\varepsilon^2}\mathcal{D}_y^2 p_{i,j+\frac{1}{2}}^{n+1} \tag{4.4}$$

which is an elliptic equation where

$$\begin{aligned}
\phi_{i+\frac{1}{2},j+\frac{1}{2}}^n &= \rho_{i+\frac{1}{2},j+\frac{1}{2}}^n - \lambda\mathcal{D}_x m_{i+\frac{1}{2},j+\frac{1}{2}}^n - \mu\mathcal{D}_y \mathfrak{n}_{i+\frac{1}{2},j+\frac{1}{2}}^n \\[2mm]
&+ \lambda^2 \mathcal{D}_x^2 f_{i+\frac{1}{2},j+\frac{1}{2}}^n + 2\lambda\mu\mathcal{D}_x\mathcal{D}_y h_{i+\frac{1}{2},j+\frac{1}{2}}^n \\[2mm]
&+ \mu^2 \mathcal{D}_y^2 g_{i+\frac{1}{2},j+\frac{1}{2}}^n
\end{aligned} \tag{4.5}$$

and

$$
\begin{aligned}
\mathcal{D}_x^2 p_{i+\frac{1}{2},j}^{n+1} &= p_{i+\frac{3}{2},j}^{n+1} - 2p_{i+\frac{1}{2},j}^{n+1} + p_{i-\frac{1}{2},j}^{n+1} \\
\mathcal{D}_y^2 p_{i,j+\frac{1}{2}}^{n+1} &= p_{i,j+\frac{3}{2}}^{n+1} - 2p_{i,j+\frac{1}{2}}^{n+1} + p_{i,j-\frac{1}{2}}^{n+1}
\end{aligned}
\tag{4.6}
$$

$\phi^n$ in Equation (4.5) denotes a quantity that can be computed explicitly (in a conservative way). Now we observe that if we approximate again the Laplace operator $\Delta p^{n+1}$, discretized in (4.4), by the approximation

$$
\Delta(p(\rho^{n+1})) \approx \nabla(p'(\rho^n)\nabla\rho^{n+1})
$$

a semi-implicit approach is involved in (4.4) for the numerical solution $\overline{\rho}_{i+\frac{1}{2},j+\frac{1}{2}}^{n+1}$ and then this implies to solve a linear system in (4.4).

## 4.1.2   Asymptotic Preserving Property

Now, we prove the AP property for our scheme (4.2), (4.3), and (4.4). Here we consider again well-prepared initial conditions (1.31), and the asymptotic expansions (3.8). Now, when $\varepsilon \to 0$ the $\mathcal{O}(1/\varepsilon^2)$ terms of (4.2) give

$$
(p_{0,i+1,j}^{n+1} - p_{0,i,j}^{n+1}) = 0, \quad (p_{0,i,j+1}^{n+1} - p_{0,i,j}^{n+1}) = 0.
$$

Using periodic boundary conditions, by $p(\rho) = \rho^\gamma$ one gets space independence of the density, i.e., $\rho_{0,i,j}^{n+1} = \rho_0^{n+1}$. Now, similarly to the one dimensional case, by summing the first equation in (4.2) over all the grid points, we obtain the time independence of the density

$$
\overline{\rho}_{0,i+\frac{1}{2},j+\frac{1}{2}}^{n+1} = \overline{\rho}_{0,i+\frac{1}{2},j+\frac{1}{2}}^{n} = \overline{\rho}_0.
\tag{4.7}
$$

Using this result in the first equation in (4.2) we get, by $m_0 = \rho_0 u_0$ and $\mathfrak{n}_0 = \rho_0 v_0$,

$$
\lambda(\mathcal{D}_x u_0^{n+1})_{i+\frac{1}{2},j+\frac{1}{2}} + \mu(\mathcal{D}_y v_0^{n+1})_{i+\frac{1}{2},j+\frac{1}{2}} = 0
\tag{4.8}
$$

This equation represents the discrete incompressibility condition for the vector velocity $\vec{u}_0^{n+1}$. Now, we consider $\mathcal{O}(1)$ terms in (4.4):

$$
\overline{\rho}_{0,i+\frac{1}{2},j+\frac{1}{2}}^{n+1} = \phi_{0,i+\frac{1}{2},j+\frac{1}{2}}^{n} + \frac{\Delta t^2}{\Delta x^2}\mathcal{D}_x^2 p_{2,i+\frac{1}{2},j}^{n+1} + \frac{\Delta t^2}{\Delta y^2}\mathcal{D}_y^2 p_{2,i,j+\frac{1}{2}}^{n+1}
$$

Then, by (4.8) and $m_0 = \rho_0 u_0$, $\mathfrak{n}_0 = \rho_0 v_0$, we get in (4.5):
$(\mathcal{D}_x m_0^n)_{i+\frac{1}{2},j+\frac{1}{2}} = 0$, and $(\mathcal{D}_y \mathfrak{n}_0^n)_{i+\frac{1}{2},j+\frac{1}{2}} = 0$. By the fact that $\overline{\rho}_0$ is independent of the time, in (4.5) we obtain:

$$
\begin{aligned}
- & \left( \frac{1}{\varepsilon^2 \Delta x^2} \mathcal{D}_x^2 p_{2,i+\frac{1}{2},j}^{n+1} + \frac{1}{\varepsilon^2 \Delta y^2} \mathcal{D}_y^2 p_{2,i,j+\frac{1}{2}}^{n+1} \right) \\
= & \ \frac{1}{\Delta x^2} \mathcal{D}_x^2 f_{0,i+\frac{1}{2},j+\frac{1}{2}}^n + \frac{2}{\Delta x \Delta y} \mathcal{D}_x \mathcal{D}_y h_{0,i+\frac{1}{2},j+\frac{1}{2}}^n \\
+ & \ \frac{1}{\Delta y^2} \mathcal{D}_y^2 g_{0,i+\frac{1}{2},j+\frac{1}{2}}^n .
\end{aligned}
\tag{4.9}
$$

We note that (4.9) is the discretization of Equation (1.33).
Finally, the $\mathcal{O}(1)$ terms of the momentum equations of (4.2) become:

$$
\begin{aligned}
\left( \frac{\overline{u}_{0,i+\frac{1}{2},j+\frac{1}{2}}^{n+1} - \overline{u}_{0,i+\frac{1}{2},j+\frac{1}{2}}^n}{\Delta t} \right) &= -\frac{1}{\Delta x} (\mathcal{D}_x(u_0^2)^n)_{i+\frac{1}{2},j+\frac{1}{2}} - \frac{1}{\Delta y} (\mathcal{D}_y(uv)_0^n)_{i+\frac{1}{2},j+\frac{1}{2}} \\
&\quad - \frac{1}{\overline{\rho}_0 \Delta x} (\mathcal{D}_x p_2^{n+1})_{i+\frac{1}{2},j} \\
\left( \frac{\overline{v}_{0,i+\frac{1}{2},j+\frac{1}{2}}^{n+1} - \overline{v}_{0,i+\frac{1}{2},j+\frac{1}{2}}^n}{\Delta t} \right) &= -\frac{1}{\Delta x} (\mathcal{D}_x(uv)_0^n)_{i+\frac{1}{2},j+\frac{1}{2}} - \frac{1}{\Delta y} (\mathcal{D}_y(v_0^2)^n)_{i+\frac{1}{2},j+\frac{1}{2}} \\
&\quad - \frac{1}{\overline{\rho}_0 \Delta y} (\mathcal{D}_y p_2^{n+1})_{i,j+\frac{1}{2}}
\end{aligned}
\tag{4.10}
$$

This represents an equivalent formulation of the incompressible momentum equation. Thus from (4.7)-(4.8) and (4.10) we obtain a full discretization of (1.32) in the limit $\varepsilon$. Therefore, the two-dimensional scheme is AP.

## 4.1.3   GSA IMEX-JT scheme

In this section we present a globally second order scheme for the isentropic Euler equations. We combine an $s$ stage semi-implicit Runge-Kutta scheme for the time discretization and JT scheme for the space discretization. The idea here is to write the system (3.4) in the form (2.16) where the first argument $\mathbf{U}^* = (\rho^*, \vec{m}^*)$, is treated explicitly, and the second one $\mathbf{U} = (\rho, \vec{m})$ implicitly. In this case the function $\mathcal{H}(U^*, U)$ is given by:

$$
\mathcal{H}(\mathbf{U}^*, \mathbf{U}) = \left( \begin{array}{c} -\nabla \cdot \vec{m} \\ -\nabla \cdot (\rho \vec{u} \otimes \vec{u})^* + \frac{1}{\varepsilon^2} \nabla p(\rho) \end{array} \right)
\tag{4.11}
$$

with $\vec{m} = (m, \mathfrak{n})^T$. A globally second order S-IMEX scheme in time can be obtained by adopting an $s$ stage IMEX R-K scheme (here we choose a particular class of implicit R-K methods called *diagonally implicit R-K* methods

for the implicit part, [13]) and JT central scheme for the discretization of the space. Then we have the two following steps:

- **Prediction step**:

$$
K_\ell := \mathcal{H}(\mathbf{U}_{ij}^*, \mathbf{U}_{ij}) = \begin{pmatrix} -\left(\lambda\mathcal{D}_x m_{ij}^{(\ell)} + \mu\mathcal{D}_y \mathfrak{n}_{ij}^{(\ell)}\right) \\ \left(\lambda\mathcal{D}_x f_{ij}^{*(\ell)} + \mu\mathcal{D}_y h_{ij}^{*(\ell)}\right) - \frac{\lambda}{\varepsilon^2}\mathcal{D}_x p_{ij}^{(\ell)} \\ -\left(\lambda\mathcal{D}_x h_{ij}^{*(\ell)} + \mu\mathcal{D}_y g_{ij}^{*(\ell)}\right) - \frac{\mu}{\varepsilon^2}\mathcal{D}_y p_{ij}^{(\ell)} \end{pmatrix} \quad (4.12)
$$

  with

$$
\mathbf{U}_{ij}^{*(k)} = \mathbf{U}_{ij}^n - \sum_{\ell=1}^{k-1}\tilde{a}_{k,\ell}K_\ell, \quad \mathbf{U}_{ij}^{(k)} = \mathbf{U}_{ij}^n - \sum_{\ell=1}^{k}a_{k,\ell}K_\ell, \quad \forall k = 1, \cdots, s
$$
$$(4.13)$$

  where $f_{ij}^* = (m_{ij}^*)^2/\rho_{ij}^*$, $g_{ij}^* = (\mathfrak{n}_{ij}^*)^2/\rho_{ij}^*$, $h_{ij}^* = \rho_{ij}^* u_{ij}^* v_{ij}^*$.

- **Correction step:** Here we require our IMEX RK is *globally stiffly accurate*, i.e. $\tilde{b}_\ell = \tilde{a}_{s,\ell}$ and $b_\ell = a_{s,\ell}$, for $\ell = 1, \cdots s$, then, discretizing the equations on a staggered grid from time $t^n$ to $t^{n+1}$, we obtain:

$$
\overline{\mathbf{U}}_{i+\frac{1}{2},j+\frac{1}{2}}^{*n+1} = \overline{\mathbf{U}}_{i+\frac{1}{2},j+\frac{1}{2}}^n - \sum_{\ell=1}^{s-1}\tilde{a}_{s,\ell}K_\ell, \quad \overline{\mathbf{U}}_{i+\frac{1}{2},j+\frac{1}{2}}^{n+1} = \overline{\mathbf{U}}_{i+\frac{1}{2},j+\frac{1}{2}}^n - \sum_{\ell=1}^{s}a_{s,\ell}K_\ell,
$$
$$(4.14)$$

  with

$$
K_\ell = \begin{pmatrix} -\lambda\mathcal{D}_x m_{i+\frac{1}{2},j+\frac{1}{2}}^\ell - \mu\mathcal{D}_y \mathfrak{n}_{i+\frac{1}{2},j+\frac{1}{2}}^\ell \\ -\lambda\mathcal{D}_x f_{i+\frac{1}{2},j+\frac{1}{2}}^{*\ell} - \mu\mathcal{D}_y h_{i+\frac{1}{2},j+\frac{1}{2}}^{*\ell} - \lambda\mathcal{D}_x p_{i+\frac{1}{2},j+\frac{1}{2}}^\ell \\ -\lambda\mathcal{D}_x h_{i+\frac{1}{2},j+\frac{1}{2}}^{*\ell} - \mu\mathcal{D}_y g_{i+\frac{1}{2},j+\frac{1}{2}}^{*(\ell)} - \mu\mathcal{D}_y p_{i+\frac{1}{2},j+\frac{1}{2}}^\ell \end{pmatrix} \quad (4.15)
$$

Now by (4.12), (4.13) and (4.14) and (2.18), (2.19) the step from $t^n$ to $t^{n+1} = t^n + \Delta t$ of the S-IMEX scheme is given by the following algorithm:

1. **Input**: Approximate the vector $\mathbf{U}_{ij}^n = (\rho_{ij}, m_{ij}, \mathfrak{n}_{ij})$ for $t = t^n$;

2. **do** $k = 1, \cdots, s-1$;

3. compute the *explicit* stages values: $\mathbf{U}_{ij}^{*(k)} = (\rho_{ij}^*, m_{ij}^*, \mathfrak{n}_{ij}^*)$ and $\hat{\mathbf{U}}_{ij}^{(k)} = (\hat{\rho}_{ij}, \hat{m}_{ij}, \hat{\mathfrak{n}}_{ij})$ with

$$
\hat{\mathbf{U}}_{ij}^{(k)} = \mathbf{U}^n + \sum_{\ell=1}^{k-1}a_{k,\ell}K_\ell
$$

  with $\hat{\mathbf{U}}_{ij}^{(k)} = (\hat{\rho}_{ij}^{(k)}, \hat{m}_{ij}^{(k)}, \hat{\mathfrak{n}}_{ij}^{(k)})$;

4. The first equation of $\mathbf{U}_{ij}^{(k)} = \hat{\mathbf{U}}_{ij}^{(k)} + a_{k,k}K_k$ is:

$$\rho_{ij}^{(k)} = \hat{\rho}_{il}^{(k)} - a_{k,k}\left(\lambda D_x m_{ij}^{(k)} + \mu D_x \mathfrak{n}_{ij}^{(k)}\right) \tag{4.16}$$

5. Using equations $m_{ij}^{(k)}$ and $\mathfrak{n}_{ij}^{(k)}$

$$m_{ij}^{(k)} = \widehat{m^{(k)}}_{ij} + a_{k,k}\lambda D_x p_{ij}^{(k)}, \quad \mathfrak{n}_{ij}^{(k)} = \widehat{\mathfrak{n}^{(k)}}_{ij} + a_{k,k}\lambda D_y p_{ij}^{(k)} \tag{4.17}$$

where

$$\widehat{m^{(k)}}_{ij} = \hat{m}_{ij}^{(k)} + a_{kk}\left(\lambda \mathcal{D}_x f_{ij}^{*(k)} + \mu \mathcal{D}_y h_{ij}^{*(k)}\right), \quad \widehat{\mathfrak{n}^{(k)}}_{ij} = \hat{\mathfrak{n}}_{ij}^{(k)} + a_{kk}\left(\lambda \mathcal{D}_x h_{ij}^{*(k)} + \mu \mathcal{D}_y g_{ij}^{*(k)}\right),$$

and plug (4.17) in (4.16) we obtain

$$\rho_{i,j}^{(k)} = \widehat{\rho^{(k)}}_{i,j} + \frac{\Delta t^2 a_{k,k}^2}{\varepsilon^2}\left(\frac{\mathcal{D}_x^2 p_{ij}^{(k)}}{\Delta x^2} + \frac{\mathcal{D}_x^2 p_{ij}^{(k)}}{\Delta y^2}\right). \tag{4.18}$$

Note that

$$\frac{\mathcal{D}_x^2 p_{ij}}{\Delta x^2} = \frac{p_{i,j+1} - 2p_{ij} + p_{i,j-1}}{\Delta x^2} \approx \left.\frac{\partial^2 p}{\partial x^2}\right|_{(x_i,y_j)}$$

6. Solving (4.18) with respect to $\rho_{ij}^{(k)}$ we get we get: $p\left(\rho^{(k)}\right)_{i,j} = \left(\rho_{ij}^{(k)}\right)^\gamma$, $m_{ij}^{(k)}$ and $\mathfrak{n}_{ij}^{(k)}$.

   **enddo**

7. Similarly, in order to update the numerical solution at the time $t^{n+1}$, we substitute $m_{ij}^{(k)}$ and $\mathfrak{n}_{ij}^{(k)}$ in the numerical solution $\overline{\rho}_{j+\frac{1}{2}}^{(n+1)}$ in the second equation in (4.14) and we obtain

$$\overline{\rho}_{i+\frac{1}{2},j+\frac{1}{2}}^{n+1} = \widehat{\overline{\rho}^{(s)}}_{i+\frac{1}{2},j+\frac{1}{2}} + \frac{\Delta t a_{s,s}^2}{\varepsilon^2}\left(\frac{\mathcal{D}_x^2 p_{i+\frac{1}{2},j}^{(s)}}{\Delta x^2} + \frac{\mathcal{D}_y^2 p_{i+\frac{1}{2},j}^{(s)}}{\Delta y^2}\right) \tag{4.19}$$

with: $\mathcal{D}_x^2 p_{i+\frac{1}{2},j}^{(s)} = p_{i+\frac{3}{2},j}^{(s)} - 2p_{i+\frac{1}{2},j}^{(s)} + p_{i-\frac{1}{2},j}^{(s)}$ and $\mathcal{D}_y^2 p_{i,j+\frac{1}{2}}^{(s)} = p_{i,j+\frac{3}{2}}^{(s)} - 2p_{i,j+\frac{1}{2}}^{(s)} + p_{i,j-\frac{1}{2}}^{(s)}$ and $\widehat{\overline{\rho}^{(s)}}_{i+\frac{1}{2},j+\frac{1}{2}}$ denote the quantity computed explicitly (in a conservative way).

8. Finally, from $\overline{\rho}_{i+\frac{1}{2},j+\frac{1}{2}}^{(n+1)}$ we get $p_{i+\frac{1}{2},j+\frac{1}{2}}^{n+1}$ and $\overline{m}_{i+\frac{1}{2},j+\frac{1}{2}}^{n+1}$ and $\overline{\mathfrak{n}}_{i+\frac{1}{2},j+\frac{1}{2}}^{n+1}$ by

$$
\begin{aligned}
\overline{m}_{i+\frac{1}{2},j+\frac{1}{2}}^{n+1} &= \widehat{\widehat{m}}_{i+\frac{1}{2},j+\frac{1}{2}} - \lambda a_{s,s}\mathcal{D}_x p_{i+\frac{1}{2},j}^{n+1} \\
\overline{\mathfrak{n}}_{i+\frac{1}{2},j+\frac{1}{2}}^{n+1} &= \widehat{\widehat{\mathfrak{n}}}_{i+\frac{1}{2},j+\frac{1}{2}} - \mu a_{s,s}\mathcal{D}_y p_{i,j+\frac{1}{2}}^{n+1}
\end{aligned}
\tag{4.20}
$$

We observe that if we approximate the Laplace operator $\Delta p^{(k)}$, discretized in (4.18) and (4.19), by a *semi-implicit* approximation as

$$
\Delta p(\rho^{(k)}) \approx \nabla(p'(\rho^{*(k)})\nabla\rho^{(k)}),
$$

where $\rho^{*(k)}$ is a quantity computed explicitly from the first equation in (4.13), this implies to solve linear systems in (4.18) and (4.19) for $\overline{\rho}_{i+\frac{1}{2},j+\frac{1}{2}}^{n+1}$ and $\rho_{ij}^{(k)}$.
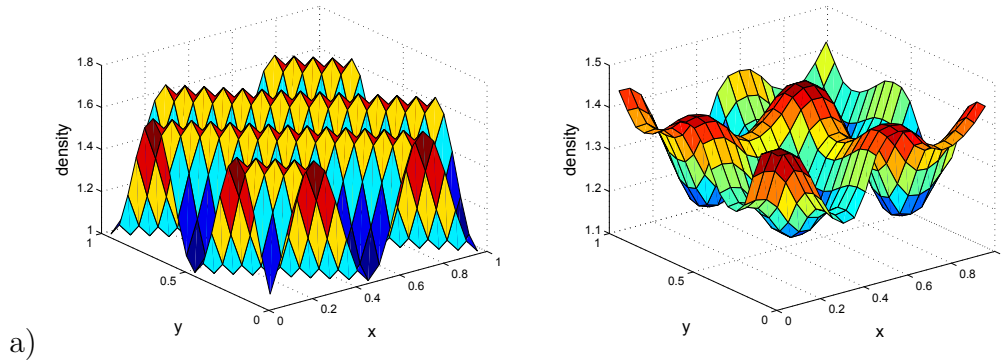
## 4.2   Numerical Tests

### 4.2.1   Example 1: isentropic problem

In this section we show numerical results for the two dimensional case with $p(\rho) = \rho^2$. The computation domain is set to $\Omega = [0,1] \times [0,1]$ with uniform cells. We use the same initial conditions as in [9]:

$$
\begin{cases}
\rho(x,y,0) = 1 + \varepsilon^2 \sin^2(2\pi(x+y)), \\
m(x,y,0) = \sin(2\pi(x-y)) + \varepsilon^2 \sin(2\pi(x+y)), \\
\mathfrak{n}(x,y,0) = \sin(2\pi(x-y)) + \varepsilon^2 \cos(2\pi(x+y)).
\end{cases}
$$

The initial conditions and the numerical results at final time, $T = 1$, are displayed in Fig. 4.1 with $\Delta x = 1/20$, $\Delta t = 1/160$.
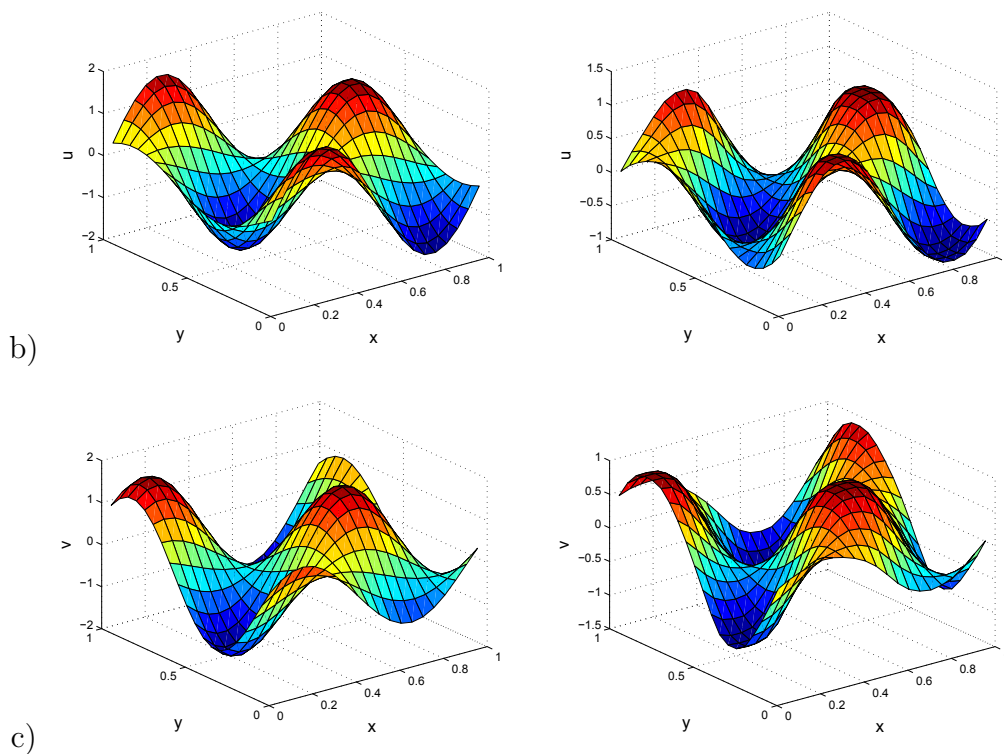


a)

b)

c)

Figure 4.1: Initial density $\rho$ and velocities $u$ and $v$ in the left column, and numerical results for $\rho$; $u$ and $v$, in the right column, with $\varepsilon = 0.8$.

In Figure 4.2, we display in a) the numerical results for the density when $\varepsilon = 0.05$ at time $T = 1$, with $\Delta x = 1/20$, $\Delta t = 1/160$ (left column) and $\Delta x = 1/80$, $\Delta t = 1/640$ (right column). In b) and c) we display the component of the velocity, $u$ and $v$, at time $T = 1$ when $\varepsilon = 10^{-4}$, these results are obtained with $\Delta x = 1/20$, $\Delta t = 1/160$ and $\Delta x = 1/80$, $\Delta t = 1/640$.
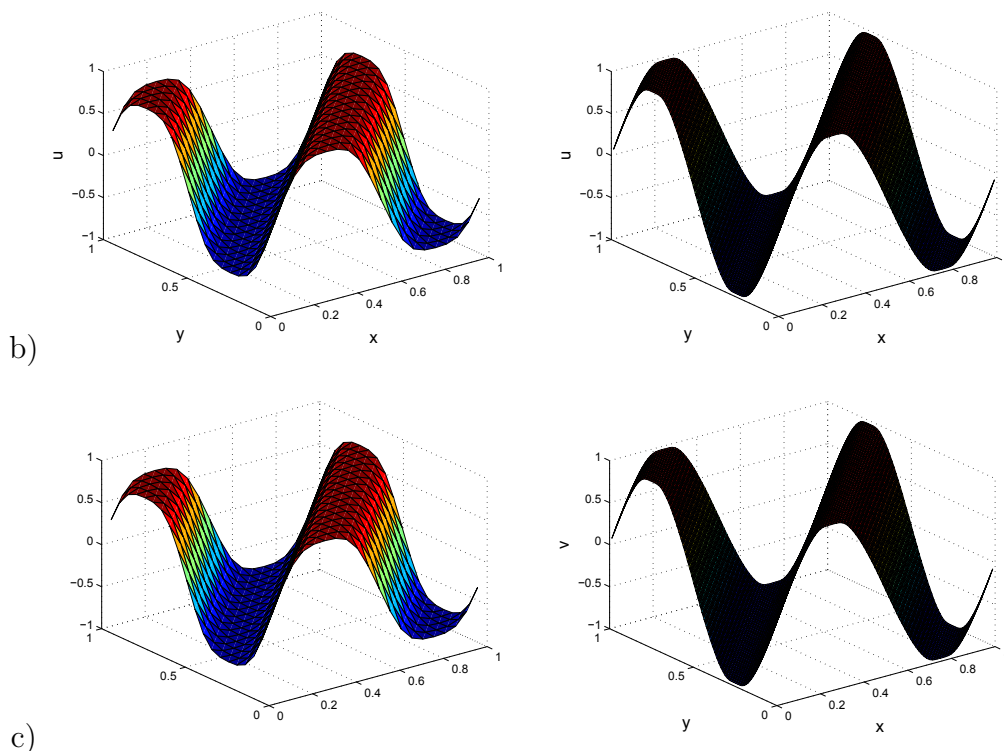


a)

b)

c)
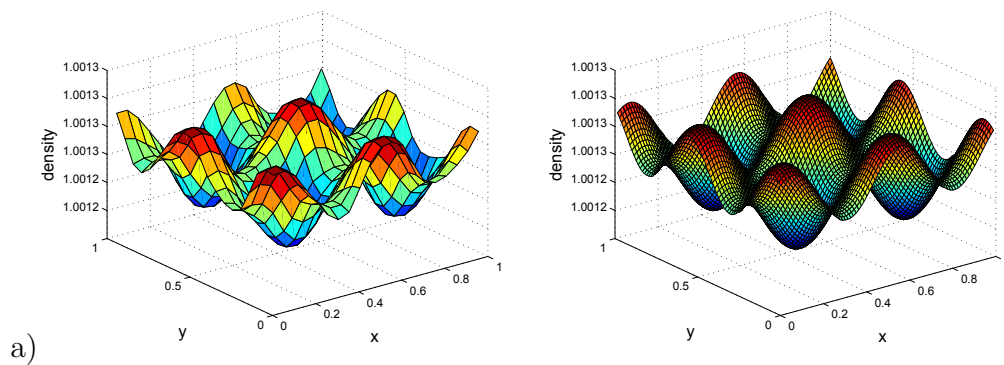
Figure 4.2: Numerical results at time $T = 1$ a): for the density with $\varepsilon = 0.05$, and b),c): for the velocity components: $\vec{u} = (u, v)^T$, when $\varepsilon = 10^{-4}$. For the space and time steps we have: $\Delta x = 1/20$, $\Delta t = 1/160$ (left panel) and $\Delta x = 1/80$, $\Delta t = 1/640$ (right panel).

## 4.2.2  Rate of convergence test

Here we verify the order of convergence in the case in which the Mach number $\varepsilon = 0.8, 0.3, 0.05$. We take a domain of $\Omega = [0, 1] \times [0, 1]$ with $\vec{u} = 0$ on $\partial\Omega$ and symmetric initial condition given by [11]:

$$\begin{cases} \rho = 1 + 0.5\varepsilon^2 e^{-100((x-1/2)^2 + (y-1/2)^2)} \\ u = 0 \\ v = 0 \end{cases}$$

To verify the order of convergence, we use the final time $T = 0.01$ and periodic boundary conditions. The initial profile is chosen in such a way that $\rho - 1$ has basically compact support.

First we verify the order of convergence away from the low Mach number regime by setting $\varepsilon = 1$.

| Density when $\varepsilon = 1$ | | | | |
|---|---|---|---|---|
| N | $L^\infty$ error | $L^\infty$ order | $L^1$ error | $L^1$ order |
| 10 | 8.856e-04 | – | 8.856e-04 | – |
| 20 | 3.984e-04 | 0.0778 | 3.984e-04 | 1.1523 |
| 40 | 1.272e-04 | 1.1666 | 1.272e-04 | 1.6469 |
| 80 | 3.567e-05 | 1.5005 | 3.567e-05 | 1.8348 |

| Density when $\varepsilon = 0.3$ | | | | |
|---|---|---|---|---|
| N | $L^\infty$ error | $L^\infty$ order | $L^1$ error | $L^1$ order |
| 10 | 2.640e-03 | – | 2.640e-03 | – |
| 20 | 1.190e-03 | 1.1497 | 1.190e-03 | 1.2859 |
| 40 | 2.894e-04 | 2.0397 | 2.894e-04 | 1.6091 |
| 80 | 1.344e-04 | 1.1070 | 1.344e-04 | 1.9256 |

We can see the second order of accuracy also for very small Mach number as $\varepsilon = 0.05$

| Density when $\varepsilon = 0.05$ | | | | |
|---|---|---|---|---|
| N | $L^\infty$ error | $L^\infty$ order | $L^1$ error | $L^1$ order |
| 10 | 6.691e-06 | – | 6.691e-06 | – |
| 20 | 3.181e-06 | 1.4761 | 3.181e-06 | 1.0726 |
| 40 | 1.266e-06 | 1.4607 | 1.266e-06 | 1.3293 |
| 80 | 3.676e-07 | 1.6931 | 3.676e-07 | 1.7842 |

## 4.3   Full Euler case

Consider the compressible Euler equations in 2D. We rescale the equations to emphasize the (possibly) small Mach number $\varepsilon$. For simplicity we assume a polytropic gas with constant $\gamma$.

$$
\begin{aligned}
\rho_t + (\rho u)_x + (\rho v)_y &= 0 \\
(\rho u)_t + (\rho u^2 + p/\varepsilon^2)_x + (\rho u v)_y &= 0 \\
(\rho v)_t + (\rho u v)_x + (\rho v^2 + p/\varepsilon^2)_y &= 0 \\
E_t + [(E + p)u]_x + [(E + p)v]_y &= 0
\end{aligned}
\tag{4.21}
$$

Closure relation

$$
p = (\gamma - 1)\left(E - \frac{\varepsilon^2}{2}\rho(u^2 + v^2)\right)
\tag{4.22}
$$

Now, we rewrite system (4.21) in an equivalent way. First of all, we set in the momentum equations $m = \rho u$ and $\mathfrak{n} = \rho v$

$$\rho_t + m_x + \mathfrak{n}_y \;= 0$$

$$m_t + \left( \frac{m^2}{\rho} + \frac{p}{\varepsilon^2} \right)_x + \left( \frac{m\mathfrak{n}}{\rho} \right)_y \;= 0$$

$$\mathfrak{n}_t + \left( \frac{m\mathfrak{n}}{\rho} \right)_x + \left( \frac{\mathfrak{n}^2}{\rho} + \frac{p}{\varepsilon^2} \right)_y \;= 0 \qquad (4.23)$$

$$E_t + \left( \frac{E+p}{\rho} m \right)_x + \left( \frac{E+p}{\rho} \mathfrak{n} \right)_y \;= 0$$

Closure relation

$$p = (\gamma - 1) \left( E - \frac{\varepsilon^2}{2} \frac{m^2 + \mathfrak{n}^2}{\rho} \right) \qquad (4.24)$$

We substitute the pressure (4.24) in the system (4.23) , then we get

$$\rho_t + m_x + \mathfrak{n}_y \;= 0$$

$$m_t + \frac{3 - \gamma}{2} f_x - \frac{\gamma - 1}{2} g_x + h_y + \frac{\gamma - 1}{\varepsilon^2} E_x \;= 0$$

$$\mathfrak{n}_t + h_x - \frac{\gamma - 1}{2} f_y + \frac{3 - \gamma}{2} g_y + \frac{\gamma - 1}{\varepsilon^2} E_y \;= 0 \qquad (4.25)$$

$$E_t - \varepsilon^2 \frac{\gamma - 1}{2} \left[ (q_1)_x + (q_2)_y \right] + \gamma \left[ \left( \frac{Em}{\rho} \right)_x + \left( \frac{E\mathfrak{n}}{\rho} \right)_y \right] \;= 0$$

Here for short we denoted

$$f = \frac{m^2}{\rho}, \quad g = \frac{\mathfrak{n}^2}{\rho}, \quad h = \frac{m\mathfrak{n}}{\rho}, \quad q_1 = \frac{m(f + g)}{\rho}, \quad q_2 = \frac{\mathfrak{n}(f + g)}{\rho}$$

### 4.3.1   Discretization

Now, discretizing again the equations on a staggered grid from time $t^n$ to $t^{n+1}$, using the JT central scheme we obtain:

$$
\begin{aligned}
\overline{\rho}_{i+\frac{1}{2},j+\frac{1}{2}}^{n+1} &= \overline{\rho}_{i+\frac{1}{2},j+\frac{1}{2}}^{n} - \lambda \mathcal{D}_x m_{i+\frac{1}{2},j+\frac{1}{2}}^{n+1} - \mu \mathcal{D}_y \mathfrak{n}_{i+\frac{1}{2},j+\frac{1}{2}}^{n+1} \\[4pt]
\overline{m}_{i+\frac{1}{2},j+\frac{1}{2}}^{n+1} &= \overline{m}_{i+\frac{1}{2},j+\frac{1}{2}}^{n} - \lambda \frac{3-\gamma}{2} \mathcal{D}_x f_{i+\frac{1}{2},j+\frac{1}{2}}^{n} + \lambda \frac{\gamma-1}{2} \mathcal{D}_x g_{i+\frac{1}{2},j+\frac{1}{2}}^{n} \\[4pt]
& \quad - \mu \mathcal{D}_y h_{i+\frac{1}{2},j+\frac{1}{2}}^{n} - \lambda \frac{\gamma-1}{\varepsilon^2} \mathcal{D}_x E_{i+\frac{1}{2},j+\frac{1}{2}}^{n+1} \\[4pt]
\overline{\mathfrak{n}}_{i+\frac{1}{2},j+\frac{1}{2}}^{n+1} &= \overline{\mathfrak{n}}_{i+\frac{1}{2},j+\frac{1}{2}}^{n} - \lambda \mathcal{D}_x h_{i+\frac{1}{2},j+\frac{1}{2}}^{n} + \mu \frac{\gamma-1}{2} \mathcal{D}_y f_{i+\frac{1}{2},j+\frac{1}{2}}^{n} \\[4pt]
& \quad - \mu \frac{3-\gamma}{2} \mathcal{D}_y g_{i+\frac{1}{2},j+\frac{1}{2}}^{n} - \mu \frac{\gamma-1}{\varepsilon^2} \mathcal{D}_y E_{i+\frac{1}{2},j+\frac{1}{2}}^{n+1} \\[4pt]
\overline{E}_{i+\frac{1}{2},j+\frac{1}{2}}^{n+1} &= \overline{E}_{i+\frac{1}{2},j+\frac{1}{2}}^{n} + \varepsilon^2 \frac{\gamma-1}{2} \left( \lambda \mathcal{D}_x (q_1)_{i+\frac{1}{2},j+\frac{1}{2}}^{n} + \mu \mathcal{D}_y (q_2)_{i+\frac{1}{2},j+\frac{1}{2}}^{n} \right) \\[4pt]
& \quad - \gamma \lambda \mathcal{D}_x \left( \frac{E_{i+\frac{1}{2},j+\frac{1}{2}}^{n}}{\rho_{i+\frac{1}{2},j+\frac{1}{2}}^{n}} m_{i+\frac{1}{2},j+\frac{1}{2}}^{n+1} \right) - \gamma \mu \mathcal{D}_y \left( \frac{E_{i+\frac{1}{2},j+\frac{1}{2}}^{n}}{\rho_{i+\frac{1}{2},j+\frac{1}{2}}^{n}} \mathfrak{n}_{i+\frac{1}{2},j+\frac{1}{2}}^{n+1} \right)
\end{aligned}
\tag{4.26}
$$

where $\forall h$:

$$
\mathcal{D}_x h_{i+\frac{1}{2},j+\frac{1}{2}} = \frac{1}{2}(\mathcal{D}_x h_{i+\frac{1}{2},j} + \mathcal{D}_x h_{i+\frac{1}{2},j+1}) \quad , \quad \mathcal{D}_y h_{i+\frac{1}{2},j+\frac{1}{2}} = \frac{1}{2}(\mathcal{D}_y h_{i,j+\frac{1}{2}} + \mathcal{D}_y h_{i+1,j+\frac{1}{2}})
$$

and

$$
\begin{aligned}
\mathcal{D}_x h_{i+\frac{1}{2},j} &= h_{i+1,j} - h_{i,j} \quad , \quad \mathcal{D}_x h_{i+\frac{1}{2},j+1} = h_{i+1,j+1} - h_{i,j+1}, \\[4pt]
\mathcal{D}_y h_{i,j+\frac{1}{2}} &= h_{i,j+1} - h_{i,j} \quad , \quad \mathcal{D}_y h_{i+1,j+\frac{1}{2}} = h_{i+1,j+1} - h_{i+1,j},
\end{aligned}
$$

with $\lambda = \dfrac{\Delta t}{\Delta x}$, $\mu = \dfrac{\Delta t}{\Delta y}$.

Just as in the case of isentropic gas dynamics, an equation for $m_{i,j}^{n+1}$ and $\mathfrak{n}_{i,j}^{n+1}$ is adopted

$$
\begin{aligned}
m_{i,j}^{n+1} &= m_{i,j}^{n} - \lambda \frac{3-\gamma}{2} \mathcal{D}_x f_{i,j}^{n} + \lambda \frac{\gamma-1}{2} \mathcal{D}_x g_{i,j}^{n} - \mu \mathcal{D}_y h_{i,j}^{n} - \lambda \frac{\gamma-1}{\varepsilon^2} \mathcal{D}_x E_{i,j}^{n+1} \\[4pt]
\mathfrak{n}_{i,j}^{n+1} &= \mathfrak{n}_{i,j}^{n} - \lambda \mathcal{D}_x h_{i,j}^{n} + \mu \frac{\gamma-1}{2} \mathcal{D}_y f_{i,j}^{n} - \mu \frac{3-\gamma}{2} \mathcal{D}_y g_{i,j}^{n} - \lambda \frac{\gamma-1}{\varepsilon^2} \mathcal{D}_y E_{i,j}^{n+1}
\end{aligned}
\tag{4.27}
$$

and by replacing $m_{i,j}^{n+1}$ and $n_{i,j}^{n+1}$ into the energy equation, we get:

$$\overline{E}^{n+1}_{i+\frac{1}{2},j+\frac{1}{2}} = \phi^n_{i+\frac{1}{2},j+\frac{1}{2}}$$

$$+\frac{\gamma(\gamma-1)}{\varepsilon^2}\lambda^2\left(\frac{E^n_{i+1,j+\frac{1}{2}}}{\rho^n_{i+1,j+\frac{1}{2}}}E^{n+1}_{i+\frac{3}{2},j+\frac{1}{2}} - \left(\frac{E^n_{i+1,j+\frac{1}{2}}}{\rho^n_{i+1,j+\frac{1}{2}}} + \frac{E^n_{i,j+\frac{1}{2}}}{\rho^n_{i,j+\frac{1}{2}}}\right)E^{n+1}_{i+\frac{1}{2},j+\frac{1}{2}} + \frac{E^n_{i,j+\frac{1}{2}}}{\rho^n_{i,j+\frac{1}{2}}}E^{n+1}_{i-\frac{1}{2},j+\frac{1}{2}}\right)$$

$$+\frac{\gamma(\gamma-1)}{\varepsilon^2}\mu^2\left(\frac{E^n_{i+\frac{1}{2},j+1}}{\rho^n_{i+\frac{1}{2},j+1}}E^{n+1}_{i+\frac{1}{2},j+\frac{3}{2}} - \left(\frac{E^n_{i+\frac{1}{2},j+1}}{\rho^n_{i+\frac{1}{2},j+1}} + \frac{E^n_{i+\frac{1}{2},j}}{\rho^n_{i+\frac{1}{2},j}}\right)E^{n+1}_{i+\frac{1}{2},j+\frac{1}{2}} + \frac{E^n_{i+\frac{1}{2},j}}{\rho^n_{i+\frac{1}{2},j}}E^{n+1}_{i+\frac{1}{2},j-\frac{1}{2}}\right)$$

$$\tag{4.28}$$

with

$$\begin{aligned}
\phi^n_{i+\frac{1}{2},j+\frac{1}{2}} &= E^*_{i+\frac{1}{2},j+\frac{1}{2}} - \gamma\lambda\mathcal{D}_x\left(\frac{E^n_{i+\frac{1}{2},j+\frac{1}{2}}}{\rho^n_{i+\frac{1}{2},j+\frac{1}{2}}}m^n_{i+\frac{1}{2},j+\frac{1}{2}}\right) - \gamma\mu\mathcal{D}_y\left(\frac{E^n_{i+\frac{1}{2},j+\frac{1}{2}}}{\rho^n_{i+\frac{1}{2},j+\frac{1}{2}}}\mathfrak{n}^n_{i+\frac{1}{2},j+\frac{1}{2}}\right) \\
&+ \gamma\frac{3-\gamma}{2}\lambda^2\mathcal{D}_x\left\{\frac{E^n_{i+\frac{1}{2},j+\frac{1}{2}}}{\rho^n_{i+\frac{1}{2},j+\frac{1}{2}}}\mathcal{D}_x f^n_{i+\frac{1}{2},j+\frac{1}{2}}\right\} - \gamma\frac{\gamma-1}{2}\lambda^2\mathcal{D}_x\left\{\frac{E^n_{i+\frac{1}{2},j+\frac{1}{2}}}{\rho^n_{i+\frac{1}{2},j+\frac{1}{2}}}\mathcal{D}_x g^n_{i+\frac{1}{2},j+\frac{1}{2}}\right\} \\
&+ \gamma\lambda\mu\mathcal{D}_x\left\{\frac{E^n_{i+\frac{1}{2},j+\frac{1}{2}}}{\rho^n_{i+\frac{1}{2},j+\frac{1}{2}}}\mathcal{D}_y h^n_{i+\frac{1}{2},j+\frac{1}{2}}\right\} + \gamma\lambda\mu\mathcal{D}_y\left\{\frac{E^n_{i+\frac{1}{2},j+\frac{1}{2}}}{\rho^n_{i+\frac{1}{2},j+\frac{1}{2}}}\mathcal{D}_x h^n_{i+\frac{1}{2},j+\frac{1}{2}}\right\} \\
&- \gamma\frac{\gamma-1}{2}\mu^2\mathcal{D}_y\left\{\frac{E^n_{i+\frac{1}{2},j+\frac{1}{2}}}{\rho^n_{i+\frac{1}{2},j+\frac{1}{2}}}\mathcal{D}_y f^n_{i+\frac{1}{2},j+\frac{1}{2}}\right\} + \gamma\frac{3-\gamma}{2}\mu^2\mathcal{D}_y\left\{\frac{E^n_{i+\frac{1}{2},j+\frac{1}{2}}}{\rho^n_{i+\frac{1}{2},j+\frac{1}{2}}}\mathcal{D}_y g^n_{i+\frac{1}{2},j+\frac{1}{2}}\right\}
\end{aligned}$$

$$\tag{4.29}$$

where

$$E^*_{i+\frac{1}{2},j+\frac{1}{2}} = \overline{E}^n_{i+\frac{1}{2},j+\frac{1}{2}} + \varepsilon^2\frac{\gamma-1}{2}\left(\lambda\mathcal{D}_x(q_1)^n_{i+\frac{1}{2},j+\frac{1}{2}} + \mu\mathcal{D}_y(q_2)^n_{i+\frac{1}{2},j+\frac{1}{2}}\right)$$

The quantity $\phi^n_{i+\frac{1}{2},j+\frac{1}{2}}$ contains what can be computed explicitly. Solving the elliptic Equation (4.28), one obtains $\overline{E}^{n+1}_{i+\frac{1}{2},j+\frac{1}{2}}$, which is then used in the second and third equation of (4.26), and finally the density $\overline{\rho}^{n+1}_{i+\frac{1}{2},j+\frac{1}{2}}$ is computed from the first equation.

## 4.3.2   Asymptotic Preserving Property

Now we show that the scheme is AP, in the sense that it leads to consistent and stable discretization of the limit Equations (1.39). Here the AP property is restricted only to the first order S-IMEX RK scheme (4.26). The extantion to high order scheme in time is straightforward. We consider the two-term

asymptotic *ansatz*

$$p_{ij}^n = p_{0,ij}^n + \varepsilon^2 p_{2,ij}^n + \cdots,$$
$$\rho_{ij}^n = \tilde{\rho}_{0,ij} + \varepsilon^2 \rho_{2,ij}^n + \cdots, \tag{4.30}$$
$$E_{ij}^n = E_{0,ij}^n + \varepsilon^2 E_{2,ij}^n + \cdots.$$

Using an argument similar to the one adopted in Section 1.4.1 to derive the expansion, we assume density $\tilde{\rho}_{0,ij}$ constant in time for all $n$ and the pressure $p_0^n$ independent of space and time with $E_0^n = p_0^n/(\gamma - 1)$ and

$$E_{2,ij}^n = \left( \frac{p_{2,ij}^n}{(\gamma - 1)} + \frac{\rho_{0,ij}^{n-1} |\vec{u}_{0,ij}^{n-1}|^2}{2} \right). \tag{4.31}$$

Furthermore, by (1.41) we take into account the following *well-prepared* initial conditions

$$\rho^0 = \tilde{\rho}_{0,ij} + \varepsilon^2 \rho_{2,ij}^0,$$
$$p^0 = p_{*,ij} + \varepsilon^2 p_{2,ij}^0, \tag{4.32}$$
$$u^0 = u_{0,ij}^0 + \mathcal{O}(\varepsilon),$$

with $p_{*,ij}$ a positive constant. We consider periodic boundary conditions. Now inserting (4.30) in (4.25) we obtain, to the order $\mathcal{O}(\varepsilon^{-2})$, spatially constant energy, i.e.:

$$\frac{\gamma - 1}{\Delta x}(E_{0,j+1,i}^{n+1} - E_{0,j,i}^{n+1}) = 0, \quad \frac{\gamma - 1}{\Delta y}(E_{0,j,i+1}^{n+1} - E_{0,j,i}^{n+1}) = 0,$$

and this yields a space independent energy: $E_{0,ij}^{n+1} = E_0^{n+1}$ and, by

$$p^{n+1} = (\gamma - 1) \left( E^{n+1} - \frac{\varepsilon^2}{2}(\rho\vec{u})^n \right) \tag{4.33}$$

we have $p_{0,ij}^{n+1} = p_0^{n+1} = (\gamma - 1)E_0^{n+1}$. Then we deduce that $E_0^{n+1}$ and $p_0^{n+1}$ are independent of $\mathbf{x}$. For the order $\mathcal{O}(1)$, by summing in the equation for the energy in (4.25) over all $i$, $j$ the expression:

$$\overline{E}_0^{n+1} = \overline{E}_{0,i+\frac{1}{2},j+\frac{1}{2}}^n - \gamma \left[ \lambda \left( \mathcal{D}_x \frac{E_0^n}{\rho_0^n} m_0^{n+1} \right)_{i+\frac{1}{2},j+\frac{1}{2}} + \mu \left( \mathcal{D}_y \frac{E_0^n}{\rho_0^n} \mathfrak{n}_0^{n+1} \right)_{i+\frac{1}{2},j+\frac{1}{2}} \right] \tag{4.34}$$

and recalling that the leading order energy is a constant, and noting that the flux terms telescope and the resulting boundary terms cancel out, we get:

$$\overline{E}_0^{n+1} = \frac{1}{N} \sum_{i,j} \overline{E}_{0,i+\frac{1}{2},j+\frac{1}{2}}^n$$

where $N$ is the total number of grid points in each direction. This tells us that the energy is equal to the average value of the energy, to the previous time step. Furthermore, from (4.30) the energy in the previous step $E_0^n$ is constant in space, and this means that the two quantities coincide. The energy $E_0^{n+1}$ and the pressure $p_0^{n+1} = p^*$ are constant for each $n$, just as in the continuous case. By (4.34), $\tilde{\rho}_{0,ij} = \rho_{0,ij}^{n+1} = \rho_{0,ij}^n$ and by the fact that $\tilde{E} = E_0^n = E_0^{n+1}$ is constant in time and space we get:

$$\gamma\tilde{E}\left[\lambda\left(\mathcal{D}_x u_0^{n+1}\right)_{i+\frac{1}{2},j+\frac{1}{2}} + \mu\left(\mathcal{D}_y v_0^{n+1}\right)_{i+\frac{1}{2},j+\frac{1}{2}}\right] = 0,$$

and, this gives to us the discrete incompressibility condition

$$\overline{\rho}_{0,i+\frac{1}{2},j+\frac{1}{2}}^{n+1} = \overline{\rho}_{0,u+\frac{1}{2},j+\frac{1}{2}}^n - \lambda u_0(\mathcal{D}_x\rho_0^{n+1})_{i+\frac{1}{2},j+\frac{1}{2}} - \mu v_0(\mathcal{D}_y\rho_0^{n+1})_{i+\frac{1}{2},j+\frac{1}{2}}$$

Now by (4.33) and (4.31) we get:

$$\frac{E_{2,ij}^{n+1}}{\gamma - 1} = p_{2,ij}^{n+1} + \rho_{0,ij}^n|\vec{u}^n|_{0,ij}^2,$$

and inserting this expression in the $\mathcal{O}(1)$ term in (4.25) we obtain:

$$\begin{aligned}
\overline{m}_{0,i+\frac{1}{2},j+\frac{1}{2}}^{n+1} &= \overline{m}_{0,i+\frac{1}{2},j+\frac{1}{2}}^n - \lambda\mathcal{D}_x f_{0,i+\frac{1}{2},j+\frac{1}{2}}^n - \mu\mathcal{D}_y h_{0,i+\frac{1}{2},j+\frac{1}{2}}^n - \lambda D_x p_{2,i+\frac{1}{2},j}^{n+1}\\
\overline{\mathfrak{n}}_{0,i+\frac{1}{2},j+\frac{1}{2}}^{n+1} &= \overline{\mathfrak{n}}_{0,i+\frac{1}{2},j+\frac{1}{2}}^n - \lambda\mathcal{D}_x h_{0,i+\frac{1}{2},j+\frac{1}{2}}^n - \mu\mathcal{D}_y g_{0,i+\frac{1}{2},j+\frac{1}{2}}^n - \mu D_y p_{2,i,j+\frac{1}{2}}^{n+1}
\end{aligned}$$
$$(4.35)$$

with $f_{0,ij}^{(n)} = (m^n)_{0,ij}^2/\rho_{0,ij}^n$, $g_{0,ij}^{(n)} = (\mathfrak{n}^n)_{0,ij}^2/\rho_{0,ij}^n$ and $h_{0,ij}^{(n)} = (\rho u v)_{0,ij}^n$. These are the discrete momentum equations at the order $\mathcal{O}(1)$ for the second equation in

$$\begin{cases}
\partial_t\rho_0 + \vec{u}_0 \cdot \nabla(\rho_0) & = 0,\\
\partial_t(\rho_0\vec{u})_0 + \nabla\cdot(\rho_0\vec{u}_0\otimes\vec{u}_0) + \nabla p_2 & = 0,
\end{cases} \qquad (4.36)$$

Therefore our scheme is asymptotic preserving, i.e., in the limit case $\varepsilon \to 0$, with well-prepared initial conditions, we have a consistent approximation of the incompressible Euler equations, i.e. (4.36).

**Remark 9.** *We note that for the leading order terms we have: $\tilde{E} = E_0^n$ constant and $\tilde{\rho}_{0,ij}$ independent of time. Then, we obtain, by (4.3.1), in the case $\varepsilon = 0$, that $E^*_{i+\frac{1}{2},j+\frac{1}{2}} = \overline{E}^n_{i+\frac{1}{2},j+\frac{1}{2}}$, and by (4.29), as proved for the isentropic case from (4.5), the pressure satisfies Eq. (4.9), which is a discretization of the equation: $-\Delta p_2 = \rho_0\nabla^2 : (\vec{u}\otimes\vec{u})$.*

### 4.3.3   GSA S-IMEX-JT scheme

In this section we show how to construct high order (in time) scheme, making us of the first order one described in the previous section. In particular, we obtain a second order accuracy *globally stiffly accurate* GSA S-IMEX method. The idea is to write Equations (4.25) as a system of the form (2.16) where the first argument $\mathbf{U}^* = (\rho^*, \vec{m}^*, E^*)$ is treated explictly and the second argument $\mathbf{U} = (\rho, \vec{m}, E)$ is treated implictly. In our case the function $\mathcal{H}(\mathbf{U}^*, \mathbf{U})$ is defined as follows:

$$
\mathcal{H}(\mathbf{U}^*, \mathbf{U}) = \begin{pmatrix} -\nabla \cdot \vec{m} \\ (\gamma - 2)\nabla \cdot \left( \dfrac{(\vec{m}^*)^2}{\rho^*} \right) - \nabla h^* - \dfrac{\gamma - 1}{\varepsilon^2} \nabla E \\ \dfrac{\gamma - 1}{2} \varepsilon^2 \nabla \cdot \left( \dfrac{|\vec{m}^*|^2 \vec{m}^*}{(\rho^*)^2} \right) - \gamma \nabla \cdot \left( \dfrac{E^*}{\rho^*} \vec{m} \right) \end{pmatrix} \tag{4.37}
$$

with $\mathbf{m} = (m, \mathfrak{n})^T$. Then, by the previous section, the simplest first-order S-IMEX-RK scheme applied to (3.18) is given by (4.26), i.e.,

$$
\mathcal{H}(\mathbf{U}^n, \mathbf{U}^{n+1}) = \begin{pmatrix} -\nabla \vec{m}^{n+1} \\ (\gamma - 2)\nabla \cdot \left( \dfrac{(\vec{m}^n)^2}{\rho^n} \right) - \nabla h^n - \dfrac{\gamma - 1}{\varepsilon^2} \nabla \cdot E^{n+1} \\ \nabla \cdot \left( \dfrac{\gamma - 1}{2} \varepsilon^2 \dfrac{|\vec{m}^n|^2 \vec{m}^n}{(\rho^n)^2} \right) - \nabla \cdot (\gamma E^n \dfrac{\vec{m}^{n+1}}{\rho^n}). \end{pmatrix} \tag{4.38}
$$

In this new approach the system (2.19) is linear in the variable $\mathbf{U}$ as for the first order (4.28).

Of course high order S-IMEX-RK schemes in time can be obtained by adopting high order IMEX R-K schemes. Then, if $s$ represents the number of the internal stages of an IMEX RK scheme, and considering the JT central scheme for the space discretization, a direct extension of the compressible Euler system, as done for the isentropic case, is given by:

- **Prediction step**:

$$
\mathbf{U}_{ij}^{*(k)} = \mathbf{U}_{ij}^n + \sum_{\ell=1}^{k-1} \tilde{a}_{k,\ell} K_\ell, \quad \hat{\mathbf{U}}_{ij}^{(k)} = \mathbf{U}_{ij}^n + \sum_{\ell=1}^{k-1} a_{k,\ell} K_\ell,
$$

with

$$
K_\ell := \mathcal{H}(\mathbf{U}_{ij}^{*(\ell)}, \mathbf{U}_{ij}^{(\ell)}) =
$$

$$
\begin{pmatrix}
-\left(\lambda\mathcal{D}_x m_{ij}^{(\ell)} + \mu\mathcal{D}_y n_{ij}^{(\ell)}\right) \\[4pt]
-\lambda\frac{3-\gamma}{2}\mathcal{D}_x f_{ij}^{*(\ell)} + \lambda\frac{\gamma-1}{2}\mathcal{D}_x g_{ij}^{*(\ell)} - \mu\mathcal{D}_y h_{ij}^{*(\ell)} - \lambda\frac{\gamma-1}{\varepsilon^2}\mathcal{D}_x E_{ij}^{(\ell)} - \cdots \\[4pt]
\cdots - \lambda\mathcal{D}_x h_{ij}^{*(\ell)} + \mu\frac{\gamma-1}{2}\mathcal{D}_y f_{ij}^{*(\ell)} - \mu\frac{3-\gamma}{2}\mathcal{D}_y g_{ij}^{*(\ell)} - \mu\frac{\gamma-1}{\varepsilon^2}\mathcal{D}_y E_{ij}^{(\ell)} \\[4pt]
\frac{\gamma-1}{2}\varepsilon^2\left[\lambda\mathcal{D}_x q_{1,ij}^{*(\ell)} + \mu\mathcal{D}_y q_{2,ij}^{*(\ell)}\right] - \gamma\left[\lambda\mathcal{D}_x\left(\frac{E^{*(\ell)}}{\rho^{*(\ell)}}m^{(\ell)}\right)_{ij} + \mu\mathcal{D}_y\left(\frac{E^{*(\ell)}}{\rho^{*(\ell)}}\mathfrak{n}^{(\ell)}\right)_{ij}\right]
\end{pmatrix}
$$

and

$$
\mathbf{U}_{ij}^{(k)} = \hat{\mathbf{U}}_{ij}^{(k)} + a_{k,k}K_k
$$

- **Correction step:** Here we require that our IMEX RK is *globally stiffly accurate*, then, from time $t^n$ to $t^{n+1}$, the numerical solution reads:

$$
\overline{\mathbf{U}}{}^{*n+1}_{i+\frac{1}{2},j+\frac{1}{2}} = \overline{\mathbf{U}}{}^{n}_{i+\frac{1}{2},j+\frac{1}{2}} + \sum_{\ell=1}^{s-1}\tilde{a}_{s,\ell}K_\ell, \quad \overline{\mathbf{U}}{}^{n+1}_{i+\frac{1}{2},j+\frac{1}{2}} = \overline{\mathbf{U}}{}^{n}_{i+\frac{1}{2},j+\frac{1}{2}} + \sum_{\ell=1}^{s}a_{s,\ell}K_\ell,
$$

with

$$
K_\ell =
\begin{pmatrix}
-\left(\lambda\mathcal{D}_x m^{(\ell)}_{i+\frac{1}{2},j+\frac{1}{2}} + \mu\mathcal{D}_y n^{(\ell)}_{i+\frac{1}{2},j+\frac{1}{2}}\right) \\[4pt]
-\lambda\frac{3-\gamma}{2}\mathcal{D}_x f^{*(\ell)}_{i+\frac{1}{2},j+\frac{1}{2}} + \lambda\frac{\gamma-1}{2}\mathcal{D}_x g^{*(\ell)}_{i+\frac{1}{2},j+\frac{1}{2}} - \mu\mathcal{D}_y h^{*(\ell)}_{i+\frac{1}{2},j+\frac{1}{2}} - \cdots \\[4pt]
\cdots - \lambda\frac{\gamma-1}{\varepsilon^2}\mathcal{D}_x E^{(\ell)}_{i+\frac{1}{2},j+\frac{1}{2}} - \lambda\mathcal{D}_x h^{*(\ell)}_{i+\frac{1}{2},j+\frac{1}{2}} + \mu\frac{\gamma-1}{2}\mathcal{D}_y f^{*(\ell)}_{i+\frac{1}{2},j+\frac{1}{2}} - \cdots \\[4pt]
\cdots - \mu\frac{3-\gamma}{2}\mathcal{D}_y g^{*(\ell)}_{i+\frac{1}{2},j+\frac{1}{2}} - \mu\frac{\gamma-1}{\varepsilon^2}\mathcal{D}_y E^{(\ell)}_{i+\frac{1}{2},j+\frac{1}{2}} \\[4pt]
\frac{\gamma-1}{2}\varepsilon^2\left[\lambda\mathcal{D}_x q^{*(\ell)}_{1,i+\frac{1}{2},j+\frac{1}{2}} + \mu\mathcal{D}_y q^{*(\ell)}_{2,i+\frac{1}{2},j+\frac{1}{2}}\right] - \cdots \\[4pt]
\cdots - \gamma\left[\lambda\mathcal{D}_x\left(\frac{E^{*(\ell)}}{\rho^{*(\ell)}}m^{(\ell)}\right)_{i+\frac{1}{2},j+\frac{1}{2}} + \mu\mathcal{D}_y\left(\frac{E^{*(\ell)}}{\rho^{*(\ell)}}\mathfrak{n}^{(\ell)}\right)_{i+\frac{1}{2},j+\frac{1}{2}}\right]
\end{pmatrix}
$$

In a similar fashion as done in the first order semi-impicit scheme, by using equations $m_{ij}^{(\ell)}$ and $\mathfrak{n}_{ij}^{(\ell)}$, we obtain for the energy

$$
\overline{E}^{n+1}_{i+\frac{1}{2},j+\frac{1}{2}} = \phi^n_{i+\frac{1}{2},j+\frac{1}{2}}
$$

$$
+\frac{\gamma(\gamma-1)}{\varepsilon^2}a_{s,s}\lambda^2\left(\frac{E^{*(s)}_{i+1,j+\frac{1}{2}}}{\rho^{*(s)}_{i+1,j+\frac{1}{2}}}E^s_{i+\frac{3}{2},j+\frac{1}{2}} - \left(\frac{E^{*(s)}_{i+1,j+\frac{1}{2}}}{\rho^{*(s)}_{i+1,j+\frac{1}{2}}} + \frac{E^{*(s)}_{i,j+\frac{1}{2}}}{\rho^{*(s)}_{i,j+\frac{1}{2}}}\right)E^s_{i+\frac{1}{2},j+\frac{1}{2}} + \frac{E^{*(s)}_{i,j+\frac{1}{2}}}{\rho^{*(s)}_{i,j+\frac{1}{2}}}E^s_{i-\frac{1}{2},j+\frac{1}{2}}\right)
$$

$$
+\frac{\gamma(\gamma-1)}{\varepsilon^2}a_{s,s}\mu^2\left(\frac{E^{*(s)}_{i+\frac{1}{2},j+1}}{\rho^{*(s)}_{i+\frac{1}{2},j+1}}E^s_{i+\frac{1}{2},j+\frac{3}{2}} - \left(\frac{E^{*(s)}_{i+\frac{1}{2},j+1}}{\rho^{*(s)}_{i+\frac{1}{2},j+1}} + \frac{E^{*(s)}_{i+\frac{1}{2},j}}{\rho^{*(s)}_{i+\frac{1}{2},j}}\right)E^s_{i+\frac{1}{2},j+\frac{1}{2}} + \frac{E^{*(s)}_{i+\frac{1}{2},j}}{\rho^{*(s)}_{i+\frac{1}{2},j}}E^s_{i+\frac{1}{2},j-\frac{1}{2}}\right)
$$

$$
\tag{4.39}
$$

where, as usual, by $\phi^n_{i+\frac{1}{2},j+\frac{1}{2}}$ we denote something that can be computed explicitly and we can solve the linear Equation (4.39) to compute $\overline{E}^{n+1}_{i+\frac{1}{2},j+\frac{1}{2}}$.

## 4.4 Numerical Tests

### 4.4.1 Example 1: Travelling vortex

We consider a test that does not contain acoustic waves, a *Travelling Vortex*, that represents a moving vortex with compact support vorticity. [2] The initial data are given by

$$
\begin{cases}
\rho(x,y,0) = 110 + \left(\frac{1.5\varepsilon}{4\pi}\right)^2 (k(4\pi r) - k(\pi))\chi_{4r\leqslant 1}, \\
u(x,y,0) = 0.6 + 1.5(1 + \cos(4\pi r))(0.5 - y)\chi_{4r\leqslant 1}, \\
v(x,y,0) = 1.5(1 + \cos(4\pi r))(x - 0.5)\chi_{4r\leqslant 1}
\end{cases}
$$

where $r = \|\mathbf{x} - (0.5, 0.5)^T\|$, and Froude number: $Fr = \dfrac{u_0}{\sqrt{gL}} = \dfrac{0.6\varepsilon}{\sqrt{110}}$,

$$
k(r) = 2\cos(r) + 2r\sin(r) + \frac{\cos(2r)}{8} + \frac{r}{4}\sin(2r) + \frac{3}{4}r^2.
$$

The initial data describes a rotating vortex that is placed in the middle of a computational domain $\Omega$. The computational domain is $\Omega = [0,1] \times [0,1]$ and periodic boundary conditions are considered in this model.
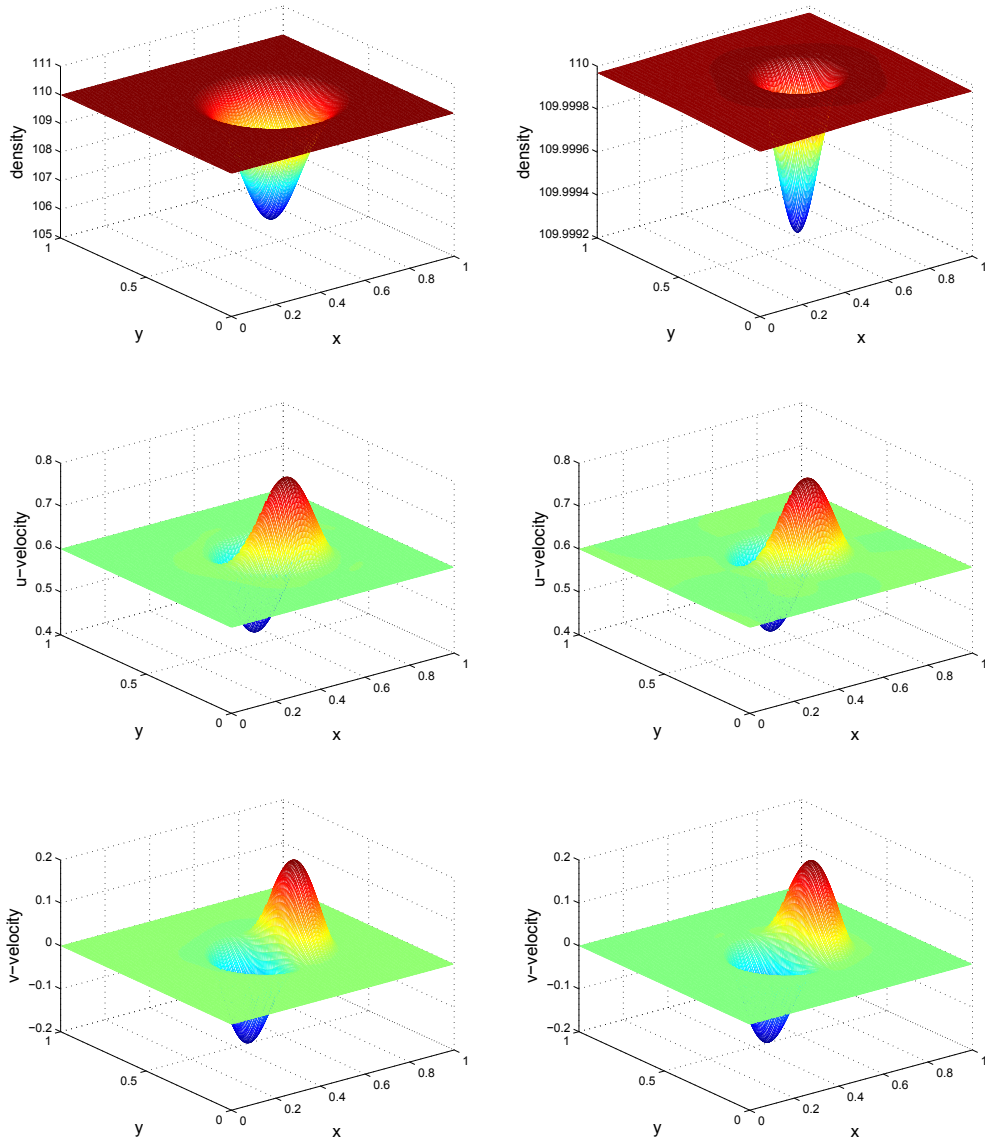
Figure 4.3: Numerical Solutions for the travelling vortex at final time $T = 0.1$, $Fr = 0.8$ (left panel) and $Fr = 0.01$ (right panel). From the top: density, $u$-component of the velocity and the $v$-component of the velocity.

In Figure 4.3 we show numerical solutions for the travelling vortex at final time $T = 0.1$ with Froude number $Fr = 0.8$ (left panel) and $Fr = 0.01$ (right panel). On the top the density of the fluid, in the middle the $u$-component of the velocity and on the bottom the $v$-component of the velocity.

Furthermore, in this example the convergence of the second order time discretization, coupled with the second order space JT discretization is investigated. In the tables we report the results for the cases in which the value of the Froude number are $Fr = 0.8$ (compressible case), moderately small $Fr = 0.01$ (intermediate case), and very small $Fr = 10^{-4}$ (incompressible case).

We set the final time $T = 0.1$ for the two cases $Fr = 0.8$ and $Fr = 0.01$ and $T = 0.01$ for the last one, so that we can appreciate second order accuracy also when the Mach number is very small.

| Mach = 0.8,   T= 0.1 | | | | |
|---|---|---|---|---|
| N | $L^1$-error $m$ | EOC $m$ | $L^1$-error $n$ | EOC $n$ |
| 10 | 2.736e-03 | – | 1.700e-01 | – |
| 20 | 2.344e-03 | 0.2232 | 1.184e-01 | 0.5217 |
| 40 | 7.247e-04 | 1.6934 | 3.566e-02 | 1.7312 |
| 80 | 1.700e-04 | 2.0923 | 8.314e-03 | 2.1006 |
| 160 | 4.101e-05 | 2.0512 | 1.997e-03 | 2.0580 |

| Mach = 0.01,   T= 0.1 | | | | |
|---|---|---|---|---|
| N | $L^1$-error $m$ | EOC $m$ | $L^1$-error $n$ | EOC $n$ |
| 10 | 2.748e-03 | – | 1.683e-01 | – |
| 20 | 2.378e-03 | 0.2085 | 1.198e-01 | 0.4912 |
| 40 | 7.478e-04 | 1.6690 | 3.682e-02 | 1.7015 |
| 80 | 1.765e-04 | 2.0828 | 8.664e-03 | 2.0875 |
| 160 | 4.311e-05 | 2.0337 | 2.114e-03 | 2.0352 |

| Mach = $10^{-4}$,   T= 0.01 | | | | |
|---|---|---|---|---|
| N | $L^1$-error $m$ | EOC $m$ | $L^1$-error $n$ | EOC $n$ |
| 10 | 1.857e-03 | – | 9.200e-02 | – |
| 20 | 5.500e-04 | 1.7556 | 2.698e-02 | 1.7697 |
| 40 | 1.072e-04 | 2.3596 | 5.325e-03 | 2.3411 |
| 80 | 2.886e-05 | 1.8927 | 1.407e-03 | 1.9201 |
| 160 | 8.191e-06 | 1.8171 | 4.016e-04 | 1.8087 |
| 320 | 2.164e-06 | 1.9203 | 1.061e-04 | 1.9205 |

## 4.4.2 Example2: Vorticity stream-function

In the sections 4.1.2 and 4.3.2 we have discussed the asymptotic preserving property for the globally second order IMEX-RK scheme and for the globally second order S-IMEX-RK scheme. The aim of this section is to verify the AP property, numerically. We recall here that: a numerical scheme applied to the compressible (or isentropic) Euler equations is called to be AP if in the limit as $\varepsilon \to 0$ (here, $\varepsilon$ is the scaled Mach number), such scheme provides a consistent discretization of the incompressible Euler equation.

In this chapter, we show that the AP property is satisfied for our scheme when applied to the 2D compressible isentropic Euler equations and to the 2D (3.4) complete Euler ones (3.17) in the limit case $\varepsilon \to 0$, i.e., for low Mach numbers. In particular, what we show is the convergence of the solutions of our scheme to the ones of the 2D incompressible Euler equations. Furthermore, this confirm that our second order scheme is stable and accurate for low Mach numbers.

As a test case, we consider the 2D incompressible Euler equation in the vorticity stream-function formulation as following:

$$\omega_t + \vec{u} \cdot \nabla \omega = 0, \quad (x, y) \in [0, 2\pi] \times [0, 2\pi] \tag{4.40}$$

where

$$w = \frac{\partial v}{\partial x} - \frac{\partial u}{\partial y}$$

Since $\nabla \cdot \vec{u} = 0$, there exists a function $\psi$ such that $\vec{u} = (\partial_y \psi, -\partial_x \psi)$. Inserting this relation in the expression for $w$ one obtains the Poisson equation $-\Delta \psi = \omega$.

For our numerical test we assume periodic boundary conditions and we consider as initial conditions, the shear flow given by [25]

$$\omega(x, y, 0) = \begin{cases} \delta \cos(x) - \dfrac{1}{\rho} sech^2((y - \pi/2)/\rho), & y \leqslant \pi \\ \delta \cos(x) + \dfrac{1}{\rho} sech^2((3\pi/2 - y)/\rho), & y > \pi \end{cases} \tag{4.41}$$

where $\delta = 0.05$ and $\rho = \frac{\pi}{15}$. In the Figure 4.4 we solved (4.40) by an accurate spectral method with $N = 160$ points per direction at final time $T = 6.0$.
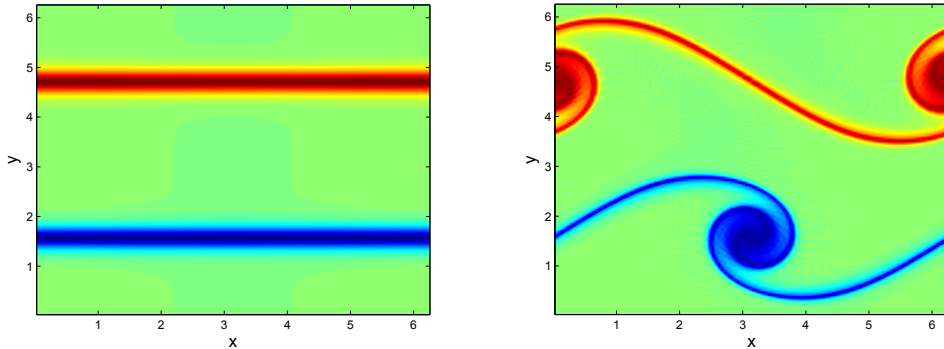
75

Figure 4.4: Plot of the numerical solution of the equation (4.41) at initial time $t = 0$ (left) and at final time $T = 6$ (right).

We test the performance of our scheme at low Mach number applied to the isentropic Euler equations (3.4) and to the complete Euler ones (3.17). We set $\varepsilon = 10^{-4}$, initial conditions (4.41), periodic boundary conditions $N = 160$ and final time $T = 6.0$. We consider as reference solution the numerical one computed by solving system (4.40) by an accurate spectral method in space and a fourth order Runge-Kutta scheme in time as in Fig. 4.4 (right panel). Results in Fig. (4.5) are consistent when compared with the reference solution in Fig. (4.41). This test suggests that our scheme satisfies the asymptotic preserving property.
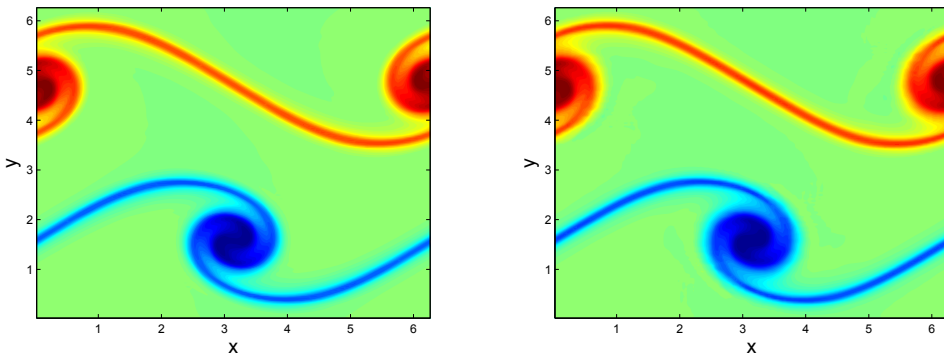


Figure 4.5: Plot of the numerical solutions of the Euler systems (3.4) (left isentropic case), and (3.17) (right full case) when the Mach number $\varepsilon = 10^{-4}$ at final time $T = 6$

Finally, in Figure 4.6 we can see the behaviour of the $L^1$ error, as the difference between the numerical solution of our scheme and the reference one, while the Mach number decreases from $10^{-1}$ to $10^{-4}$. When Mach number becomes smaller and smaller, we observe that the model error reduces, i.e,

the numerical solution of our system is converging exactly to the reference one of the incompressible system (4.40).

We begin with $\Delta x = 2\pi/16$ and $\Delta t$ given by CFL gas dynamics condition

$$\Delta t \leqslant \frac{\text{CFL}}{\dfrac{\lambda_{max}}{\Delta x} + \dfrac{\mu_{max}}{\Delta y}} \tag{4.42}$$

where $\lambda_{max} = \max\left(|u|\right) + c_s$ and $\mu_{max} = \max\left(|v|\right) + c_s$ with $c_s = \sqrt{\frac{\gamma p}{\rho}}$ and refine the simulation to the final time $T = 0.01$, using $1024 \times 1024$ computation as reference solution. The result show second-order convergence, as expected. For moderate Mach numbers, as $\varepsilon = 10^{-1}$, the error initially decreases as the grid is refined, but then it settles to an approximately constant value, which measure the different behavior of slightly compressible and incompressible Euler equation (model error).
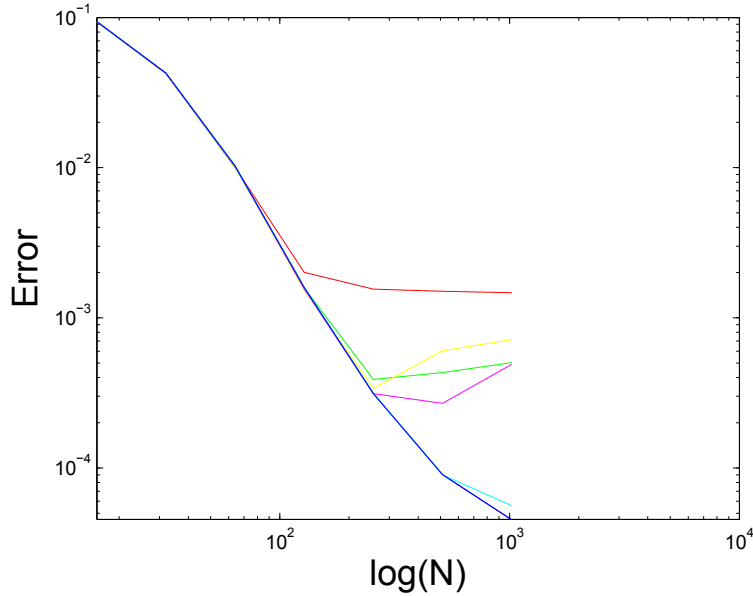


Figure 4.6: $L^1$ error between incompressible fluid complete Euler system at difference Mach values: $\varepsilon = 10^{-1}$, $7.7 \cdot 10^{-2}$, $5.5 \cdot 10^2$, $3.25 \cdot 10^{-2}$, $10^{-2}$, $10^{-3}$ and $N = 16, 32, 64, \cdots, 1024$. The final time is $T = 1$.

# Application

## 5.1 Lagrangian form

We start rewriting the Euler equations in Lagrangian form. Starting from the full Euler equations in conservative form

$$\rho_t + (\rho u)_x = 0$$

$$(\rho u)_t + (\rho u^2 + p)_x = 0$$

$$E_t + [(E + p)u]_x = 0$$

taking into account the relation $E = \rho \xi = \rho \left(e + \frac{1}{2}u^2\right)$, where $e = \frac{1}{\gamma-1}\frac{p}{\rho}$ denotes the polytropic gas. We consider the following change of variable and coordinates by introducing the specific volume $v = 1/\rho$, and mass coordinate $\alpha$ defined by $\rho dx = d\alpha$. In these new coordinates the starting system becomes:

$$\begin{aligned} v_t - u_\alpha &= 0 \\ u_t + p_\alpha &= 0 \\ \xi_t + (pu)_\alpha &= 0 \end{aligned} \tag{5.1}$$

where the **equation of state** takes the form

$$p = \frac{\gamma - 1}{v}\left(\xi - \frac{1}{2}u^2\right) \tag{5.2}$$

System (5.1) with closure (5.2) is hyperbolic, and can be written in the form

$$U_t + F(U)_\alpha = 0,$$

with

$$U = \begin{pmatrix} v \\ u \\ \xi \end{pmatrix}, \quad F(U) = \begin{pmatrix} -u \\ p \\ pu \end{pmatrix} \tag{5.3}$$

For smooth solutions one has $U_t + AU_\alpha = 0$, where the Jacobian matrix is equal to

$$A = \begin{bmatrix} 0 & -\frac{1}{v^2} & 0 \\ 0 & 0 & 1 \\ 0 & c_L^2 & 0 \end{bmatrix}$$

where $c_L = \sqrt{\frac{\gamma p}{v}}$ represents the Lagrangian *speed of sound* and the respective eigenvalues are

$$\lambda_1 = -c_L, \quad \lambda_2 = 0, \quad \lambda_3 = +c_L$$

when discretizing (5.1) by classical explicit finite volume scheme, one has to satisfy a CFL type stability restriction of the form

$$\Delta t \leqslant \frac{\text{CFL } \Delta x}{c_{max}}$$

where $c_{max} = \max\limits_j (c_L)_j^n$.

## 5.2 Time Discretization

In this section we apply the semi-implicit scheme developed before to the Euler equations in the Lagrangian formulation. Let us discretize system (5.1) to the first order in time using an S-IMEX approach from $t^n$ to $t^{n+1}$, and consider central difference method in space on a Cartesian grid keeping the conservative form.

$$
\begin{aligned}
v_j^{n+1} &= v_j^n + \Delta t \mathcal{D}_\alpha u_j^{n+1} \\
u_j^{n+1} &= u_j^n - \Delta t \mathcal{D}_\alpha p_j^{n+1} \\
\xi_j^{n+1} &= \xi_j^n - \Delta t \mathcal{D}_\alpha (p_j^n u_j^{n+1})
\end{aligned}
\tag{5.4}
$$

By replacing $u_j^{n+1}$ in the energy equation and considering the closure relation given by (5.2), we get:

$$
\begin{aligned}
\xi_j^{n+1} = \quad &\phi_j^n + (\gamma - 1)\frac{\Delta t^2}{\Delta \alpha^2} \cdots \\
\cdots &\left( \frac{p_{j+\frac{1}{2}}^n}{v_{j+1}^n} \xi_{j+1}^{n+1} - \left( \frac{p_{j+\frac{1}{2}}^n}{v_j^n} + \frac{p_{j-\frac{1}{2}}^n}{v_j^n} \right) \xi_j^{n+1} + \frac{p_{j-\frac{1}{2}}^n}{v_{j-1}^n} \xi_{j-1}^{n+1} \right)
\end{aligned}
\tag{5.5}
$$

with

$$\phi_j^n = \xi_j^* - \frac{\gamma-1}{2}\frac{\Delta t^2}{\Delta\alpha^2}\left[\left(\frac{u^2}{v}\right)_{j+1}^n p_{j+\frac{1}{2}}^n - \left(\frac{u^2}{v}\right)_j^n (p_{j+\frac{1}{2}}^n + p_{j-\frac{1}{2}}^n) + \left(\frac{u^2}{v}\right)_{j-1}^n p_{j-\frac{1}{2}}^n\right]$$
$$(5.6)$$

where

$$\xi_j^* = \xi_j^n - \Delta t \mathcal{D}_\alpha (pu)_j^n \tag{5.7}$$

The quantity $\phi_j^n$ contains something that can be computed explicitly. The result is in the solution of a simple tridiagonal system at each time step. Solving the elliptic equation (5.5), we get $\xi_j^{n+1}$, then using (5.2) we get the pressure value at time $t^{n+1}$

$$p_j^{n+1} = \frac{\gamma-1}{v_j^n}\left(\xi_j^{n+1} - \frac{1}{2}(u^2)_j^n\right) \tag{5.8}$$

**Remark 10.** *We observe that the quantity $\frac{1}{2}u^2$ is small, then we can treat it explicitly.*

Equation (5.8) is used in the second equation of (5.4), and at the end specific volume $v_j^{n+1}$ is computed from the first equation.

## 5.3 Piston Problem

Suppose to have a cylindrical container with a moving wall and a steady wall, isolated and containing a polytropic gas with certain conditions of pressure, density and temperature. If the piston moves slowly when it compresses the gas, the density is raised adiabatically, and vice versa.
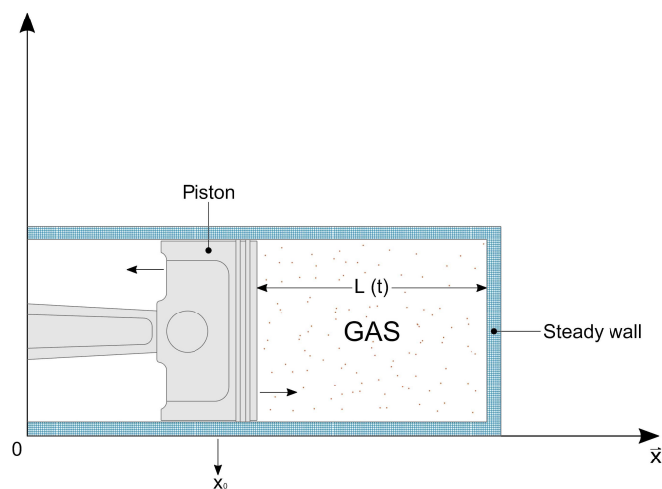


Figure 5.1

Pressure gradients are vanishingly small as the piston velocity approaches zero. Let us see that with second order method in time we are able to capture the acoustic waves with our semi-implicit method, when the piston moves slowly, for example at CFL = 1. While the profile will be smoothed out at much larger time steps, say for example at CFL = 10. In this last case we can not capture the acoustic waves.
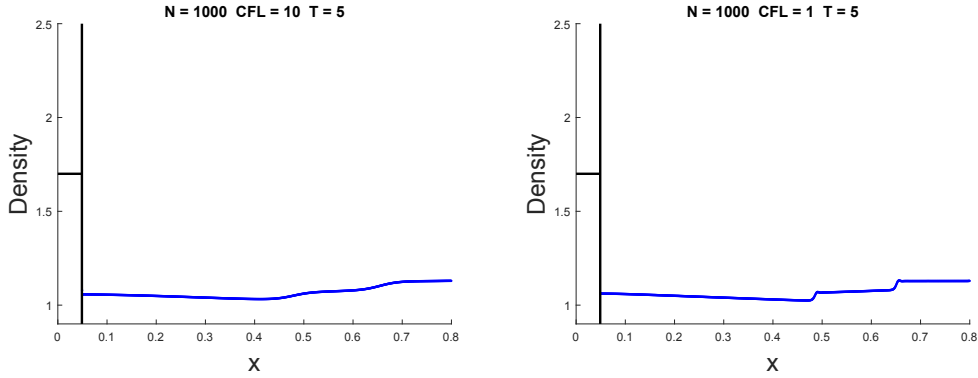
Figure 5.2

Furthermore, by moving the piston the gas undergoes a transformation. We would like to know under which conditions the behaviour can be considered adiabatic. We know that in an adiabatic transformation pressure and volume are related by the following relation:

$$pV^\gamma = const$$

Obtaining that

$$p(t) = p_0 \left( \frac{L_0}{L(t)} \right)^\gamma$$

## 5.3.1   Boundary conditions

The use of Lagrangian coordinates for a piston is convenient because the boundary conditions are easy to calculate. Furthermore, in the piston problem the computational domain is fixed, since the total amount of mass inside the domain $\Omega$ is constant, and therefore the mass variable spans from 0 to $M = \int_0^L \rho_0(x)dx = \int_{x_p(t)}^L \rho(x,t)dx$. In this model we have two types of boundaries: a moving one (the piston) and a fixed one (the wall). Divide the grid in $N$ points: $x_1, \ldots, x_N$. Suppose we know our solution on these $N$ grid points and insert two *ghost points* at the extremes of our stencil $x_0$ and $x_{N+1}$. Obviously the piston moves, therefore is subject to a velocity $v_p(t)$ and an acceleration $a_p(t)$.

So we have that $\alpha \in [0, M]$, where $M = \int_{x_p(t)}^L \rho(x,t)dx$.

**Left boundary layer** The velocity of the gas is equal to the velocity of the wall

$$u|_{\alpha=0} = v_p(t)$$

while the pressure is such that

$$\left.\frac{\partial p}{\partial \alpha}\right|_{\alpha=0} = -a_p(t) = -\frac{\gamma p}{v}\left.\frac{\partial u}{\partial \alpha}\right|_{\alpha=0}$$

Then in the moving wall the numerical conditions to assign to the variables are

$$u_0 = 2v_p - u_1$$

$$p_0 = p_1 + a_p \Delta\alpha$$

$$v_0 = v_1 \frac{(\gamma-1)p_0 + (\gamma+1)p_1}{(\gamma+1)p_0 + (\gamma-1)p_1} \qquad (5.9)$$

$$\xi_0 = \frac{1}{2}u_0^2 + \frac{v_0 p_0}{\gamma-1}$$

**Right boundary layer** In this case

$$u|_{\alpha=M} = 0$$

then the derivatives taking to be zero

$$\left.\frac{\partial p}{\partial \alpha}\right|_{\alpha=M} = 0, \quad \left.\frac{\partial u}{\partial \alpha}\right|_{\alpha=M} = 0$$

Then in the steady wall the numerical conditions to assign to the variables are the follow

$$u_{N+1} = -u_N$$

$$p_{N+1} = p_N$$

$$v_{N+1} = v_N \qquad (5.10)$$

$$\xi_{N+1} = \frac{1}{2}u_{N+1}^2 + \frac{v_{N+1} p_{N+1}}{\gamma-1}$$

## 5.4   Adiabatic Approximation

Consider as test a problem under the following conditions

$$L(t) = L_0 - x_p(t), \quad \text{with } x_p(t) = \mathcal{A}(1 - \cos(\omega t))$$

where $L_0 = L(0) = 0.8$ is the initial piston length, $\mathcal{A} = 0.2$ is the amplitude, $\omega = 2\pi/T$ is the impulse, and $T = 0.1$ represents the final time.

As initial data we are considering a simple wave since that its solution travels along a characteristic line, up to the moment in which shocks are formed.

The initial conditions on the variables are given by:

$$
\begin{aligned}
a(x) &= a_1 + \frac{\gamma - 1}{2} u(x) \\
\rho(x) &= \rho_1 \left( \frac{a(x)}{a_1} \right)^{\frac{2}{\gamma - 1}} \\
p(x) &= p_1 \left( \frac{\rho(x)}{\rho_1} \right)^{\gamma}
\end{aligned}
\tag{5.11}
$$

The function $u(x)$ is defined as

$$
u(x) = \begin{cases} 0 & \text{se } |x - x_1| > \sigma \\ a_1 \epsilon \left( 1 + \cos\left( \frac{\pi(x - x_1)}{\sigma} \right) \right) & \text{se } |x - x_1| < \sigma \end{cases}
\tag{5.12}
$$

where the parameters used have the follow values:

$$\rho_1 = 1, \quad p_1 = 10^5, \quad a_1 = \sqrt{\frac{\gamma p_1}{\rho_1}}, \quad \gamma = \frac{5}{3}$$

$$\epsilon = 0.05, \quad x_1 = 0.5, \quad \sigma = 0.2$$

Let us evaluate the behavior of these systems with the evolution of time. The initial conditions for the pressure is shown in Figure (5.3)
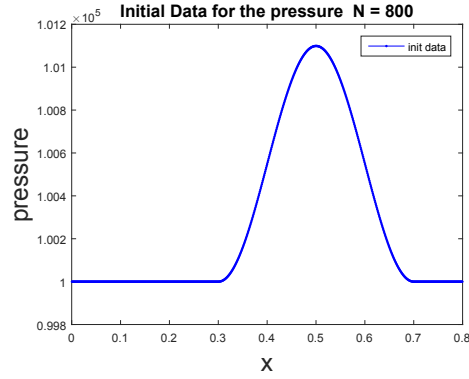


Figure 5.3

In the figures below we report the evolution of the pressure on the piston with two different values of the CFL showing a comparison between the numerical pressure and the adiabatic pressure next to the piston for $t = [0, 0.1]$
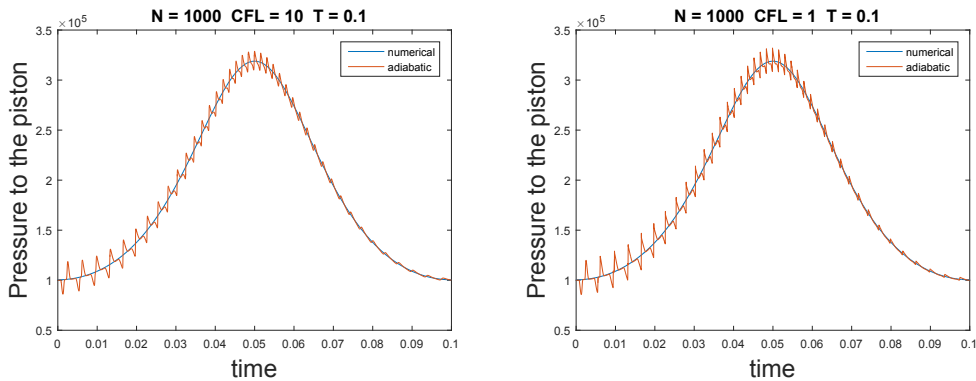


Figure 5.4

We observe that the compression ratio $r = \frac{L(0)}{L_{\min}}$ is equal to 2, namely at the instant of maximum compression the volume occupied by the gas is halved and then the density values are doubled. Even the pressure values evolve according to the adiabatic curve, noting the oscillations around it that are due to the initial simple wave, indeed its solution (even with stationary piston) is characterized by the fact that the wave bounces between the two boundaries.

**Remark 11.** *The use of a routine for the automatic control time step would lead to a more accurate scheme, in fact, if we use a step constant $\Delta t$, its value would be chosen in such a way that the CFL condition is verified at each iteration (work in progress).*

## 5.4.1   Low Mach number

Obviously starting from an initial configuration in which, density and pressure are constant and the velocity is zero, the agreement with the adiabatic approximation is better.

Consider the follow initial conditions

$$
\begin{cases}
u = & 0 \\
\rho = & 1 \\
p = & 10^5 \\
\gamma = & \dfrac{5}{3}
\end{cases}
\tag{5.13}
$$

We are considering that the Mach number $\varepsilon$ is such that:

$$
\varepsilon = \max_{t \in [0,T]} \frac{v_p(t)}{c_s}
$$

where $c_s = \sqrt{\frac{\gamma p}{\rho}}$ is the speed of sound.

We observe that for small Mach numbers if we compare numerical solutions with different values of CFL, taking a number of small points we get similar solutions and we can capture the adiabatic solution.
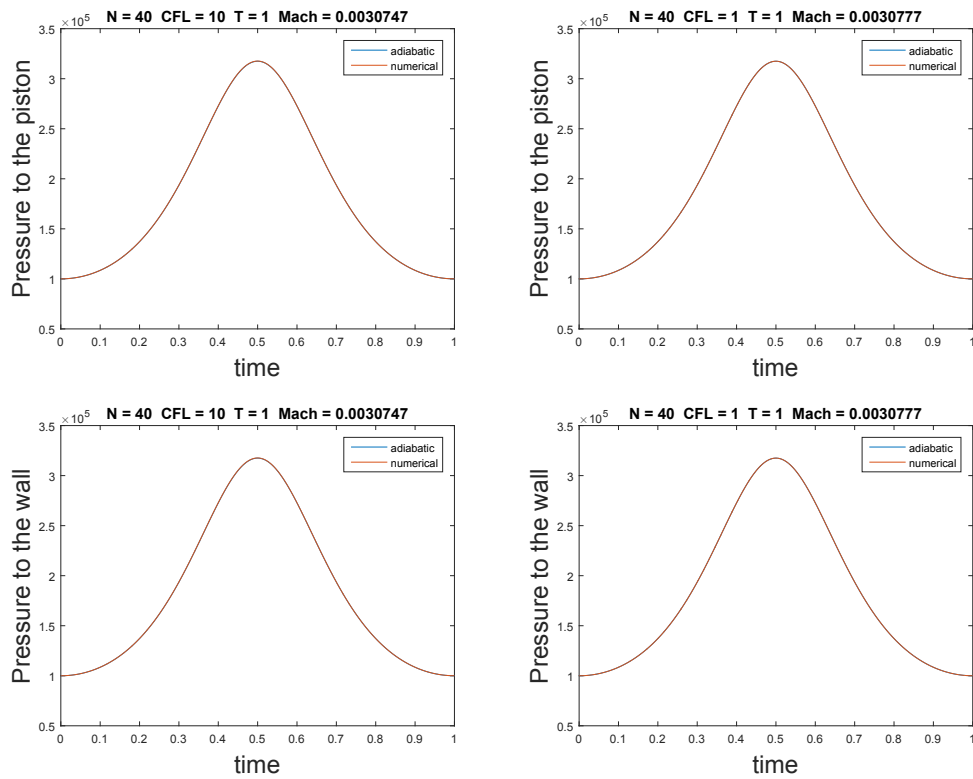
Figure 5.5

While for Mach numbers which are not too small, with a small number of points, we can observe that by comparing the solutions with different values of the CFL, the one with the highest CFL is stable but not accurate, while the one with the lowest CFL will be more correct.
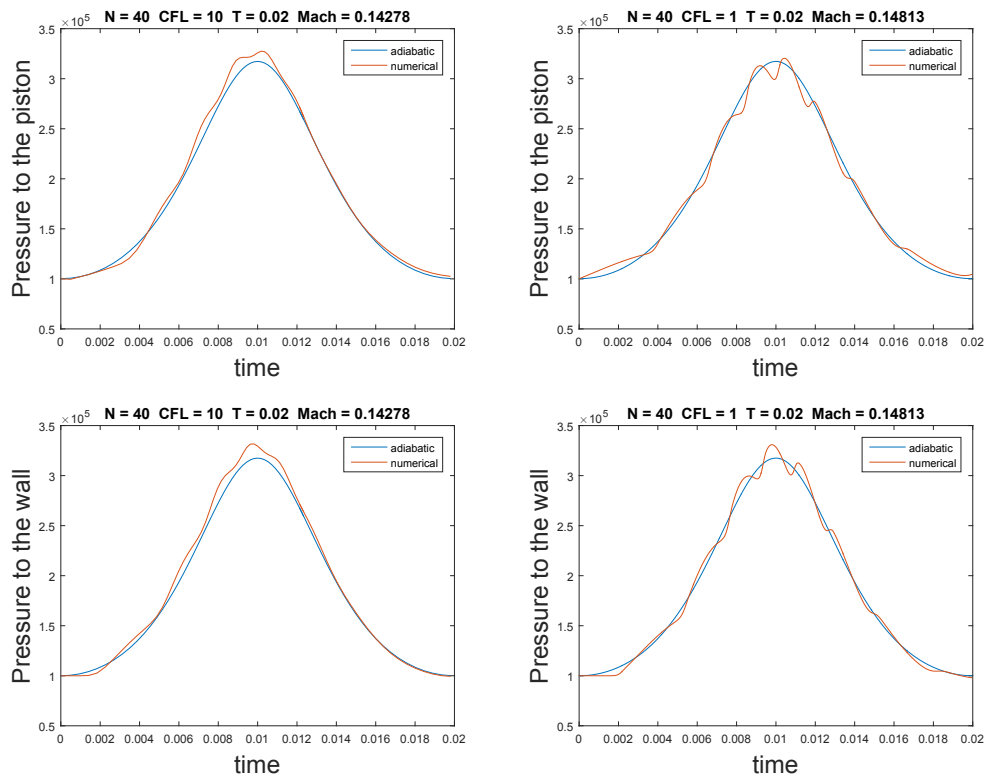
Figure 5.6

To see their accuracy, comparison them with a reference solution by considering a number of high points.
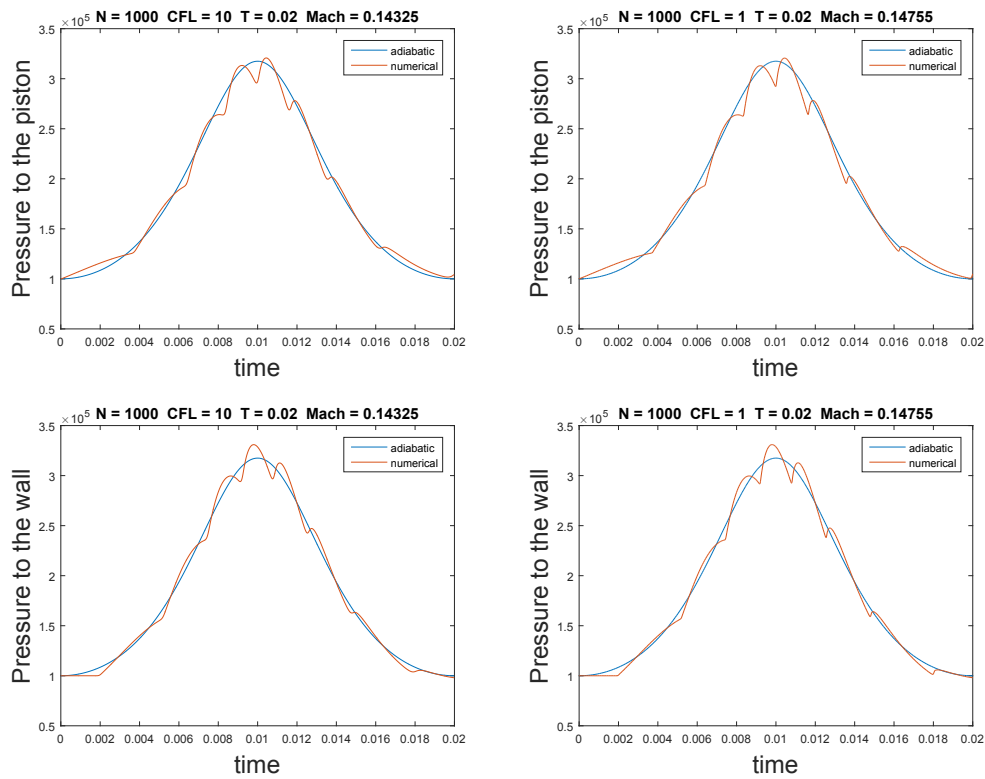
Figure 5.7

We can easily see from these graphs that the numerical method to CFL lower is more correct than that with the CFL higher as it keeps a very similar profile.

# Conclusions and Work in progress

In the thesis we present effective all-Mach number flow methods for the solution of Euler equations of gas dynamics.

Chapter 4 and 5 deal with schemes based on staggered mesh in space. It is shown that, in spite of their simplicity, the schemes are able to reproduce several results of the semi-implicit schemes that can be found in the literature. In particular, the schemes have been shown to be AP, in the sense that they become a consistent discretizzation of the incompressible Euler equation as the Mach number approaches zero. Numerical evidence of such AP property is provided on a two dimensional test case.

Second order in space is guaranteed by classical non-oscillatory reconstruction commonly adopted for such central schemes on a staggered mesh.

The last chapter deals with the piston problem in Lagrangian coordinates treated by a semi-implicit scheme. The implicit treatment of the boundary conditions is originally developed in the thesis. It is shown that for very law Mach number the scheme is able to recover the adiabatic solution with very large CFL numbers. For moderate Mach numbers, or in presence of an initial acoustic wave, loss of accuracy is observerd if the CFL is too large. This drawback can be cured by using a suitable time step control, which will be subject of future investigation.

# Bibliography

[1] U. Ascher, S. Ruuth, and R.J. Spiter. Implicit-explicit rungekutta methods for time dependent partial differential equations. *Appl. Numer.Math.*, 25:151–167, 1997.

[2] G. Bispen. Imex finite volume methods for the shallow water equations. *Ph.D. thesis, Johannes Gutenberg-Universität*, 2015.

[3] S. Boscarino, F. Filbet, and G. Russo. High order semi-implicit schemes for time dependent partial differential equations. *Journal of Scientific Computing*, pages 1–27, 2016.

[4] S. Boscarino, L. Pareschi, and G. Russo. Implicit-explicit runge–kutta schemes for hyperbolic systems and kinetic equations in the diffusion limit. *SIAM Journal on Scientific Computing*, 35(1):A22–A51, 2013.

[5] Sebastiano Boscarino and Giovanni Russo. Flux-explicit imex runge–kutta schemes for hyperbolic to parabolic relaxation problems. *SIAM Journal on Numerical Analysis*, 51(1):163–190, 2014.

[6] Christopher A. Kennedy Carpenter and Mark H. Additive runge-kutta schemes for convection-diffusion-reaction equations. *Applied Numerical Mathematics*, 44:139–181, 2003.

[7] R. Cockburn, C. Johnson, C.-W. Shu, and E. Tadmor. Advanced numerical approximation of nonlinear hyperbolic equations. 1997.

[8] F. Cordier, P. Degond, and A. Kumbaro. An asymptotic-preserving all-speed scheme for the euler and navier-stokes equations. *J. Comput. Phys.*, Vol. 231(No. 17):pp. 5685–5704, 2012.

[9] P. Degond and M. Tang. All speed scheme for the low mach number limit of the isentropic euler equations. *Commun. Comput. Phys.*, Vol. 10(No. 1):pp. 1–31, 2011.

[10] Edwige Godlewski and Pierre-Arnaud Raviart. Numerical approximation of hyperbolic systems of conservation laws. 2014.

[11] J. Haack, S. Jin, and J. Liu. An all-speed asymptotic-preserving method for the isentropic euler and navierstokes equations. *Commun. Comput. Phys.*, 12:pp. 955–980, 2012.

[12] Jeffrey Haack, Shi Jin, and Jian-Guo Liu. An all-speed asymptotic-preserving method for the isentropic euler and navier-stokes equations. *Communications in Computational Physics*, 12(04):955–980, 2012.

[13] E. Hairer, S. P. Nørsett, and G. Wanner. *Solving Ordinary Differential Equations I (2Nd Revised. Ed.): Non-stiff Problems.* Springer-Verlag New York, Inc., New York, NY, USA, 1993.

[14] Ami Harten and Stanley Osher. Uniformly high-order accurate nonoscillatory schemes. i. *SIAM Journal on Numerical Analysis*, 24(2):279–309, 1987.

[15] G.-S. Jiang and E. Tadmor. Non-oscillatory central schemes for multidimensional hyperbolic conservation laws. *SIAM J. Sci. Comput.*, Vol. 19(No. 6):pp. 1892–1917, 1998.

[16] Shi Jin. Efficient asymptotic-preserving (ap) schemes for some multiscale kinetic equations. *SIAM Journal on Scientific Computing*, 21(2):441–454, 1999.

[17] Shi Jin. Asymptotic preserving (ap) schemes for multiscale kinetic and hyperbolic equations: a review. *Lecture Notes for Summer School on Methods andModels of Kinetic Theory (M&MKT), Porto Ercole (Grosseto, Italy)*, pages 177–216, 2010.

[18] S. Kleinerman and A. Majda. Singular limits of quasilinear hyperbolic systems with large parameters and the incompressible limit of compressible fluids. *Commun. Pure. Appl. Math.*, 34(4):pp. 481–524, 1981.

[19] S. Kleinerman and A. Majda. Compressible and incompressible fluids. *Commun. Pure. Appl. Math.*, 35(5):pp. 629–651, 1982.

[20] R. Kleinm. Semi-implicit extension of a godunov-type scheme based on lowmach number asymptotics. i. one-dimensional flow. *J. Comput. Phys.*, 121(2):213–237, 1995.

[21] Randall J LeVeque. Finite volume methods for hyperbolic problems. 31, 2002.

[22] H. Nessyahu and E. Tadmor. Non-oscillatory central differencing for hyperbolic conservation laws. *J. Comput. Phys.*, Vol.(No. 87):pp. 408–463, 1990.

[23] S. Noelle, G. Bispen, K. R. Arun, and C.-D. Munz Lukáčová-Medvidová, M. An asymptotic preserving all mach number scheme for the euler equations of gas dynamics. *Technical Report 348, IGPM , RWTH-Aachen, Germany*, 2012.

[24] Lorenzo Pareschi and Giovanni Russo. Implicit-explicit runge-kutta schemes and applications to hyperbolic systems with relaxation. *Journal of Scientific computing*, 25(1-2):129–155, 2005.

[25] J.-M. Qiu and C.-W. Shu. Conservative high order semi-lagrangian finite difference weno methods for advection in incompressible flow. *J. Comput. Phys.*, 230(4):863–889, 2011.

[26] Eleuterio F Toro. Riemann solvers and numerical methods for fluid dynamics: a practical introuduction. third edition. 2009.